Reversible and Selective Bimolecular Interactions Using γPNA

Submitted in Partial Fulfillment of the Requirements for

The Degree of Doctor of Philosophy

The Department of Chemistry

Taylor D. Canady

Carnegie Mellon University
Pittsburgh, PA

June 1, 2017

Abstract

On-demand selective regulation of gene expression in living cells is a central goal of chemical biology and antisense therapeutic development. While significant advances have allowed regulatory modulation through inserted genetic elements, on-demand control of the expression/translation state of a given native gene by complementary sequence interactions remains a technical challenge.

Toward this objective, in the second chapter, we demonstrate the reversible suppression of a luciferase gene in cell-free translation using Watson-Crick base pairing between the mRNA and a complementary gamma-modified peptide nucleic acid (γPNA) sequence with a non-complementary toehold. Exploiting the favorable thermodynamics of γPNA–γPNA interactions, the antisense sequence can be removed by hybridization of a second, fully complementary γPNA, through a strand displacement reaction, allowing translation to proceed. Additionally, we characterize the displacement reaction via surface plasmon resonance (SPR).

The third chapter continues the theme of reversible translation control and SPR measurements of strand displacement. However, we do so through the orthogonal recognition capability of chiral γPNA. In addition to reversible translation control, we characterize the chimeric probe displacement reaction via surface plasmon resonance (SPR) and demonstrate specific chiral recognition of the chimeric γPNA probes.

The fourth chapter explores increasing the selectivity of complementary γPNA by incorporating intramolecular stem-loop structure. Using SPR, we investigated the selectivity of a structured γPNA against several mutations types and at different target positions. To this end, we identify several mutations which are kinetically discriminated

against compared to an unstructured γPNA control. Additionally, we replicated the

enhanced selectivity findings in an antisense knockdown assay.

Table of Contents

List of Figures

Chapter 1

Chapter 2

Chapter 3

Chapter 4

Chapter 5

List of Tables

Acknowledgements

forever grateful to her. I thank her for her support of Genoa Warner as well. I would also like to thank Dr. Jim Schneider who served as my outside committee member and helped me think through some of my SPR-related issues.

To the wonderful Armitage and Bruchez students, who created an exciting scientific and engaging environment to be a part of, I thank you. In Marcel's lab, I especially thank Dr. Yi Wang, Dr. Cheryl Telmer, Lydia Perkins for their biology teachings, research collaboration, and coffee outings. I thank Alex Carpenter for being a kind friend and working to improve the health and well-being of Mellon Institute. In the Armitage lab, I especially thank Dr. Lisa Rastede and Dr. Ha Pham for training me early on, Dr. Stanley Oyaghire and Dr. Karen Kormouth for their research collaboration and mentorship, and Dr. Munira Fouz for being a friendly lab-mate and research colleague. April Berylyoung really deserves a special acknowledgement section all to herself. April has been a wonderful presence in the Armitage lab and in the Mellon Institute, I thank her for the many hours she has put in to help me and her dedication to make Mellon a healthier place overall.

To the undergraduates to which I had the pleasure of working with: Chris Hong, Lauren Xu, Adam Barsouk (high school student), Joe Martinez, Mallory Evanoff, Steve (Sukjin) Jang (undergrad and masters), and Cole Emanuelson, I thank you all. I especially worked closely with the last four names given. To this group, I will cherish our time together, and I say to you all now: go get your own PhDs!

From the chemistry department, I want to thank the Rea Freeland, Sara Wainer-your help with the CNAST speaker invite was extremely helpful, Valerie Bridge, and Tim Sager. Each are a wonderful asset to the university. To my fellow graduate student

peers, namely, Jon Willcox-your MellonFIT work is appreciated, Matthew Mackenzie-beers and soccer, Chris Collins-our lunch conversations were wonderful, Sushil Lathwal, and Dr. Matteus Tanha-I thank you both for your friendship. Of CNAST, I would like to thank Donna Smith, and Hannah Diorio-Toth for working with me at several outreach events and going above and beyond to make those events exciting. I would like to thank Bruce McWilliams for the endowing the McWilliams fellowship which funded my last year of research.

To my parents, I owe my deepest thanks. My parents worked very hard to get me where I am today. I thank them for their continued support and dedication to helping me get somewhere in life. I would also like to thank Genoa's parents, Dr. Steven Warner and Ruth Warner, for their support through this adventure.

I thank my undergraduate advisor Dr. David Whitten for his mentorship, teachings, and support of my graduate career. I would not be here without David extending himself on multiple occasions. I would also like to thank Dr. Maggie Werner-Washburne, Lupe Atencio, and Dr. Stephen Phillips for taking me into IMSD and supporting my research career in the earliest of stages at UNM.

Finally, I would like to say a few things about Genoa Warner. She deserves more than my acknowledgement, she deserves my everything. We met at CMU in August 2012. We fell in love over the course of the first semester and got married in May 2015. We did it all together. I love you and I look dearly forward to meeting our baby girl. To Genoa Warner, thank you.

Chapter 1: Conjugated- and Backbone Modified-PNA as Bioactive Probes

1.1 Background

From the combined effort of four Danish scientists who set out to build a selective and avid ligand to Nature's singular molecule, the DNA double helix, peptide nucleic acid (PNA) was invented.[1] After their seminal PNA publication in 1991[1], subsequent studies were focused on understanding and exploring the *in vitro* chemical and biological properties, and in turn, the immediate applications of this DNA analog. For example, it was quite exciting when PNA was used as a *sequence targeted* antisense and antigene probe.[2, 3] The immediate attraction (and publicity) surrounding PNA was immense due to the untapped clinical and experimental potential of PNA.[4]

The potential to modify PNA further, through the modularity of solid phase synthesis and the rather simple PNA backbone, further added to the scientific wonderment around what might be possible. However, the therapeutic excitement and promise turned to outright speculation, when it was demonstrated that PNA does not penetrate the cell membrane, nor was it generally obvious how to get PNA to do so in an *effective* manner.[5] Even if the lipid bilayer could be breached through the addition of delivery assists, further doubt set in surrounding being able to achieve targeted control over PNA biodistribution (for example, having the PNA target only heart tissue) and intracellular delivery (does PNA escape endosomes?). In short, for PNA to realize its

early promise, investigators had (have) to solve a "body-to-cell-to-gene" drug delivery problem.

1.2   Introduction

It is the goal of this review to detail some of the impressive synthetic advancements of backbone modified and/or conjugated PNA, which together have lowered the barrier to cellular applications. To this end, a brief overview of the early PNA functionalization work will be given to provide a historical context to the "newer generation" PNA biotechnologies. A summary of key improvements to physiochemical and cell delivery properties will be given in separate sections. The highlighted applications will follow, with an emphasis placed on backbone-modified PNA with biological activity. To conclude, a brief account of the remaining challenges that impede broad use of PNA, and the potential directions for future work, will be given.

PNA has an achiral pseudopeptide backbone with methylenecarbonyl-linked nucleobases capable of complementary hybridization of DNA, RNA, and PNA (Figure 1.1).
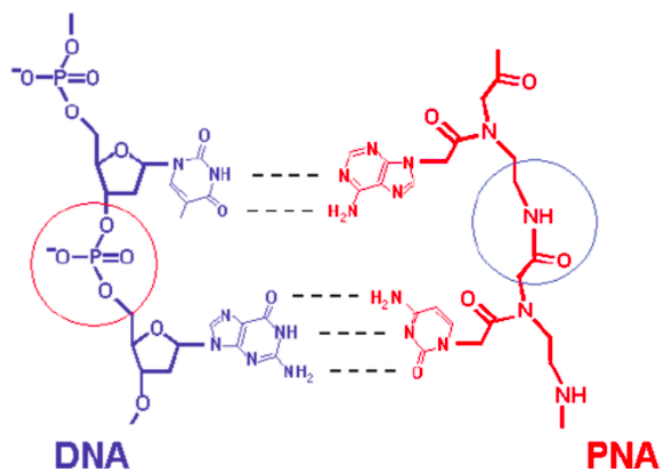
Figure 1.1 Example of a Watson-Crick DNA-PNA structure. Adapted from reference 6.

PNA-target recognition can occur along any face of the cognate target nucleobase. Specifically, PNA binding modes employ Watson-Crick (duplex), Hoogsteen (triplex or quadruplex), or if the PNA is designed accordingly, both types of interaction simultaneously (bisPNA or "tail clamp"). The PNA-target duplex is generally the most stable in the antiparallel conformation, however Hoogsteen-mediated interactions are commonly parallelly directed. Regardless of the exact register of binding used, specific targets are recognized by "programming" the PNA to include the complementary (*homologous* in the case of heteroquadruplex formation) target sequence (**Figure 1.2**).
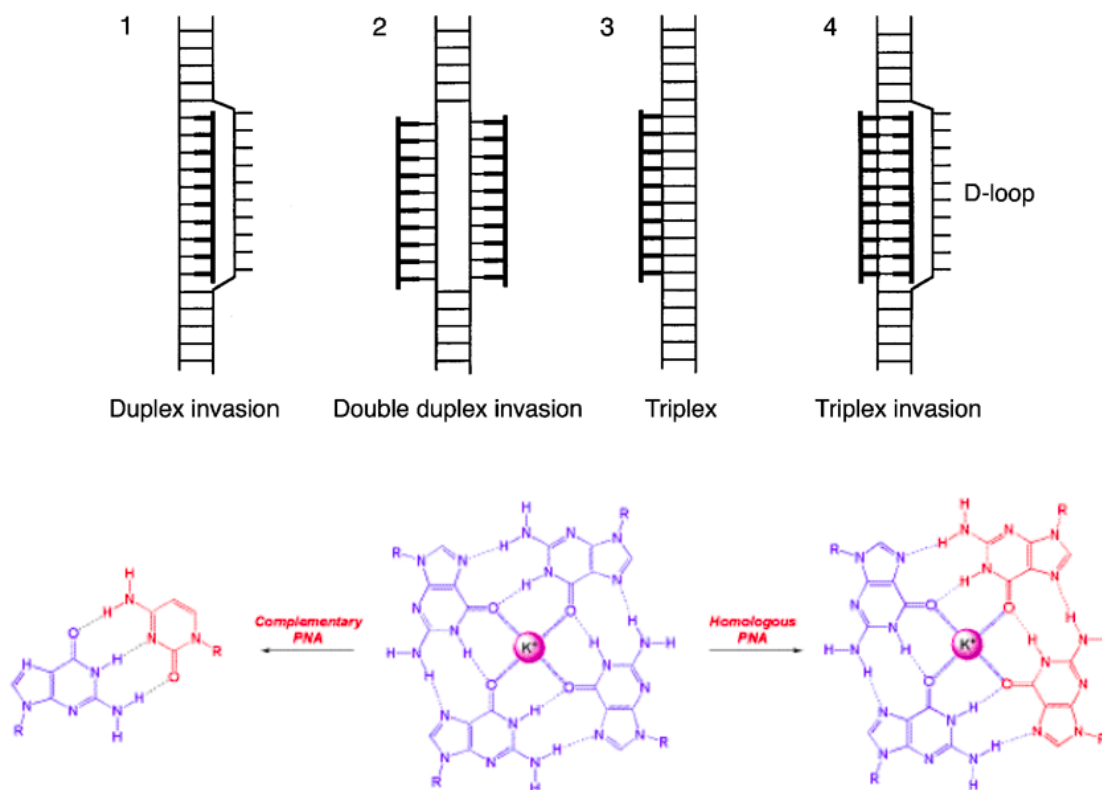
Figure 1.2 (**Above**) PNA binding modes with duplex DNA. (**Below**) Invasion of a Guanine quartet structure by a homologous (right) or a complementary (left) PNA. Adapted from reference 7, 8.

With the effortless ability to define probe-target interactions, increased biological stability[9] and high binding affinity, PNA was proven to be a useful and pluralistic *in vivo* and *in vitro* biotechnology. Further expanding the application space of PNA is the relative synthetic ease to incorporate additional molecules (e.g., amino acids, fluorescent dyes, metals, etc.) along the backbone via solid phase synthesis directly or through "post-synthetic" addition.

The lack of a PNA backbone charge leads to salt insensitivity, allowing for beneficial buffer manipulations *in vitro*, and high affinity binding due to the lack of intermolecular electrostatic repulsion. However, the overall hydrophobicity of

unmodified PNA limits its water solubility and therefore has stinted its bioactive 'plug and play' nature. Again, as highlighted above, the poor cellular uptake and uncertain systemic distribution and tissue localization profile have slowed PNA therapeutic progress. Recognizing these issues, several groups have set out to improve PNA biocompatibility by synthetic alteration of the parent PNA design.

1.3 Conjugated and backbone modified PNA: increased solubility properties

With its displayed hydrophobic nucleobases and non-polar backbone, unmodified PNA is a globular molecule in water. However, the PNA skeleton contains an alpha (α), beta (β), and gamma (γ) positions, which can be modified to improve its biochemical properties (**Figure 1.3**). Moreover, applying monomers that are compatible with solid phase synthesis and post-functionalization allow for the terminal conjugation of orthogonal chemical groups to the PNA main chain. In part, the synthetic modularity of PNA has allowed for continued biotechnology progress.
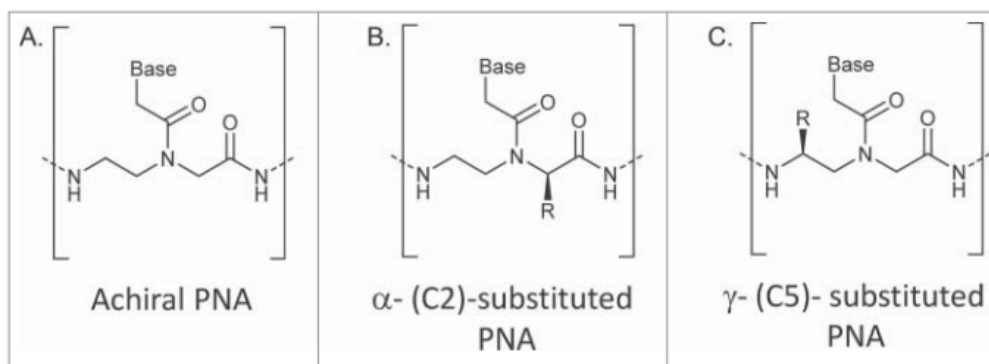
Figure 1.3 Structure of unmodified and backbone-modified (R substituents) PNAs. Adapted from reference 10.

The conjugation of a positively-charged lysine to the PNA C-terminus increased water solubility and maintained high probe-target affinity and mismatch sensitivity.[11] Similar in effect, α-substitution derived from a positively-charged, chiral amino acid in forming the PNA skeleton also granted increased water solubility.[12] Specifically, the incorporation of two D-lysine modifications within a PNA dodecamer led to a 5-fold solubility enhancement over the analogous unmodified PNA. Interestingly, the α-substituted D-lysine PNA/DNA binding affinity was dependent on the amino acid charge and stereochemistry due to electrostatic contributions and α-substituent/groove-accommodation, respectively. Biophysically, the α-substituted D-lysine PNA-DNA hybrid adopts a P-form duplex with limited PNA backbone flexibility, and thus, the potential for increased mismatch target discrimination.[13] In short, the increased selectivity of backbone-modified is due to the limited conformational space that can be explored, by the PNA, in order to energetically compensate for a mismatch base pair. It should be noted that backbone incorporation of solubilizing negative-charge through internal glutamic acid- or phosphono-incorporation has been pursued as well.[12, 14-16] Whether a positive or negative charge is chosen, the incorporation of charge in the backbone will likely affect the affinity/selectivity for DNA/RNA targets. Furthermore, solution ionic strength, through counterion masking effects, can alter PNA/DNA heteroduplex stability when the PNA backbone is charged.[17]

In addition to incorporating solubilizing agents inspired by nature, synthetic units have been applied to improve PNA's physiochemical properties and increase its biocompatibility. For example, polyethylene glycol (PEG) incorporation is often pursued due to its noted high water solubility, low immunogenicity and cytotoxicity profile.[18]

Thus it is no surprise that PNA-PEG conjugation has been carried out as well, with demonstrated applications on surface[19] and in solution[20, 21]. Notably, the hydrophilic diethylene glycol (miniPEG) unit has also been placed at the γ-carbon position of the PNA backbone, termed [R-MP]γPNA, to improve water solubility. Excitingly, the core installation of *R*-substituent at the γ-carbon transforms the collapsed PNA globule into a rigid (relative to DNA/RNA) right-handed helix, with helical propagation occurring in a C- to N-direction (**Figure 1.4**).[22] Probe preorganization confers enhanced stability to the [R-MP]γPNA/target heteroduplex by lowering the entropic cost of binding and increasing mismatch discrimination through backbone rigidity.[23]
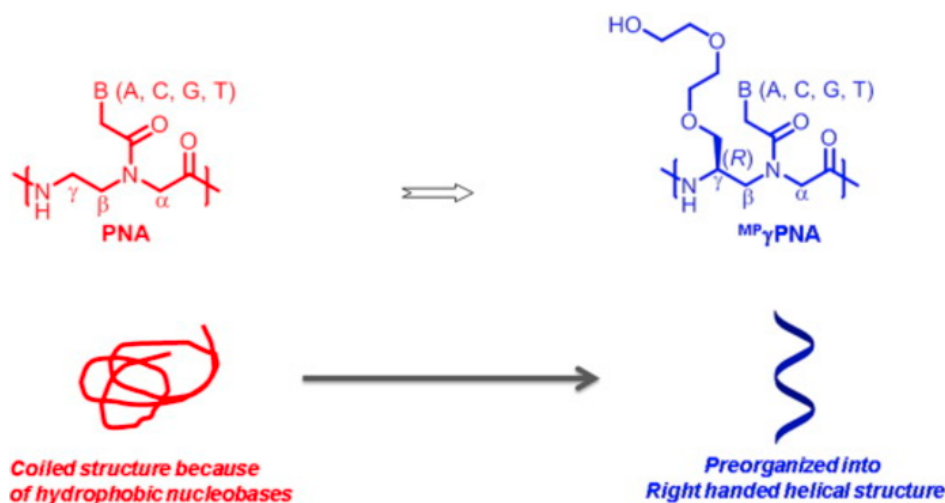
Figure 1.4 Gamma-substitution leads to helical preorganization (blue) compared to the unmodified PNA globular state (red). Adapted from reference 24.

By studying the γPNA-DNA (P-form) crystal and NMR structural information[25], the helical sense of the γPNA was determined to be the result of a series of steric clashes between the internal amide bond and proximal γ-substituent, followed by helical stabilization through base stacking.[18] Interestingly, the right- or left-handed chirality can

be "programmed" into the γPNA probe through a judicious choice of the γ-position stereochemistry during monomer synthesis, thus adding another layer[10] of hybridization "encoding" that can be used in bimolecular applications (**Figure 1.5**).[26, 27] It should be noted that helical preorganization is also seen in the trans-cyclopentyl backbone PNA derivative.[28] The chiral constrained pyrrolidinyl PNA represents another promising backbone derivative, especially when considering their high sequence discrimination.[29, 30] Although trans-cyclopentyl and pyrrolidinyl PNAs have not been heavily explored as an intracellular bioactive tool (and are not highlighted in depth in this review), they have been employed in a couple impressive *in vitro* diagnostic contexts.[31, 32]
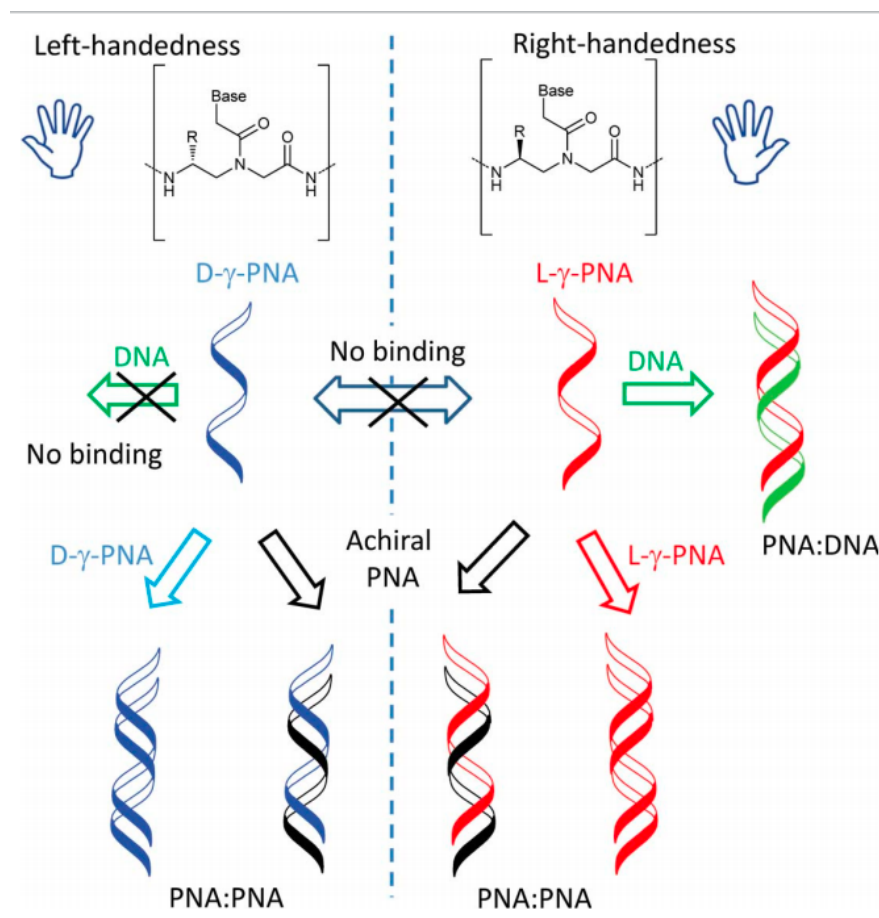
Figure 1.5 Helical handedness is determined by the gamma-substituent stereochemistry which leads to a intramolecular steric interaction within the backbone. Thus, bimolecular interactions are defined by *both* sequence *and* helical complementarity. Adapted from reference 10.

Another interesting strategy to increase the aqueous solubility of PNA, although not implemented for this feature alone, is the synthesis of PNA-DNA oligonucleotide chimeras.[33-35] The intense clinical interest as well as the accompanying literature breadth of DNA-modified oligonucleotides[36-38] present an exciting opportunity to study systems that leverage both the PNA and the DNA properties. For example, engagement of RNase H machinery and high target binding affinity has been achieved using PNA-DNA chimeric probes.

1.4 Conjugated and backbone-modified PNA: increased cell-permeability

The intracellular application of nucleic acids as target-specific probes affords a promising technology that has clearly been stinted by uptake and distribution problems. [39, 40] The strategies employed to deliver oligonucleotides are quite varied, but in general use chemical, mechanical, and/or electrical transduction means (**Figure 1.6**). A common *in vitro* PNA-delivery strategy has been to form PNA-DNA heteroduplexes that are complexed to lipid delivery vectors.[41, 42] However, this method is not without its limits in terms of systemic delivery and cytotoxicity.[41] That being said, the following section will primarily focus on chemical delivery methods that incorporate "main-chain" PNA modifications and allow for "naked" probe delivery. Some mention will be made of non-toxic nanoparticle approaches to increase modified PNA delivery.
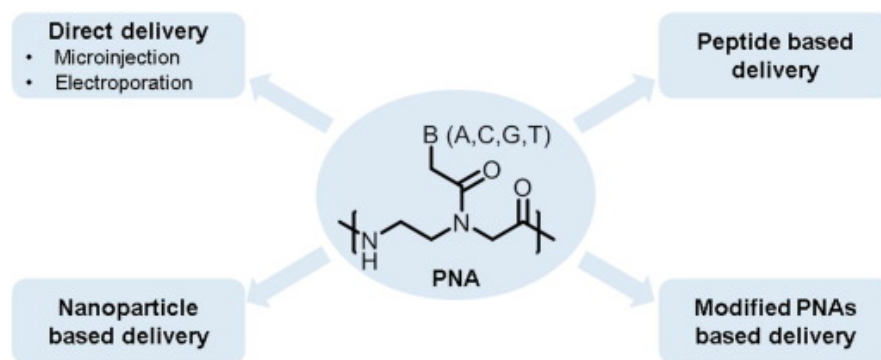
Figure 1.6 Various methods to delivery PNA probes. Adapted from reference 24.

Conjugation of short cationic peptides to the PNA termini was used to deliver PNA cargo to mammalian cells without a liposome aid. PNA-peptide conjugates commonly include positively charged cell penetrating peptides (CPPs), such as the HIV Tat[43] and the *Drosophila* Antennapedia[44] (termed penetratin), as well several other

natural and synthetic variants, for mammalian cell delivery.[5] For example, in a seminal study by Nielsen and coworkers the mammalian-based delivery efficacy of PNA-Antennapedia versus PNA-Tat was compared.[45] Additionally, the authors investigated the delivery efficacy as a function of the CPP placement and the particular conjugation chemistry used to attach PNA cargo.[45] Importantly, cell-specific instances of both endosomal inclusion and limited escape were observed for various CPP designs, which was similarly observed in earlier PNA conjugate delivery work.[46]

After observing some initial PNA delivery progress, an expanded comparison of 7 CPP peptides conjugated to splice-site correcting antisense PNAs by several different linker chemistries was made.[47] In addition to relating the overall antisense efficacy of the various CPPs, the authors noted that the PNA-CPP serum sensitivity and linker position- and chemical- composition effect delivery. Similarly, in another comparative PNA-CPP study, it was again suggested that intracellular trafficking (and therefore biological PNA activity) and CPP enzymatic stability is likely influenced by CPP chemical composition.[48] Collectively, this work laid important experimental and control rules for how PNA delivery experiments should be carried out, as well as, included some clear examples of successful PNA delivery.

Terminal conjugations of PNA to various sugar and lipophilic ligands have been studied for cell targeting as well. For example, conjugation of an adamantyl sugar group to PNA led to increased cellular uptake in some mammalian cell lines. However, the use of a cationic lipid aid was effective endosomal release observed.[46] Further exploring the possible PNA-conjugation chemistries, Nielsen and coworkers also investigated lipid-mediated delivery of an array of hetero-aromatic and lipophilic PNA-conjugates. The

PNA-conjugates were screened based on splice site correction efficacy in cell culture, with several variants showing promising bioactivity.[49] In an effort to try and strike a balance between the hydrophilicity and lipophilicity required for effective cellular uptake without the need for additional lipid delivery aids, researchers synthesized steroidal cholic acid-PNA "umbrella" conjugates and measured their *in vivo* uptake and bioactivity.[50] Unfortunately, this design showed limited delivery, and thus antisense activity.[50] In a similar design that strives to balance chemical properties, the conjugation of a lipid-CPP (CatLip) motif to an antisense PNA increased the delivery and biological effect of the PNA, however noticeable toxicity effects were also observed as a function of lipid conjugate length.[51] Nevertheless, the application of various sugars/lipids combinations to the PNA scaffold is still underexplored and warrants closer investigation.

Apart from terminally conjugating chemical groups, increasing PNA cell delivery can be acquired through altering the backbone chemical composition. For example, inspired by the mammalian uptake properties of the arginine-rich HIV-1 Tat transduction domain, Ly and coworkers studied the cellular delivery and targeting potential of α-guanidine PNA, named GPNA (**Figure 1.7**).[52]
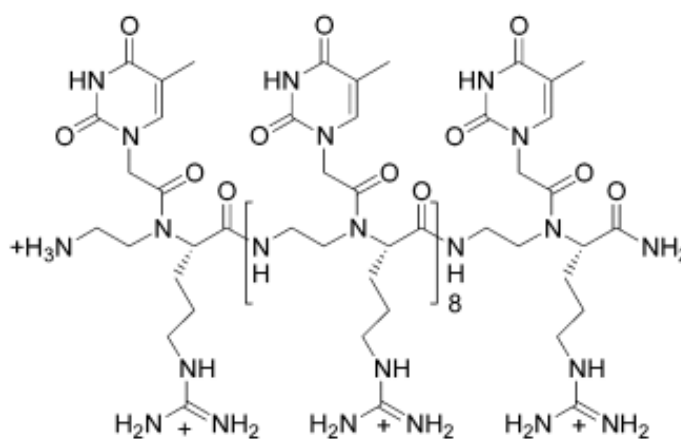
Figure 1.7 Structure of α-guanidine PNA. Adapted from reference 52.

The direct *in vitro* application of fluorescently labeled GPNA to HCT116 (colon) cells resulted in cellular uptake, which was consistent with the uptake of earlier lysine-backbone modified PNA.[45] In subsequent studies[53, 54], GPNA cellular uptake was observed in human somatic and embryonic stem cells, with optimal delivery requiring alternating α-D-guanidine functionalization of the PNA backbone. Delivery to stem cells is especially exciting given the transfection difficulties associated with this cell type. Additionally, this result may become more relevant for future embryonic PNA gene editing technologies. Beside the GPNA's delivery potential, stable duplex and triplex GPNA-DNA complexes were studied through circular dichroism and UV melting spectroscopy, thus providing important biophysical characterization of the antigene/antisense potential of these "newer" generation probes. The highest GPNA-target affinity was achieved with GPNA probes that contained alternating spaced guanidine groups, likely due to reduced intramolecular steric clash.[55] Furthermore, the α-D-guanidine configuration granted higher GPNA-RNA binding affinity, compared to the stereoisomer α-L-guanidine GPNA.[55, 56] Additionally of note, PNA has been modified at the γ-position with guanidine, which grants both increased cellular delivery properties and, as noted above, higher binding affinity to targets due to helical preorganization.[54]

The general consensus is that PNA-CPP delivery is endocytosis-dependent[57], but the exact internalization pathways leading to cytoplasmic PNA-CPP release remains unclear.[57-59] In addition, effective PNA delivery is thwarted by endosomal entrapment which limits the overall bioavailability of PNA.[60] To address endocytosis challenges, researchers have applied external chemical aids[61] and/or further PNA core additions to

potentiate endosomal disruption and escape.[58, 62, 63] For example, PNA conjugation to a

'proton sponge' polyethyleneimine (PEI) polymer for purposes of endosomal-disruption

has successfully increased the antisense activity of PNA.[64] In addition, delivery via

polymeric nanoparticle formulations is becoming increasingly common and affords the

opportunity to build upon decades worth of nanoparticle encapsulation research.[24]

       The fact that many of the hurdles in early nucleic acid delivery research, namely

achieving and *understanding* mechanisms and routes of intracellular delivery, exist today

speaks to the complexity of intracellular trafficking. It is recommended that oligo-

delivery experiments include bioactivity (for example, antisplice activity) measurements

and scrambled probe controls to avoid delivery and activity misinterpretation,

respectively. An increased focus on the identification of intracellular pathways as a

function of probe design is essential to achieve a higher understanding of how probes

must be designed to locate to specific tissues/targets. In an early example, Dowdy and

coworkers have presented an interesting experimental tool which may help to understand

how and where PNA-peptides traffic, although this tool has not been adapted to PNA yet.

Specifically, cellular internalization mechanisms and transduction efficiency of several

peptide conjugates were studied through the application of a GFP-complementation

fluorescence assay (**Figure 1.8**).[65] Furthermore, the reconstitution of a split GFP

construct is dependent efficient cellular uptake and cytosolic delivery of a CPP

conjugated to a GFP-fragment. In short, this approach allows for the localized expression

(via cellular address tags) of protein constructs that can be targeted by a synthetic nucleic

acid construct, thus simultaneously reporting on the specific trafficking profile and

potential bioactivity of the probe. In a similar manner, targeting cell-permeable

fluorogenic dyes to genetically-encoded proteins at various cellular sites, which *may* also provide a technological platform to help understand oligonucleotide trafficking biology.[66] However, the fluorogenic dye-protein technology has not been explicitly applied to nucleic acid trafficking questions and will require some "re-tooling" of the technology to oligonucleotides. Nevertheless, further engaging with technology that can interface with genetically-encoded machinery is under explored and much needed in the nucleic acid field.
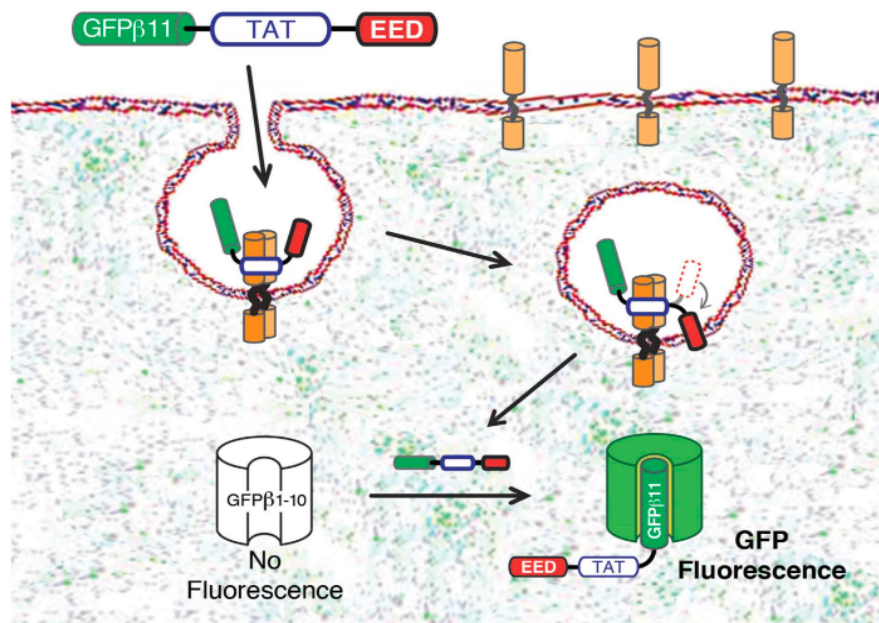
Figure 1.8 Experimental system employed by Dowdy et al. Here, intracellular delivery of GFFβ11 cargo is mediated by CPP and EED (endosomal release) peptides. Verification of cargo localization is established through GFP complexation. Adapted from reference 65.

1.5   Applications of backbone-modified PNA

It is impossible to give a comprehensive summary without leaving out several informative examples because there exists a tremendous amount of PNA literature replete with impressive applications. With that said, the goal of this section is to highlight some common uses of backbone-modified PNA into *bioactive* categories.

When considering the potential applications of modified PNA, it is worthwhile to first start with a general understanding of the Central Dogma of Molecular Biology, which states that genetic information passes through three discrete levels: DNA replication, RNA transcription, and protein translation. Of course, this description is too simplified, considering the important role epigenetics and intermediate RNA processing and modifications have on gene expression. Nevertheless, this model allows for a scientist to hypothesize points of therapeutic PNA intervention (or any other base sequence cognate technology for that matter).

For example, one may build a complementary PNA to block transcription (antigene strategy) at a specific gene or construct a transcript-specific PNA to inhibit translation (antisense strategy). Of course, antigene efforts have an added challenge, that of invading the cell *and* entering the nucleus. Hence, many of the published intracellular examples include antisense data. Indeed, a vast amount of PNA literature revolves around antisense developments in mammalian or bacterial systems. Nevertheless, as the above sections hopefully detailed, the main challenge has been in building PNA technologies that work in water and can effectively access the intracellular environment where the genetic information is housed. These challenges are the reasons for which research on backbone-modified PNA has remarkable progress. Next sections highlight some of the

antigene, RNA interference, and gene editing advancements using backbone-modified-
and conjugate-PNAs.

1.6   Antigene

In vitro antigene studies typically include 2PNA/DNA or bisPNA/DNA triplexes,
which are constrained to purine-rich DNA duplex targets. Furthermore, these studies are
often performed at relatively low salt concentrations, which limit their potential target
scope and clinical utility. Although it is possible to lower the target sequence stringency
by incorporating pH-independent, "non-Watson-Crick" nucleobases (i.e.,
pseudoisocytosine) or employing a PNA-mediated duplex strand displacement strategy,
the overall progress using these approaches has been slow due to the nuclear targeting
and energetic challenges of invading duplex DNA.[67, 68] Nevertheless, there are examples
that have demonstrated chromosomal antigene activity of PNA in cells. For example,
Corey and coworkers have demonstrated liposome-mediated and CPP-mediated delivery
of a progesterone-receptor promoter-directed PNA inside cells.[69, 70] However, several
complications were observed related to overall PNA-CPP potency and delivery
efficiency, leading the authors to suggest that further PNA modifications may need to be
explored. To this end, much of the PNA antigene work has been limited to targeting non-
nuclear DNA (plasmid or linear DNA) in culture or cell-free systems because targeting
chromosomal DNA *in vivo* is much more challenging due to several factors including
nuclear localization, nucleosome packaging, and the inability to manipulate the
surrounding buffer.[41]

Interestingly, recent studies of single stranded γPNA (γ = miniPEG) modified with "G-clamp" bases showed promise in invading and binding duplex DNA under physiologically-relevant conditions. The high binding affinity of γPNA affords thermodynamically favorable double helical DNA recognition in a sequence-unrestricted manner.[71, 72] However, as seen in unmodified PNA examples[73], γPNA duplex invasion is kinetically hindered by the native double stranded structure. The fact that γPNA "nucleation" to duplex DNA is slow may warrant applying "breathing-mode" independent intercalation groups directly to the probe. As shown previously with acridine-PNA and acridine-γPNA conjugates, a conjugated intercalator "anchors" the PNA probe proximal to the DNA target, thus raising the local probe concentration and increasing the probability of duplex invasion.[74, 75] Additionally, designing experiments which take advantage of transiently formed transcription bubbles[68] in order to bind the PNA near the DNA invasion site may also be a useful approach.[76] Upon solving the kinetic challenges, the high binding affinity coupled with the unrestricted sequence recognition properties demonstrated *in vitro*, should allow γPNA variants to function as a potent transcriptional agent. Further, selecting a γPNA capable of cell-delivery and nuclear localization may be a promising strategy for achieving nuclear antigene activity.

1.7   Antisense

PNA inhibits translation by the steric blockage of ribosomal assembly or translocation through PNA-RNA duplex formation (PNA-mediated degradation of the mRNA has also been hypothesized).[77] An important contribution to the PNA antisense field was the discovery that targeting the terminal end of the 5'-UTR with a

complementary PNA results in potent luciferase knockdown, relative to other transcript

binding sites, including the Kozak-AUG protein start site (**Figure 1.9**).[78] It has been

noted that the high antisense activity observed at the terminal transcript site is likely due

to the bound PNA probe sterically hindering small ribosomal subunit association at the

5'-cap region.
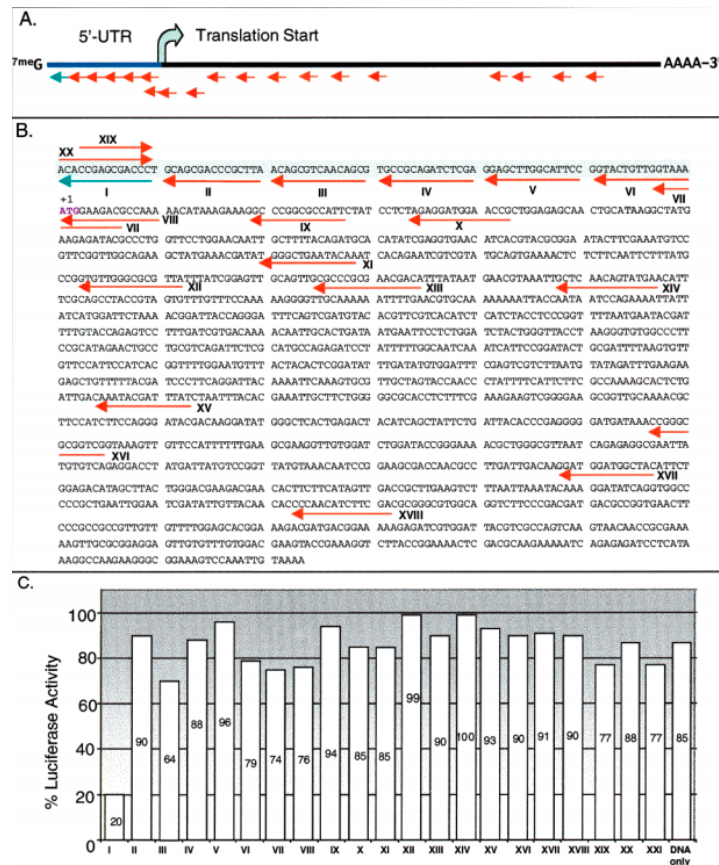
Figure 1.9 PNA Gene walk antisense study (in cells) along the length of a luciferase reporter transcript. A) Cartoon representation of the PNA binding sites (1 blue arrow and rest are red arrows) and (B) demonstrates the actual PNA probe length and name labels. C) Luciferase activity is measured for each PNA probe, with probe I (blue arrow) demonstrating the highest knockdown at the 5'-terminal end. Adapted from reference [78].

Subsequent PNA antisense studies that targeted other gene transcripts in

mammalian cell culture have identified high potency via terminal binding, thus giving

credence to the general antisense potency of this site.[79, 80] Nevertheless, there are examples of successful mammalian antisense demonstrations that targeted alternative transcript sites, such as translation start site.[81, 82] Additionally, it is worth noting that although targeting the terminal 5'-UTR is an effective strategy in eukaryotic systems, prokaryotic-based antisense studies generally require targeting the Shine-Delgano and translation start site (RBS-AUG) region for high potency.[83] The difference in the probe target site selection within the transcript is largely guided by the differences in eukaryotic and prokaryotic ribosomal association mechanisms.[84] In eukaryotes, the small ribosomal subunit associates at the 5'-cap of the transcript and proceeds to scan (5' --> 3') the UTR until it encounters the Kozak-AUG start site. Thus, the introduction of a 5'-terminal complementary probe is likely to yield potent eukaryotic antisense knockdown by sterically blocking the small-subunit association. In contrast, prokaryotes direct small subunit association with the ribosome binding site (Shine-Dalgarno). Thus, prokaryotic antisense probes which directly target the start codon are effective ribosome steric blocks.

Backbone-modified PNAs are attractive antisense agents due to their un-aided delivery potential and relatively high binding RNA affinity, compared to unmodified PNA. After initially studying the intracellular delivery properties of α-guanidine GPNA, subsequent GPNA work demonstrated sequence specific *in vitro* antisense knockdown of human E-cadherin.[59] In a recent example, the Ly lab demonstrated GPNA antisense-mediated antitumour efficacy in cancer cells both *in vitro* and *in vivo*.[62] Specifically, anti-EGFR antisense GPNA was administered intraperitoneally in a xenograft mouse model resulting in sequence specific tumor reduction over the GPNA treatment time course. Interestingly, GPNA effectively inhibited *in vitro* cancer cell growth in a

cetuximab (FDA-approved EGFR inhibitor) resistant EGFR-mutant model. γ-guanidine GPNAs, which allows for un-aided cell-delivery and preorganization-mediated enhanced target affinity, has also been used as an antisense probe in β-catenin mutated liver tumor cells.[85] This study demonstrated high γ-guanidine GPNA sequence selectivity and antitumor potency when targeted to the transcription start site. Additionally, a recent combined approach which coupled the "newer generation" γPNA with nanoparticle delivery methods, specifically PGLA-mediated delivery, anti-Chemokine Receptor 5 (CCR5) antisense was demonstrated *in vitro*.[86] Moreover, the specific antisense γPNAs studied included both the γ-miniPEG and the γ-guanidine monomers in an individual probe, thereby granting the ability to compare the encapsulated nanoparticle delivery to naked probe delivery efficacy.

Antisense targeting of double stranded RNA (in cells) through PNA-CPPs has resulted in a few successful demonstrations worth noting. In an impressive example, Corey and coworkers demonstrated effective *in vitro* antisense targeting of the mutant huntingtin (*HTT*) allele CAG repeat (forms a repeating hairpin structure) with a single stranded PNA-peptide probe.[87] In addition, experimental evidence pointed to the benefits of applying a shorter (13-mer) PNA probe for increased selectivity without compromising potency. In a separate approach, the incorporation of physiologically charged (positive) nucleobases into a PNA, allowed for triplex-mediated targeting of dsRNA structures within the 5'-UTR. The authors noted the nucleobase-modified PNA had selective (mutation sensitive) and potent translation knockdown.[88] In addition to the triplex-mediated strategy, the incorporation of nucleobases which can "bifacially" invade and interact with double stranded RNA targets presents an exciting strategy for *in vivo*

manipulation, however this strategy has only been applied to *in vitro* RNA targets.[89] Although, the above probes used for double stranded RNA invasion apply unmodified PNA, they do provide potential targets and inspiration to test future backbone modified PNAs. For example, motivated by the work of duplex DNA invasion by γPNA, it would be interesting to investigate if the high target affinity of γPNA can be leveraged in order to invade duplex RNA targets.

In addition to mRNA targeting, application of antimiRNAs PNA-CCPs can be conducted as well. In an impressive recent example, Slack and coworkers conjugated a low pH-induced transmembrane structure (pHLIP) peptide to a PNA (antimiRNA) to target the acidic tumor microenvironment within a mouse model.[90] The pHLIP mechanism for intracellular delivery is endocytosis-independent and involves (1) pH activated helical folding and lipid bilayer invasion of the pHLIP peptide, followed by (2) the reduction of the disulfide PNA-peptide linker and (3) intracellular PNA bioavailability (**Figure 1.10**). Additional, backbone modified PNAs have been applied as an antimiRNA agent in leukaemic K562 cells (GPNA against miR-210), resulting in efficient probe delivery and bioactivity.[91]
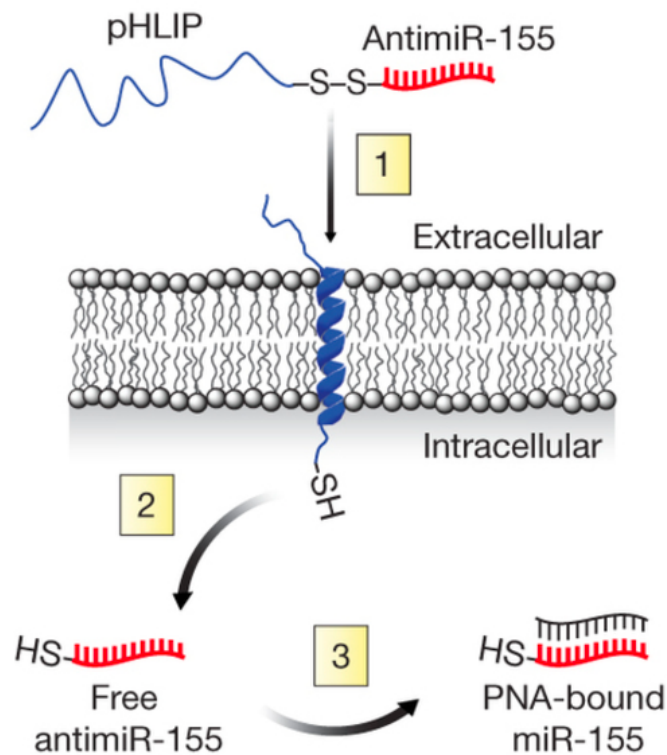
Figure 1.10 Non-endosomal mediated delivery of an anti-microRNA pH sensitive CPP-PNA (CPP = pHLIP) conjugate. Adapted from reference [90].

Alteration of pre-mRNA processing through antisense PNA (unmodified backbone) splice site obstruction has led to corrective protein expression *in vitro*.[92] However, tissue- and target-specific effects, as well as, delivery challenges often confound the general rules for building effective antisplice agents. For example, a 4-lysine PNA conjugate (18-mer) administered intraperitoneally resulted in corrective splice switching in numerous mouse tissues.[93] However, the application of a 14-mer 4-lysine PNA conjugate failed to demonstrate effective splice switching in patient muscle cells, likely hinting at the role of probe length-affinity effects.[94] In a set of muscular related examples, intramuscular and intravenous delivery of antisplice PNA was studied in a Duchenne muscular dystrophy mouse model (*mdx*). Although earlier work showed increased muscular uptake (via direct muscle injection) and splice-site correction[95, 96] with a PNA-CPP (PNA-Pip2b),

intravenous injection of PNA-Pip2b as well as other candidate PNA-CPPs all performed therapeutically worse than the analogous unmodified 20mer PNA (which also performed relatively poorly).[97] The authors noted PNA sequence length may be a causative factor in observing low PNA and PNA-CPP systemic activity, and thus evaluated intramuscular delivery and splice correction as a function of applying shorter (<20mer) and longer (>20mer) length PNA probes. From this, a 25mer PNA showed enhanced activity, thereby hinting at the interplay between steric blockage, affinity, and selectivity towards achieving effective bioactivity.[97] In another antisplice study, PNA conjugated to lysine rich (up to 8 lysines) peptides showed substantial and preferential inhibition of PTEN expression in adipose tissue *in vivo*, however nephrotoxicity was observed, which raised concerns about future PNA-CPP work.[98] These features do seem to warrant the application of naked backbone modified PNA variants for systemic delivery and antisense-mediated splice correction due to their more attractive physiochemical properties, however experiments using backbone modified PNA as an antisplice agent have yet to be done.

1.8   Gene repair

The application of backbone modified PNA for targeted gene repair arguably represents the most exciting demonstration of PNA yet. However, the capability of PNA as a potent and selective "gene editor" was not discovered by fortuitous happenstance. In fact, for nearly 25 years the Glazer lab has worked on PNA-mediated gene repair, publishing across a spectrum of disciplines. For example, the early gene repair work focused on understanding DNA-PNA triplexes[99-101] in cell culture and in parallel, the

Glazer lab aimed to understand how the endogenous DNA repair machinery engages with the PNA-DNA triplex.[102, 103] Recently, the Glazer lab has employed a strategy that uses a nanoparticle formulation to aid in PNA delivery (also formulated with the "corrective" DNA template), thus working around many of PNA's delivery short comings (Figure 1.11). In short, the Glazer lab is well on its way in building a bona-fide competitor to the CRIPSR-Cas technology.
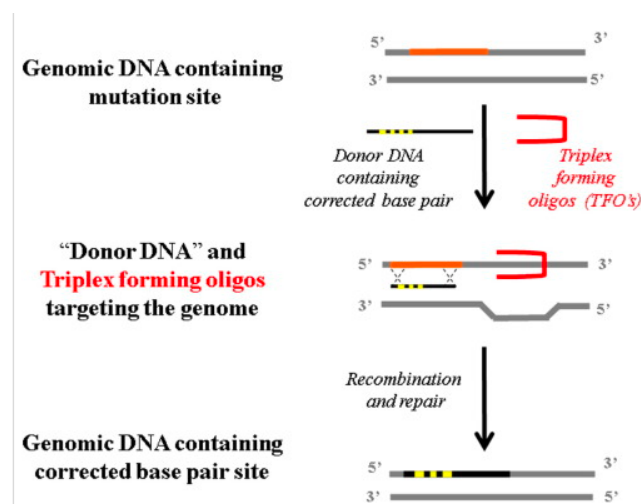
Figure 1.11 General PNA-mediated gene editing strategy. Nanoparticle delivery of both the donor DNA and triplex forming PNA (red) target allow for gene specific correction of a mutated locus. Adapted from reference 24.

Recently, researchers have achieved *in vivo* gene therapy through the corrective action of a triplex forming PNA. Two impressive *in animal* experimental results are worth noting here. First, through intranasal delivery of a PLGA nanoparticle with an entrapped triplex-forming bisPNA and donor DNA template, corrective editing of the F508del mutation in the *CFTR* gene was demonstrated.[104] Impressively, no statistically

significant off-target modifications were observed. In a closely followed publication, Glazer and coworkers systemically delivered a PLGA nanoparticle formulation consisting of a tail-clamp forming γPNA (γ = miniPEG) and the "wild type" DNA donor template, in a human β-thalassemia mouse model. This treatment course resulted in disease phenotype correction with "extremely" low off-target effects.[105] Additionally, elevated gene repair was achieved upon co-administration of a stimulatory cytokine (SCF) for increased homology dependent repair (HDR) gene expression, thus evidencing a role for adjuvants in PNA triplex gene editing.

Future work is likely to include additional disease corrections and, speculatively, should include other correction examples across various cell lineages and differentiation states. Irrespective of the specific route of the future work, the PNA gene editing is an exciting technology that, so far at least, leverages the best features of γPNA (i.e., solubility, affinity, unrestricted targeting) and the nanoparticle delivery platform (i.e., high delivered dose, non-toxic, biodistribution, etc.) to construct a clinically exciting technology.

1.9   Conclusions

The above sections highlight the tremendous >25-year effort spent in developing PNA into a powerful tool for genetic manipulation. Over this time, the PNA water solubility problem has been solved through hydrophilic group incorporation. Yet, when considering "naked" probes, the cell-delivery and cell-internalization problem is not completely solved. There are several examples of effective delivery to be sure, however the exact internalization pathways and intracellular biomolecule associations (especially

if the probes contain charged groups) that lead to PNA bioactivity are still unclear. Further, in hopes of developing a truly impactful PNA-based pharmacology, additional focus on PNA biodistribution and toxicity are needed. Lastly, additional focus should be placed on selectivity of binding, and not just affinity, especially as we enter the realm of irreversible gene-editing technologies. Lessons from the recent progress in building ultra-specific DNA hybridization technologies may become quite relevant as we look to build precise PNA materials.[106]

As we learn increasingly more about the various internal structures and UTR modifications RNA employs for regulation/function, new targets become apparent. To this end, further development and continued application of high affinity backbone/base modified PNAs is warranted against various RNA structures and sequences. Additionally, the synthesis of different PNA monomers with different displayed stereochemistry and/or functionalization hinders their broad use and limits modified PNA studies to a handful of labs across the world. Therefore, building "modular" backbones that can easily functionalized, where the exact pendant group used depends on the downstream application, may also accelerate wide spread use of backbone modified PNAs. To this end, placing orthogonal chemistry functional groups, such as azide-alkyne "click", in key backbone positions will likely lower the barrier to use.

1.10 Research overview

Cell-free reversible translation control through toehold-mediated γPNA strand displacement is demonstrated in chapter 2. In addition to achieving control over the translation state of a reporter gene, we also developed a surface plasmon resonance (SPR)

method to measure the displacement reaction. In chapter 3, we aimed to leverage additional properties of γPNA to dictate the strand displacement reaction; specifically, we constructed helical chimeric probes that contained complementary left- and right-handed domains. With the chimeric probe set we demonstrate helical-dependent (orthogonal) displacement using our SPR method. Chapter 4 presents our efforts to improve γPNA selectivity through incorporating intramolecular structure into the antisense probe. We investigate γPNA binding discrimination on the SPR and in a cell-free context. In short, we observe enhanced binding selectivity and detail how mutational type and placement effects the kinetic discrimination of the structured γPNA. Chapter 5 provides an improved example of γPNA-mediated strand displacement measured by SPR. Lastly, chapter 5 gives potential forward direction of the strand displacement system.

1.11 References

1.   Nielsen, P. E.; Egholm, M.; Berg, R. H.; Buchardt, O., Sequence-selective recognition of DNA by strand displacement with a thymine-substituted polyamide. *Science* **1991,** *254* (5037), 1497-500.

2.   Nielsen, P. E.; Egholm, M.; Buchardt, O., Sequence-specific transcription arrest by peptide nucleic acid bound to the DNA template strand. *Gene* **1994,** *149* (1), 139-45.

3.   Hanvey, J. C.; Peffer, N. J.; Bisi, J. E.; Thomson, S. A.; Cadilla, R.; Josey, J. A.; Ricca, D. J.; Hassman, C. F.; Bonham, M. A.; Au, K. G.; et al., Antisense and antigene properties of peptide nucleic acids. *Science* **1992,** *258* (5087), 1481-5.

4.   Nielsen, P. E., Peptide nucleic acid (PNA): A lead for gene therapeutic drugs. *Perspect Drug Discovery* **1996,** *4*, 76-84.

5.   Koppelhus, U.; Nielsen, P. E., Cellular delivery of peptide nucleic acid (PNA). *Adancedv Drug Deliver Reviews* **2003,** *55* (2), 267-280.

6.   Mateo-Marti, E.; Pradier, C. M., A Novel Type of Nucleic Acid-based Biosensors: the Use of PNA Probes, Associated with Surface Science and Electrochemical Detection Techniques. *Intelligent and Biosensors* **2010**, 323-344.

7.   Paulasova, P.; Pellestor, F., The peptide nucleic acids (PNAs): a new generation of probes for genetic and cytogenetic analyses. *Annales De Genetique* **2004,** *47* (4), 349-358.

8.   Lusvarghi, S.; Murphy, C. T.; Roy, S.; Tanious, F. A.; Sacui, I.; Wilson, W. D.; Ly, D. H.; Armitage, B. A., Loop and backbone modifications of peptide nucleic acid improve g-quadruplex binding selectivity. *Journal of the American Chemical Society* **2009,** *131* (51), 18415-24.

9.   Demidov, V. V.; Potaman, V. N.; Frank-Kamenetskii, M. D.; Egholm, M.; Buchard, O.; Sonnichsen, S. H.; Nielsen, P. E., Stability of peptide nucleic acids in human serum and cellular extracts. *Biochemical Pharmacology* **1994,** *48* (6), 1310-3.

10.   Manicardi, A.; Corradini, R., Effect of chirality in gamma-PNA: PNA interaction, another piece in the picture. *Artifical DNA PNA XNA* **2014,** *5* (3), e1131801.

11.   Egholm, M.; Buchardt, O.; Nielsen, P. E.; Berg, R. H., Peptide Nucleic-Acids (Pna) - Oligonucleotide Analogs with an Achiral Peptide Backbone. *Journal of the American Chemical Society* **1992,** *114* (5), 1895-1897.

12.   Haaima, G.; Lohse, A.; Buchardt, O.; Nielsen, P. E., Peptide nucleic acids (PNAs) containing thymine monomers derived from chiral amino acids: Hybridization and solubility properties of D-lysine PNA. *Angewandte Chemie-Internation Edition* **1996,** *35* (17), 1939-1942.

13.   Menchise, V.; De Simone, G.; Tedeschi, T.; Corradini, R.; Sforza, S.; Marchelli, R.; Capasso, D.; Saviano, M.; Pedone, C., Insights into peptide nucleic acid (PNA) structural features: The crystal structure of a D-lysine-based chiral PNA-DNA duplex. *Proceedings of the Natational Academy of Sciences USA* **2003,** *100* (21), 12021-12026.

14.   Boyarskaya, N. P.; Kirillova, Y. G.; Stotland, E. A.; Prokhorov, D. I.; Zvonkova, E. N.; Shvets, V. I., Synthesis of two new thymine-containing negatively charged PNA monomers. *Doklady Chemistry* **2006,** *408*, 57-60.

15.   Peyman, A.; Uhlmann, E.; Wagner, K.; Augustin, S.; Breipohl, G.; Will, D. W.; Schafer, A.; Wallmeier, H., Phosphonic ester nucleic acids (PHONAs): Oligonucleotide

analogues with an achiral phosphonic acid ester backbone. *Angewandte Chemie-International Edition in English* **1996,** *35* (22), 2636-2638.

16.   Efimov, V. A.; Choob, M. V.; Buryakova, A. A.; Kalinkina, A. L.; Chakhmakhcheva, O. G., Synthesis and evaluation of some properties of chimeric oligomers containing PNA and phosphono-PNA residues. *Nucleic Acids Research* **1998,** *26* (2), 566-575.

17.   Tilani, N.; De Costa, S.; Heemstra, J. M., Evaluating the Effect of Ionic Strength on Duplex Stability for PNA Having Negatively or Positively Charged Side Chains. *Plos One* **2013,** *8* (3).

18.   Webster, R.; Elliott, V.; Park, B. K.; Walker, D.; Hankin, M.; Taupin, P., PEG and PEG conjugates toxicity: towards an understanding of the toxicity of PEG and its relevance to PEGylated biologicals. *Milestones Drug Therapy* **2009**, 127-146.

19.   Cattani-Scholz, A.; Pedone, D.; Blobner, F.; Abstreiter, G.; Schwartz, J.; Tornow, M.; Andruzzi, L., PNA-PEG modified silicon platforms as functional bio-interfaces for applications in DNA microarrays and biosensors. *Biomacromolecules* **2009,** *10* (3), 489-96.

20.   Morin, T. J.; Shropshire, T.; Liu, X.; Briggs, K.; Huynh, C.; Tabard-Cossa, V.; Wang, H.; Dunbar, W. B., Nanopore-Based Target Sequence Detection. *PLoS One* **2016,** *11* (5), e0154426.

21.   Bonora, G. M.; Drioli, S.; Ballico, M.; Faccini, A.; Corradini, R.; Cogoi, S.; Xodo, L., PNA conjugated to high-molecular weight poly(ethylene glycol): synthesis and properties. *Nucleosides Nucleotides Nucleic Acids* **2007,** *26* (6-7), 661-4.

22.   Dragulescu-Andrasi, A.; Rapireddy, S.; Frezza, B. M.; Gayathri, C.; Gil, R. R.; Ly, D. H., A simple gamma-backbone modification preorganizes peptide nucleic acid into a helical structure. *Journal of the American Chemical Society* **2006,** *128* (31), 10258-67.

23.   Sahu, B.; Sacui, I.; Rapireddy, S.; Zanotti, K. J.; Bahal, R.; Armitage, B. A.; Ly, D. H., Synthesis and characterization of conformationally preorganized, (R)-diethylene glycol-containing gamma-peptide nucleic acids with superior hybridization properties and water solubility. *Journal Organic Chemistry* **2011,** *76* (14), 5614-27.

24.   Gupta, A.; Bahal, R.; Gupta, M.; Glazer, P. M.; Saltzman, W. M., Nanotechnology for delivery of peptide nucleic acids (PNAs). *Journal of Controlled Release* **2016,** *240*, 302-311.

25.   Yeh, J. I.; Shivachev, B.; Rapireddy, S.; Crawford, M. J.; Gil, R. R.; Du, S. C.; Madrid, M.; Ly, D. H., Crystal Structure of Chiral gamma PNA with Complementary DNA Strand: Insights into the Stability and Specificity of Recognition and Conformational Preorganization. *Journal of the American Chemical Society* **2010,** *132* (31), 10717-10727.

26.   Sacui, J.; Hsieh, W. C.; Manna, A.; Sahu, B.; Ly, D. H., Gamma Peptide Nucleic Acids: As Orthogonal Nucleic Acid Recognition Codes for Organizing Molecular Self-Assembly. *Journal of the American Chemical Society* **2015,** *137* (26), 8603-8610.

27.   Chang, D.; Lindberg, E.; Winssinger, N., Critical Analysis of Rate Constants and Turnover Frequency in Nucleic Acid-Templated Reactions: Reaching Terminal Velocity. *Journal of the American Chemical Society* **2017,** *139* (4), 1444-1447.

28.   Englund, E. A.; Xu, Q.; Witschi, M. A.; Appella, D. H., PNA-DNA duplexes, triplexes, and quadruplexes are stabilized with trans-cyclopentane units. *Journal of the American Chemical Society* **2006,** *128* (51), 16456-16457.

29.   Vilaivan, T.; Srisuwannaket, C., Hybridization of pyrrolidinyl peptide nucleic acids and DNA: Selectivity, base-pairing specificity, and direction of binding. *Organic Letters* **2006,** *8* (9), 1897-1900.

30.   Nielsen, P. E., Peptide nucleic acids (PNA) in chemical biology and drug discovery. *Chemistry & Biodiversity* **2010,** *7* (4), 786-804.

31.   Zhao, C.; Hoppe, T.; Setty, M. K. H. G.; Murray, D.; Chun, T. W.; Hewlett, I.; Appella, D. H., Quantification of plasma HIV RNA using chemically engineered peptide nucleic acids. *Nature Communications* **2014,** *5*.

32.   Jampasa, S.; Wonsawat, W.; Rodthongkum, N.; Siangproh, W.; Yanatatsaneejit, P.; Vilaivan, T.; Chailapakul, O., Electrochemical detection of human papillomavirus DNA type 16 using a pyrrolidinyl peptide nucleic acid probe immobilized on screen-printed carbon electrodes. *Biosensors & Bioelectronics* **2014,** *54*, 428-434.

33.   Petersen, K. H.; Jensen, D. K.; Egholm, M.; Nielsen, P. E.; Buchardt, O., A Pna-DNA Linker Synthesis of N-((4,4'-Dimethoxytrityloxy)Ethyl)-N-(Thymin-1-Ylacetyl)Glycine. *Bioorganic & Medical Chemistry Letters* **1995,** *5* (11), 1119-1124.

34.   Bergmann, F.; Bannwarth, W.; Tam, S., Solid-Phase Synthesis of Directly Linked Pna-DNA-Hybrids. *Tetrahedron Lett* **1995,** *36* (38), 6823-6826.

35.   Finn, P. J.; Gibson, N. J.; Fallon, R.; Hamilton, A.; Brown, T., Synthesis and properties of DNA-PNA chimeric oligomers. *Nucleic Acids Research* **1996,** *24* (17), 3357-3363.

36.   Juliano, R. L.; Ming, X.; Nakagawa, O., Cellular Uptake and Intracellular Trafficking of Antisense and siRNA Oligonucleotides. *Bioconjugate Chemistry* **2012,** *23* (2), 147-157.

37.   Crooke, S. T.; Wang, S.; Vickers, T. A.; Shen, W.; Liang, X. H., Cellular uptake and trafficking of antisense oligonucleotides. *Nature Biotechnology* **2017,** *35* (3), 230-237.

38.   Khvorova, A.; Watts, J. K., The chemical evolution of oligonucleotide therapies of clinical utility. *Nature Biotechnology* **2017,** *35* (3), 238-248.

39.   Hamzavi, R.; Dolle, F.; Tavitian, B.; Dahl, O.; Nielsen, P. E., Modulation of the pharmacokinetic properties of PNA: Preparation of galactosyl, mannosyl, fucosyl, N-acetylgalactosaminyl, and N-acetylglucosaminyl derivatives of aminoethylglycine peptide nucleic acid monomers and their incorporation into PNA oligomers. *Bioconjugate Chemistry* **2003,** *14* (5), 941-954.

40.   De Rosa, G.; La Rotonda, M. I., Nano and microtechnologies for the delivery of oligonucleotides with gene silencing properties. *Molecules* **2009,** *14* (8), 2801-23.

41.   Kaihatsu, K.; Janowski, B. A.; Corey, D. R., Recognition of chromosomal DNA by PNAs. *Chemistry & Biology* **2004,** *11* (6), 749-758.

42.   Hamilton, S. E.; Simmons, C. G.; Kathiriya, I. S.; Corey, D. R., Cellular delivery of peptide nucleic acids and inhibition of human telomerase. *Chemical Biology* **1999,** *6* (6), 343-51.

43.   Turner, J. J.; Ivanova, G. D.; Verbeure, B.; Williams, D.; Arzumanov, A. A.; Abes, S.; Lebleu, B.; Gait, M. J., Cell-penetrating peptide conjugates of peptide nucleic

acids (PNA) as inhibitors of HIV-1 Tat-dependent trans-activation in cells. *Nucleic Acids Research* **2005,** *33* (21), 6837-6849.

44.   Abes, S.; Turner, J. J.; Ivanova, G. D.; Owen, D.; Williams, D.; Arzumanov, A.; Clair, P.; Gait, M. J.; Lebleu, B., Efficient splicing correction by PNA conjugation to an R6-Penetratin delivery peptide (vol 35, pg 4495, 2007). *Nucleic Acids Research* **2007,** *35* (21), 7396-7396.

45.   Koppelhus, U.; Awasthi, S. K.; Zachar, V.; Holst, H. U.; Ebbesen, P.; Nielsen, P. E., Cell-dependent differential cellular uptake of PNA, peptides, and PNA-peptide conjugates. *Antisense Nucleic Acid Drug Develiry* **2002,** *12* (2), 51-63.

46.   Ljungstrom, T.; Knudsen, H.; Nielsen, P. E., Cellular uptake of adamantyl conjugated peptide nucleic acids. *Bioconjugate Chemistry* **1999,** *10* (6), 965-972.

47.   Bendifallah, N.; Rasmussen, F. W.; Zachar, V.; Ebbesen, P.; Nielsen, P. E.; Koppelhus, U., Evaluation of cell-penetrating peptides (CPPs) as vehicles for intracellular delivery of antisense peptide nucleic acid (PNA). *Bioconjugate Chemistry* **2006,** *17* (3), 750-758.

48.   Maier, M. A.; Esau, C. C.; Siwkowski, A. M.; Wancewicz, E. V.; Albertshofer, K.; Kinberger, G. A.; Kadaba, N. S.; Watanabe, T.; Manoharan, M.; Bennett, C. F.; Griffey, R. H.; Swayze, E. E., Evaluation of basic amphipathic peptides for cellular delivery of antisense peptide nucleic acids. *Journal of Medicinal Chemistry* **2006,** *49* (8), 2534-42.

49.   Shiraishi, T.; Bendifallah, N.; Nielsen, P. E., Cellular delivery of polyheteroaromate-peptide nucleic acid conjugates mediated by cationic lipids. *Bioconjugate Chemistry* **2006,** *17* (1), 189-94.

50.   Shiraishi, T.; Nielsen, P. E., Nanomolar cellular antisense activity of peptide nucleic acid (PNA) cholic acid ("umbrella") and cholesterol conjugates delivered by cationic lipids. *Bioconjugate Chemistry* **2012,** *23* (2), 196-202.

51.   Koppelhus, U.; Shiraishi, T.; Zachar, V.; Pankratova, S.; Nielsen, P. E., Improved cellular activity of antisense peptide nucleic acids by conjugation to a cationic peptide-lipid (CatLip) domain. *Bioconjugate Chemistry* **2008,** *19* (8), 1526-34.

52.   Zhou, P.; Wang, M.; Du, L.; Fisher, G. W.; Waggoner, A.; Ly, D. H., Novel binding and efficient cellular uptake of guanidine-based peptide nucleic acids (GPNA). *Journal of the American Chemical Society* **2003,** *125* (23), 6878-9.

53.   Zhou, P.; Dragulescu-Andrasi, A.; Bhattacharya, B.; O'Keefe, H.; Vatta, P.; Hyldig-Nielsen, J. J.; Ly, D. H., Synthesis of cell-permeable peptide nucleic acids and characterization of their hybridization and uptake properties. *Bioorganic & Medicinal Chemistry Letters* **2006,** *16* (18), 4931-4935.

54.   Sahu, B.; Chenna, V.; Lathrop, K. L.; Thomas, S. M.; Zon, G.; Livak, K. J.; Ly, D. H., Synthesis of conformationally preorganized and cell-permeable guanidine-based gamma-peptide nucleic acids (gammaGPNAs). *Journal of Organic Chemistry* **2009,** *74* (4), 1509-16.

55.   Dragulescu-Andrasi, A.; Zhou, P.; He, G.; Ly, D. H., Cell-permeable GPNA with appropriate backbone stereochemistry and spacing binds sequence-specifically to RNA. *Chemical Communications (Camb)* **2005,** (2), 244-6.

56.   Zhou, P.; Dragulescu-Andrasi, A.; Bhattacharya, B.; O'Keefe, H.; Vatta, P.; Hyldig-Nielsen, J. J.; Ly, D. H., Synthesis of cell-permeable peptide nucleic acids and

characterization of their hybridization and uptake properties. *Bioorganic & Medicinal Chemistry Letters* **2006,** *16* (18), 4931-5.

57.   Lundin, P.; Johansson, H.; Guterstam, P.; Holm, T.; Hansen, M.; Langel, U.; S, E. L. A., Distinct uptake routes of cell-penetrating peptide conjugates. *Bioconjugate Chemistry* **2008,** *19* (12), 2535-42.

58.   Shiraishi, T.; Nielsen, P. E., Enhanced delivery of cell-penetrating peptide-peptide nucleic acid conjugates by endosomal disruption. *Nature Protocols* **2006,** *1* (2), 633-636.

59.   Erazo-Oliveras, A.; Muthukrishnan, N.; Baker, R.; Wang, T. Y.; Pellois, J. P., Improving the endosomal escape of cell-penetrating peptides and their cargos: strategies and challenges. *Pharmaceuticals (Basel)* **2012,** *5* (11), 1177-209.

60.   El-Andaloussi, S.; Johansson, H. J.; Lundberg, P.; Langel, U., Induction of splice correction by cell-penetrating peptide nucleic acids. *Journal of Gene Medicine* **2006,** *8* (10), 1262-1273.

61.   Shiraishi, T.; Pankratova, S.; Nielsen, P. E., Calcium ions effectively enhance the effect of antisense peptide nucleic acids conjugated to cationic tat and oligoarginine peptides. *Chemical Biology* **2005,** *12* (8), 923-9.

62.   Kaihatsu, K.; Huffman, K. E.; Corey, D. R., Intracellular uptake and inhibition of gene expression by PNAs and PNA-peptide conjugates. *Biochemistry* **2004,** *43* (45), 14340-14347.

63.   Shiraishi, T.; Nielsen, P. E., Photochemically enhanced cellular delivery of cell penetrating peptide-PNA conjugates. *FEBS Letters* **2006,** *580* (5), 1451-6.

64.   Berthold, P. R.; Shiraishi, T.; Nielsen, P. E., Cellular delivery and antisense effects of peptide nucleic acid conjugated to polyethyleneimine via disulfide linkers. *Bioconjugate Chemistry* **2010,** *21* (10), 1933-8.

65.   Lonn, P.; Kacsinta, A. D.; Cui, X. S.; Hamil, A. S.; Kaulich, M.; Gogoi, K.; Dowdy, S. F., Enhancing Endosomal Escape for Intracellular Delivery of Macromolecular Biologic Therapeutics. *Scientific Reports* **2016,** *6*.

66.   Grover, A.; Schmidt, B. F.; Salter, R. D.; Watkins, S. C.; Waggoner, A. S.; Bruchez, M. P., Genetically Encoded pH Sensor for Tracking Surface Proteins through Endocytosis. *Angewandte Chemie-International Edition* **2012,** *51* (20), 4838-4842.

67.   Vickers, T. A.; Griffith, M. C.; Ramasamy, K.; Risen, L. M.; Freier, S. M., Inhibition of NF-kappa B specific transcriptional activation by PNA strand invasion. *Nucleic Acids Research* **1995,** *23* (15), 3003-8.

68.   Larsen, H. J.; Nielsen, P. E., Transcription-mediated binding of peptide nucleic acid (PNA) to double-stranded DNA: sequence-specific suicide transcription. *Nucleic Acids Research* **1996,** *24* (3), 458-63.

69.   Janowski, B. A.; Kaihatsu, K.; Huffman, K. E.; Schwartz, J. C.; Ram, R.; Hardy, D.; Mendelson, C. R.; Corey, D. R., Inhibiting transcription of chromosomal DNA with antigene peptide nucleic acids. *Nature Chemical Biology* **2005,** *1* (4), 210-215.

70.   Hu, J. X.; Corey, D. R., Inhibiting gene expression with peptide nucleic acid (PNA)-peptide conjugates that target chromosomal DNA. *Biochemistry* **2007,** *46* (25), 7581-7589.

71.   Bahal, R.; Sahu, B.; Rapireddy, S.; Lee, C. M.; Ly, D. H., Sequence-Unrestricted, Watson-Crick Recognition of Double Helical B-DNA by (R)-MiniPEG-γPNAs. *Chembiochem* **2012,** *13* (1), 56-60.

72.   Rapireddy, S.; Bahal, R.; Ly, D. H., Strand invasion of mixed-sequence, double-helical B-DNA by gamma-peptide nucleic acids containing G-clamp nucleobases under physiological conditions. *Biochemistry* **2011,** *50* (19), 3913-8.

73.   Demidov, V. V.; Yavnilovich, M. V.; Belotserkovskii, B. P.; Frank-Kamenetskii, M. D.; Nielsen, P. E., Kinetics and mechanism of polyamide ("peptide") nucleic acid binding to duplex DNA. *Proceedings of the National Academy of Sciences of the United States of America* **1995,** *92* (7), 2637-41.

74.   Bentin, T.; Nielsen, P. E., Superior duplex DNA strand invasion by acridine conjugated peptide nucleic acids. *Journal of the American Chemical Society* **2003,** *125* (21), 6378-6379.

75.   Rapireddy, S.; He, G.; Roy, S.; Armitage, B. A.; Ly, D. H., Strand invasion of mixed-sequence B-DNA by acridine-linked, gamma-peptide nucleic acid (gamma-PNA). *Journal of the American Chemical Society* **2007,** *129* (50), 15596-15600.

76.   Bentin, T.; Nielsen, P. E., Superior duplex DNA strand invasion by acridine conjugated peptide nucleic acids. *Journal of the American Chemical Society* **2003,** *125* (21), 6378-9.

77.   Nielsen, P. E.; Egholm, M., An introduction to peptide nucleic acid. *Current Issues in Molecular Biology* **1999,** *1* (1-2), 89-104.

78.   Doyle, D. F.; Braasch, D. A.; Simmons, C. G.; Janowski, B. A.; Corey, D. R., Inhibition of gene expression inside cells by peptide nucleic acids: effect of mRNA target sequence, mismatched bases, and PNA length. *Biochemistry* **2001,** *40* (1), 53-64.

79.   Dragulescu-Andrasi, A.; Rapireddy, S.; He, G.; Bhattacharya, B.; Hyldig-Nielsen, J. J.; Zon, G.; Ly, D. H., Cell-permeable peptide nucleic acid designed to bind to the 5'-untranslated region of E-cadherin transcript induces potent and sequence-specific antisense effects. *Journal of the American Chemical Society* **2006,** *128* (50), 16104-12.

80.   Canady, T. D.; Telmer, C. A.; Oyaghire, S. N.; Armitage, B. A.; Bruchez, M. P., In Vitro Reversible Translation Control Using gamma PNA Probes. *Journal of the American Chemical Society* **2015,** *137* (32), 10268-10275.

81.   Fraser, G. L.; Holmgren, J.; Clarke, P. B.; Wahlestedt, C., Antisense inhibition of delta-opioid receptor gene function in vivo by peptide nucleic acids. *Molecular Pharmacology* **2000,** *57* (4), 725-31.

82.   Chiarantini, L.; Cerasi, A.; Fraternale, A.; Andreoni, F.; Scari, S.; Giovine, M.; Clavarino, E.; Magnani, M., Inhibition of macrophage iNOS by selective targeting of antisense PNA. *Biochemistry* **2002,** *41* (26), 8471-7.

83.   Dryselius, R.; Aswasti, S. K.; Rajarao, G. K.; Nielsen, P. E.; Good, L., The translation start codon region is sensitive to antisense PNA inhibition in Escherichia coli. *Oligonucleotides* **2003,** *13* (6), 427-433.

84.   Kozak, M., Initiation of translation in prokaryotes and eukaryotes. *Gene* **1999,** *234* (2), 187-208.

85.   Delgado, E.; Bahal, R.; Yang, J.; Lee, J. M.; Ly, D. H.; Monga, S. P., beta-Catenin knockdown in liver tumor cells by a cell permeable gamma guanidine-based peptide nucleic acid. *Current Cancer Drug Targets* **2013,** *13* (8), 867-78.

86.   Bahal, R.; McNeer, N. A.; Ly, D. H.; Saltzman, W. M.; Glazer, P. M., Nanoparticle for delivery of antisense gammaPNA oligomers targeting CCR5. *Artifical DNA PNA XNA* **2013,** *4* (2), 49-57.

87.   Hu, J.; Matsui, M.; Gagnon, K. T.; Schwartz, J. C.; Gabillet, S.; Arar, K.; Wu, J.; Bezprozvanny, I.; Corey, D. R., Allele-specific silencing of mutant huntingtin and ataxin-3 genes by targeting expanded CAG repeats in mRNAs. *Nature Biotechnology* **2009,** *27* (5), 478-84.

88.   Endoh, T.; Hnedzko, D.; Rozners, E.; Sugimoto, N., Nucleobase-Modified PNA Suppresses Translation by Forming a Triple Helix with a Hairpin Structure in mRNA In Vitro and in Cells. *Angewandte Chemie-International Edition* **2016,** *55* (3), 899-903.

89.   Xia, X.; Piao, X. J.; Bong, D., Bifacial Peptide Nucleic Acid as an Allosteric Switch for Aptamer and Ribozyme Function. *Journal of the American Chemical Society* **2014,** *136* (20), 7265-7268.

90.   Cheng, C. J.; Bahal, R.; Babar, I. A.; Pincus, Z.; Barrera, F.; Liu, C.; Svoronos, A.; Braddock, D. T.; Glazer, P. M.; Engelman, D. M.; Saltzman, W. M.; Slack, F. J., MicroRNA silencing for cancer therapy targeted to the tumour microenvironment. *Nature* **2015,** *518* (7537), 107-10.

91.   Manicardi, A.; Fabbri, E.; Tedeschi, T.; Sforza, S.; Bianchi, N.; Brognara, E.; Gambari, R.; Marchelli, R.; Corradini, R., Cellular uptakes, biostabilities and anti-miR-210 activities of chiral arginine-PNAs in leukaemic K562 cells. *Chembiochem* **2012,** *13* (9), 1327-37.

92.   Karras, J. G.; Maier, M. A.; Lu, T.; Watt, A.; Manoharan, M., Peptide nucleic acids are potent modulators of endogenous pre-mRNA splicing of the murine interleukin-5 receptor-alpha chain. *Biochemistry* **2001,** *40* (26), 7853-9.

93.   Sazani, P.; Gemignani, F.; Kang, S. H.; Maier, M. A.; Manoharan, M.; Persmark, M.; Bortner, D.; Kole, R., Systemically delivered antisense oligomers upregulate gene expression in mouse tissues. *Nature Biotechnology* **2002,** *20* (12), 1228-33.

94.   Aartsma-Rus, A.; Kaman, W. E.; Bremmer-Bout, M.; Janson, A. A. M.; den Dunnen, J. T.; van Ommen, G. J. B.; van Deutekom, J. C. T., Comparative analysis of antisense oligonucleotide analogs for targeted DMD exon 46 skipping in muscle cells. *Gene Therapy* **2004,** *11* (18), 1391-1398.

95.   Ivanova, G. D.; Arzumanov, A.; Abes, R.; Yin, H.; Wood, M. J.; Lebleu, B.; Gait, M. J., Improved cell-penetrating peptide-PNA conjugates for splicing redirection in HeLa cells and exon skipping in mdx mouse muscle. *Nucleic Acids Research* **2008,** *36* (20), 6418-28.

96.   Yin, H.; Lu, Q.; Wood, M., Effective exon skipping and restoration of dystrophin expression by peptide nucleic acid antisense oligonucleotides in mdx mice. *Molecular Therapy* **2008,** *16* (1), 38-45.

97.   Yin, H.; Betts, C.; Saleh, A. F.; Ivanova, G. D.; Lee, H.; Seow, Y.; Kim, D.; Gait, M. J.; Wood, M. J., Optimization of peptide nucleic acid antisense oligonucleotides for local and systemic dystrophin splice correction in the mdx mouse. *Molecular Therapy* **2010,** *18* (4), 819-27.

98.   Wancewicz, E. V.; Maier, M. A.; Siwkowski, A. M.; Albertshofer, K.; Winger, T. M.; Berdeja, A.; Gaus, H.; Vickers, T. A.; Bennett, C. F.; Monia, B. P.; Griffey, R. H.; Nulf, C. J.; Hu, J. X.; Corey, D. R.; Swayze, E. E.; Kinberger, G. A., Peptide Nucleic Acids Conjugated to Short Basic Peptides Show Improved Pharmacokinetics and Antisense Activity in Adipose Tissue. *Journal of Medicinal Chemistry* **2010,** *53* (10), 3919-3926.

99.   Havre, P. A.; Gunther, E. J.; Gasparro, F. P.; Glazer, P. M., Targeted Mutagenesis of DNA Using Triple Helix-Forming Oligonucleotides Linked to Psoralen *Proceedings of the National Academy of Sciences of the United States of America* **1993,** *90* (16), 7879-7883.

100.   Wang, G.; Levy, D. D.; Seidman, M. M.; Glazer, P. M., Targeted Mutagenesis in Mammalian-Cells Mediated by Intracellular Triple-Helix Formation - a New Approach to Gene-Therapy. *Journal of Cellular Biochemistry* **1995**, 386-386.

101.   Faruqi, A. F.; Egholm, M.; Glazer, P. M., Peptide nucleic acid-targeted mutagenesis of a chromosomal gene in mouse cells. *Proceedings of the National Academy of Sciences of the United States of America* **1998,** *95* (4), 1398-1403.

102.   Faruqi, A. F.; Datta, H. J.; Carroll, D.; Seidman, M. M.; Glazer, P. M., Triple-helix formation induces recombination in mammalian cells via a nucleotide excision repair-dependent pathway. *Molecular Cell Biology* **2000,** *20* (3), 990-1000.

103.   Datta, H. J.; Chan, P. P.; Vasquez, K. M.; Gupta, R. C.; Glazer, P. M., Triplex-induced recombination in human cell-free extracts - Dependence on XPA and HsRad51. *Journal of Biological Chemistry* **2001,** *276* (21), 18018-18023.

104.   McNeer, N. A.; Anandalingam, K.; Fields, R. J.; Caputo, C.; Kopic, S.; Gupta, A.; Quijano, E.; Polikoff, L.; Kong, Y.; Bahal, R.; Geibel, J. P.; Glazer, P. M.; Saltzman, W. M.; Egan, M. E., Nanoparticles that deliver triplex-forming peptide nucleic acid molecules correct F508del CFTR in airway epithelium. *Nature Communications* **2015,** *6*.

105.   Bahal, R.; McNeer, N. A.; Quijano, E.; Liu, Y. F.; Sulkowski, P.; Turchick, A.; Lu, Y. C.; Bhunia, D. C.; Manna, A.; Greiner, D. L.; Brehm, M. A.; Cheng, C. J.; Lopez-Giraldez, F.; Ricciardi, A.; Beloor, J.; Krause, D. S.; Kumar, P.; Gallagher, P. G.; Braddock, D. T.; Saltzman, W. M.; Ly, D. H.; Glazer, P. M., In vivo correction of anaemia in beta-thalassemic mice by gamma PNA-mediated gene editing with nanoparticle delivery. *Nature Communications* **2016,** *7*.

106.   Zhang, D. Y.; Chen, S. X.; Yin, P., Optimizing the specificity of nucleic acid hybridization. *Nature Chemistry* **2012,** *4* (3), 208-214.

Chapter 2: In Vitro Reversible Translation Control Using γPNA Probes

2.1 Eukaryotic translation overview

Controlling gene expression ectopically through synthetic molecular tools is an intriguing and challenging prospect in chemical and synthetic biology.[1, 2] In this chapter, we demonstrate translation control with complementary oligonucleotides. To fully appreciate the antisense tactic employed herein, it is important to summarize the translational initiation and scanning processes that lead to the assembly of a mature 80S ribosome on a gene transcript.

The first step in the eukaryotic initiation pathway begins with the assembly of the ternary complex (eIF2, GTP, and Met-tRNA$_i^{Met}$) and its subsequent interaction with the 40S subunit to form the 43S preinitiation complex (**Figure 2.1**).[3] The 43S complex then interacts with the mRNA in an ATP dependent manner by binding to the capped 5'-end. Here, we encounter our first antisense opportunity to inhibit the 43S subunit from binding to the 5' end of the untranslated region (UTR) via introduction of a complementary probe, a method that will be used in this project. After successful docking of the 43S small subunit, the second step in ribosomal assembly involves scanning and denaturing local secondary structure on the template in a 5' to 3' direction along the UTR. Two translation factors (eIF4A and eIF4F) have been indicated as ATP-dependent helicases capable of unwinding RNA folding to allow the 43S complex to continue scanning.[4] The scanning process completes when optimal binding interactions are established between the AUG start codon, the Met-tRNA$_i^{Met}$ anticodon, and the upstream Kozak initiation

sequence (ribosome binding sequence). Lastly, with the aid of eIF factors to recruit the

60S large subunit, the 80S mature ribosome complex forms on the transcript ready to

begin peptide elongation.
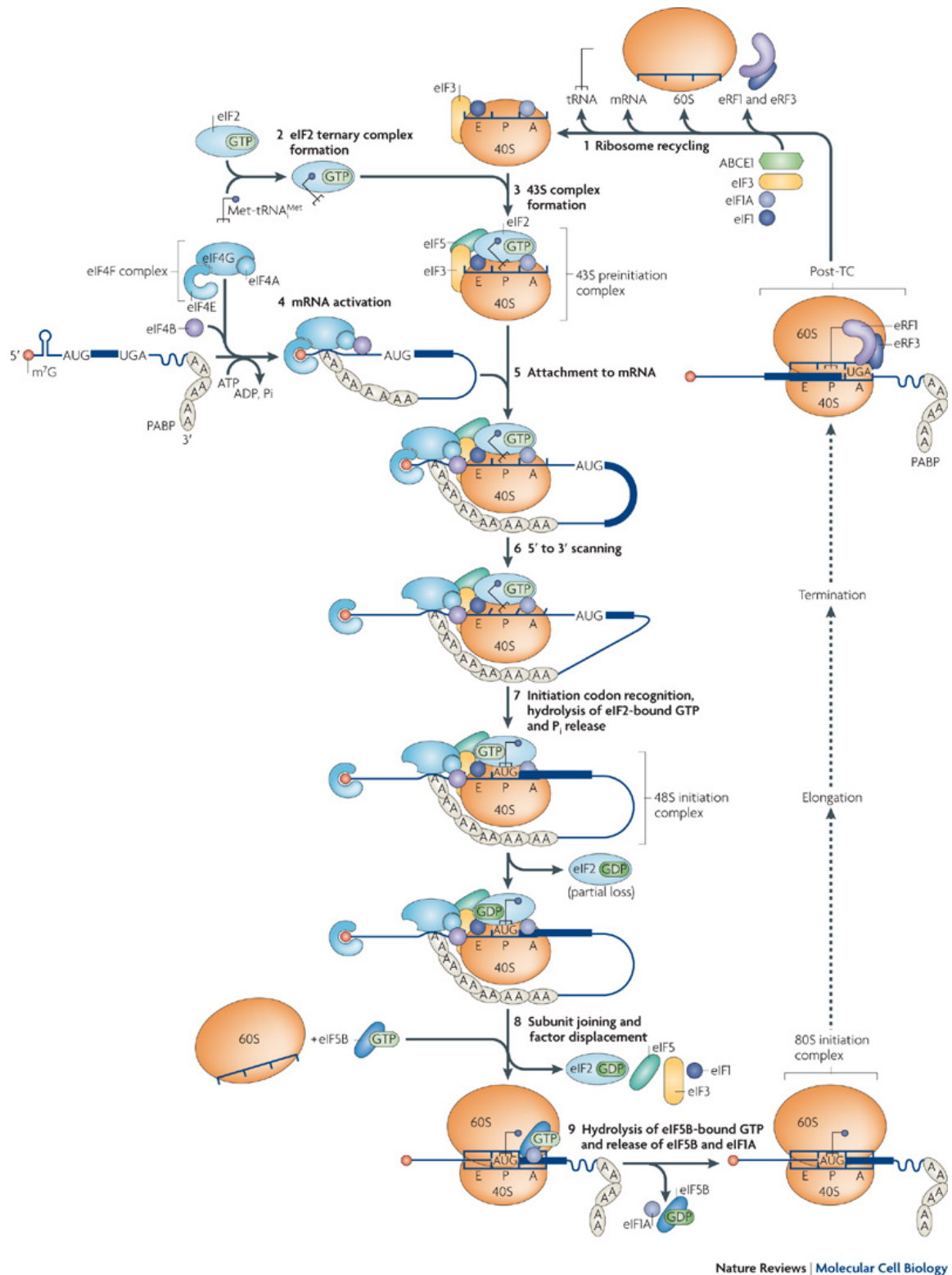
Figure 2.1 Overview of eukaryotic translation initiation pathway. Adapted from reference [5].

2.2 Introduction

Methods to irreversibly interfere with gene expression (e.g., antisense targeting of mRNA) are well-known chemical biology tools and potential therapeutic strategies.[6] Reversible regulation of gene expression offers the opportunity to perturb gene regulatory networks and signaling cascades. Through the use of a serial method of translation control, investigations related to the temporal and spatial effects of a specific transcript can be approached. Through the careful attention to chemical probe affinity and selectivity, control over protein expression is possible at the transcript level, which allows for the direct investigation at precise nodes in biochemical pathways. Importantly, achieving reversible control through the supply of an external probe can enable numerous interventions and manipulations of native genetic elements to assess or control downstream phenotypic effects. To this end, chemical probes can be introduced at precise time points, allowing for on-demand control of translation locally or systemically, depending on the method of probe delivery.

Synthetic translation regulation has been implemented through the utilization of various engineered mRNAs and antisense-probe manipulations. Facile examples of ligand-dependent (i.e. riboswitches[7]) protein expression, sequence optimization (ribosome binding site strength[8]), and direct expression knockdown through exogenous and endogenous probe hybridization[9] have provided a way to selectively (de)-activate target transcripts. Translation regulation through a strand displacement mechanism has also been realized. For example, through the careful design of toehold-driven RNA interactions, conditional RNAi mediated knockdown has been demonstrated.[10] Furthermore, the mRNA transcript itself has been engineered to display conditional

ribosome binding site (RBS) sequestration, whereupon translation is driven by a small non-coding RNA displacement reaction.[11] Using this approach, Green and coworkers recently reported improved transcript designs for higher-fold GFP activation and generalized the design to detect a much larger set of small RNA targets (triggers).[12] In terms of antisense reversible regulation, Young et al. suppressed gene expression knockdown and then subsequently re-activated it by manipulating a light-sensitive antisense agent that undergoes an intramolecular strand displacement reaction.[13] This work demonstrated the feasibility of light-defined control over reporter expression where reversibility was established through application of caged antisense probes. Nevertheless, achieving light-activated translation control is limited to a relatively small sensitized area and penetrance depth, thus precluding systemic translation control (i.e. whole animal). To achieve translation control in a systemic manner as well as limit any genetic manipulation of target transcripts, we designed a translation control system consisting of an antisense agent that inhibits translation but can be subsequently displaced from the mRNA target by a suitable complementary sense agent.

A probe that alters translation must display the requisite affinity, specificity, and solubility, and be amenable to cellular uptake to be successful in a range of applications. Peptide nucleic acids (PNA[14, 15]) provide high affinity complementary probes, with biological stability owing to the unnatural backbone configuration (**Figure 2.2**).
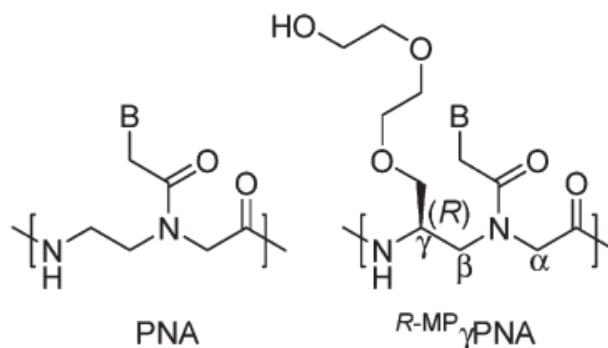
Figure 2.2 Chemical structures of PNA and γPNA (γ = *R*-miniPEG). Adapted from reference 16

The ability of PNA to interfere with gene expression has been well documented[17],
with examples including modulation of transcription[18-20], pre-mRNA splicing[21-23], mRNA
translation[24-27] and miRNA function[28, 29]. γPNA, a second generation analogue of PNA,[30]
exhibits enhanced target affinity and increased solubility compared to traditional PNA.[16]
These features arise from the fact that γ-modifications that introduce an appropriate
chirality to the PNA backbone induce right-handed helicity, presumably reducing the
entropic binding penalty to a complementary partner, and leading to enhanced target
affinity. Meanwhile, the diethylene glycol (miniPEG) substituent used in the current
work provides significantly improved water solubility to PNA. γPNA has shown
promising target selectivity with excellent mismatch discrimination,[16] and guanidinium-
modified γPNA has been shown to inhibit translation of mRNA within living cells.[31]
Moreover, γPNA-γPNA duplexes are significantly more stable than γPNA-RNA
heteroduplexes, meaning our proposed approach relies on a thermodynamically favorable
process.[32] Finally, PNA molecules are nuclease, protease, and peptidase resistant, which
makes them stable in biological milieu, such as the cell lysates we used in the following

in vitro translation experiments.[33] Herein, we demonstrate reversible translation control mediated through a γPNA-γPNA strand displacement process.

2.3   Results

Reversible translation control is achieved through two separate and fully complementary γPNA molecules. The first γPNA is required for direct mRNA target binding (antisense), which represses translation. The second (sense) γPNA de-represses translation through a γPNA-γPNA displacement interaction, mediated by a free toehold sequence on the first (antisense) γPNA strand (**Figure 2.3**).
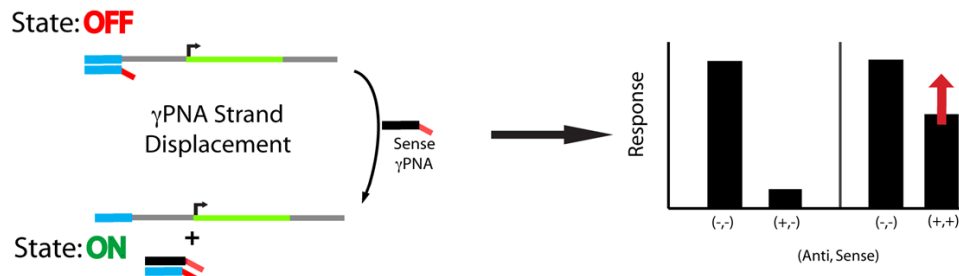
Figure 2.3 Reversible translational control through use of γPNA probes. State: OFF is established by the introduction of an antisense γPNA that binds to a partially cognate mRNA transcript, leaving the adjoining toehold domain free. With the introduction of sense γPNA, a subsequent γPNA-γPNA (toehold nucleation event) binding event initializes strand displacement, rendering the translation to State: ON. The subsequently altered luciferase expression can be plotted to measure the translation recovery (right illustration).

Reversible control of translation by base-pairing requires two functioning components: (i) a sequence-selective probe that suppresses translation effectively and (ii) an agent that can relieve this suppression. Previous antisense "gene walk" investigations with PNA established two effective native mRNA target sites[25, 34, 35] (*i*) the 5'-terminal

end of the mRNA and (*ii*) proximal to or at the Kozak initiation sequence and AUG start codon. Relative to eukaryotic translation, probe hybridization at the terminal end of the 5'-UTR is largely believed to attenuate translation by inhibiting the attachment of the 43S ribosomal pre-initiation complex to the transcript and thus blocking initiation of translation.[25, 35] When a probe is targeted to the Kozak/AUG region,[36] both ribosomal scanning of the 5'-UTR and subsequent translocation into the coding region is prevented.[5] The removal of the antisense block from the mRNA transcript via strand displacement from either site would release a fully functional native mRNA and allow translation to proceed.

2.3.1 Translation suppression by PNA and γPNA

To begin development of the translational switch, two unmodified 15-mer PNA probes were synthesized that were designed to bind to the abovementioned sites within a luciferase transcript. Both of the PNAs display IC_{50} values in the low nM range (**Figure 2.4A**), indicative of excellent in vitro targeting, while maintaining negligible activity towards an orthogonal 5'-UTR luciferase transcript that lacks the PNA target sites (**Figure 2.4B**). To improve target binding, analogous γPNA (γ = (R)-diethylene glycol, "miniPEG") oligomers were prepared. As mentioned above, γPNA has been demonstrated to exhibit favorable RNA duplex stability, while still maintaining target selectivity. Due to the higher thermodynamic stability of γPNA–RNA interactions, compared to PNA–RNA,[37] we synthesized two γPNAs (10-mer and 15-mer) targeting the 5' terminus of the mRNA (referred to as **γPNA₁₀** and **γPNA₁₅**). The luciferase mRNA target sequence and the γPNA sequences are given in **Table 2.1**.
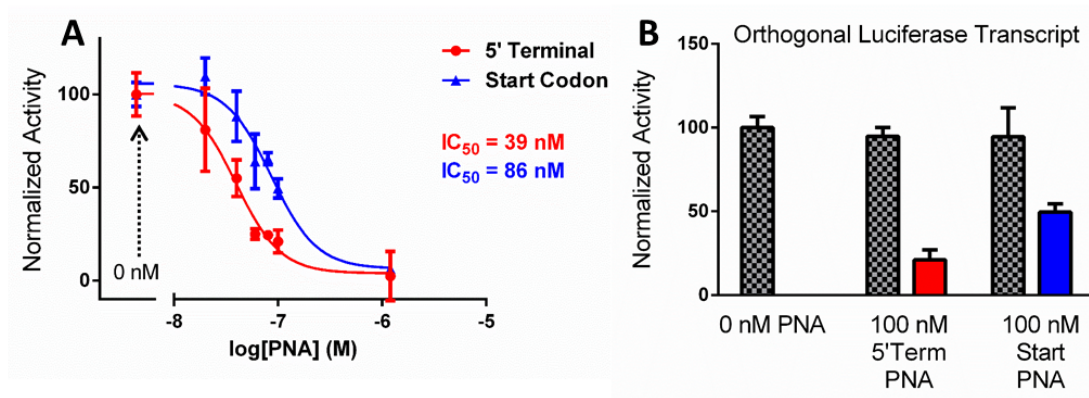
Figure 2.4 PNA (unmodified) antisense inhibition of luciferase. (**A.**) Antisense dose-response curves for both the 5'-Terminal and Start codon PNA probes (both tested at N=3) tested against the luciferase mRNA (10 nM). The PNA probe and mRNA were pre-annealed in a solution (37 $^{\circ}$C for 1 hour in RRL-matching concentration of 79 mM K^{+} and DEPC-treated H$_2$O) and then translated for 90 mins at 30 $^{\circ}$C. The given IC$_{50}$ values (mean average) represent the PNA concentration where a 50% reduction in luciferase activity is observed. (**B.**) A luciferase transcript with a 5'-UTR lacking PNA binding sites is not suppressed by the PNAs (checkered bars) as compared to the no PNA control (p >.05). Red and blue columns correspond to level of inhibition by each PNA for the specific target. The two PNAs, both tested at 100 nM, were incubated with 10 nM of the mRNA.

Table 2.1 The 5'-terminal mRNA target sequence is given. The γPNA sequences are written from the C-terminus to the N-terminus, "K" represents lysine. The 5'-end of the mRNA transcript is hybridized with the C-terminal end of the γPNA oligonucleotide. All monomers are γPNA.

mRNA Target	5´–AGACCCAAGCUUUCA–3´
γPNA$_{15}$	NH$_2$–K–TCTGGGTTCGAAAGT–H
γPNA$_{10}$	NH$_2$–K–TCTGGGTTCG–H

The antisense dose response relationship for both **γPNA$_{15}$** and **γPNA$_{10}$** probes against the luciferase reporter are presented in **Figure 2.5A**. Both probes gave low IC$_{50}$ values (<50 nM). Furthermore, a dose of 100 nM γPNA gave >85% gene knockdown for

both cases. Unexpectedly, the two γPNAs gave similar IC_{50} values despite the difference

in length. This is likely due to both probes blocking ribosome association at the termianl

end. Nonetheless, the improved efficacy of the γPNAs compared to the PNA is consistent

with the enhanced γPNA thermodynamic stability. In addition, by utilizing an mRNA

transcript with an orthogonal 5'-UTR, we observed only slight (~10-15%) off-target

luciferase knockdown (**Figure 2.5B**), again likely due to the higher affinity tradeoff with

selectivity. Having observed sufficient antisense knockdown for both lengths of γPNA,

subsequent γPNA translational control probes were based off the shorter γPNA_{10}

sequence.
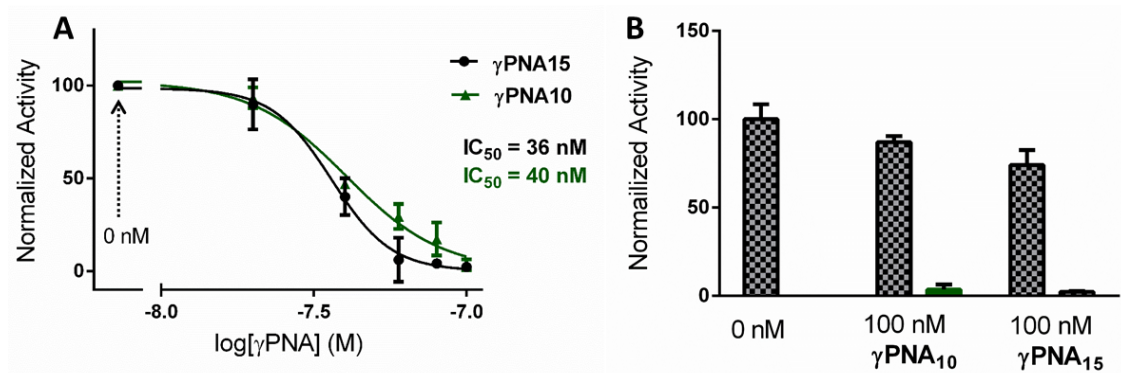
Figure 2.5 γPNA antisense gives effective and specific luciferase knockdown. (**A.**) Overlay of antisense dose-response curves for both **γPNA_{10}** and **γPNA_{15}** (both tested at n = 3) tested against the luciferase mRNA (10 nM). The γPNA probe and mRNA were pre-annealed in a buffered solution (RRL-matching concentration of 79 mM K^+ and DEPC-treated H_2O) and then placed in a 37 °C incubator for 1 hour. (**B.**) γPNA probes against a luciferase mRNA (10 nM) that has a scrambled γPNA target site (checkered bars). **γPNA_{10}** shows insignificant knockdown (p > .05) and **γPNA_{15}** shows small (~15%) but potentially significant (p < .05) luciferase knockdown. The knockdown of the perfect match luciferase is shown for **γPNA_{15}** (100 nM, black bar) and **γPNA_{10}** (100 nM, green bar).

2.3.2 Reversible translation suppression with γPNA

Because the 10-mer sequence is effective for translational suppression, we designed an extended γPNA probe containing the same 10-base mRNA binding domain and a contiguous 5-nucleobase toehold that is not complementary to any site on the mRNA (**Figure 2.3**). The toehold domain functions as a nucleation site that mediates the displacement of the bound antisense strand by addition of the second sense γPNA. The sense γPNA is fully complementary to antisense γPNA, leading to 5-extra base pairs (for specific sequence design see **Table 2.2**).

Table 2.2 Specific γPNA sequence used in reversible experiments, with complementary toehold domains indicated in red. K = lysine.

mRNA Target	5'-AGACCCAAGC-3'
Antisense γPNA	H$_2$N–K–TCTGGGTTCGTGATA–H
Sense γPNA	H–AGACCCAAGCACTAT–K–NH$_2$

The use of a 5-nucleobase toehold was determined by previous reports that show this to be a suitable length[38] for strand displacement reactions in DNA-based manipulations. However, shorter length toeholds may potentially be suitable given the higher affinity of PNA-PNA interactions relative to the analogous DNA-DNA interactions. Hence, upon the introduction of the complementary sense γPNA and through binding of the sense toehold to the complementary antisense toehold, a strand displacement reaction should free the mRNA transcript and toggle translation back ON.

To characterize the γPNA-γPNA displacement reaction we designed a series of surface plasmon resonance (SPR) experiments to verify and quantify the displacement reaction. Unfortunately, SPR is not amenable to direct immobilization of RNA due to the harsh chip regeneration conditions (i.e. NaOH wash) needed to remove bound γPNA prior to the next injection of sample. Given this, the SPR chip is functionalized with an immobilized biotinylated-DNA target, where the DNA sequence matches the target mRNA probe binding domain. Antisense γPNA is then injected (20 nM) into the flow cell to allow the target DNA-antisense γPNA hybridization reaction to occur (**Figure 2.6**). Subsequently, a short buffer wash is used to remove any unbound antisense γPNA, and then a titrated concentration (0-200 nM) of sense γPNA is flowed over the chip to allow for the γPNA-γPNA displacement reaction. A successful displacement reaction causes an overall loss of mass on the chip and generates a discernable dissociation curve on the SPR sensorgram (**Figure 2.6**). The percent displacement should increase as a function of sense concentration.
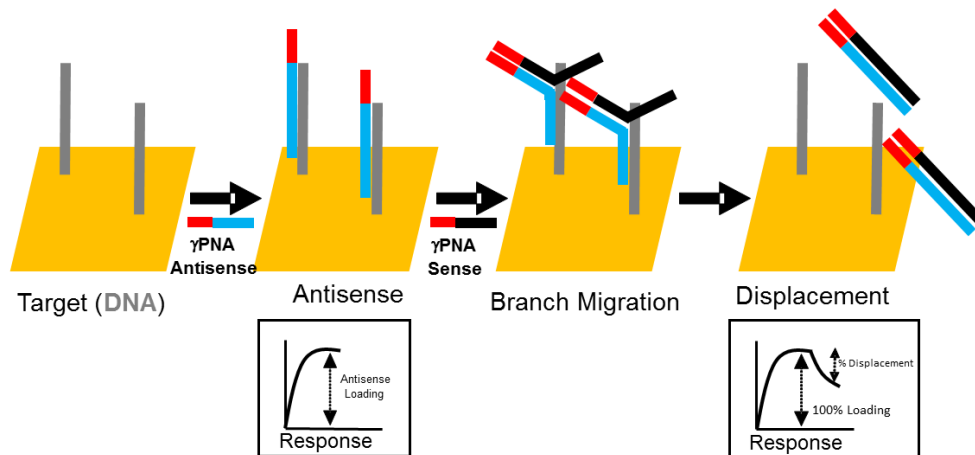
Figure 2.6 Surface Plasmon Resonance (SPR) investigation of γPNA-γPNA strand displacement. Antisense γPNA (light blue), with toehold (red), is loaded (association phase) onto the SPR chip via a hybridization reaction with the surface bound DNA (gray) capture strand. A wash step is included to

remove any residual antisense γPNA. The toehold nucleation and strand displacement reaction is initiated through sense γPNA (black) injection. Branch migration phenomena (unresolvable by SPR) leads to strand displacement, resulting in overall mass loss from the chip. The ratio of loading versus loss due to displacement is taken as the percent displacement.

Figure 2.7 demonstrates that the displacement experiment functions as illustrated in Figure 2.6. Loading of the antisense γPNA results in strong increase in signal, while subsequent addition of sense γPNA decreases the signal in a dose-dependent manner. Interestingly, only ca. 50% of the antisense γPNA could be displaced, based on the decrease in the observed response units. Although we saw clear evidence of γPNA strand displacement in the SPR (Figure 2.7C), the reaction was incomplete even when using high sense γPNA concentrations (> 200 nM).
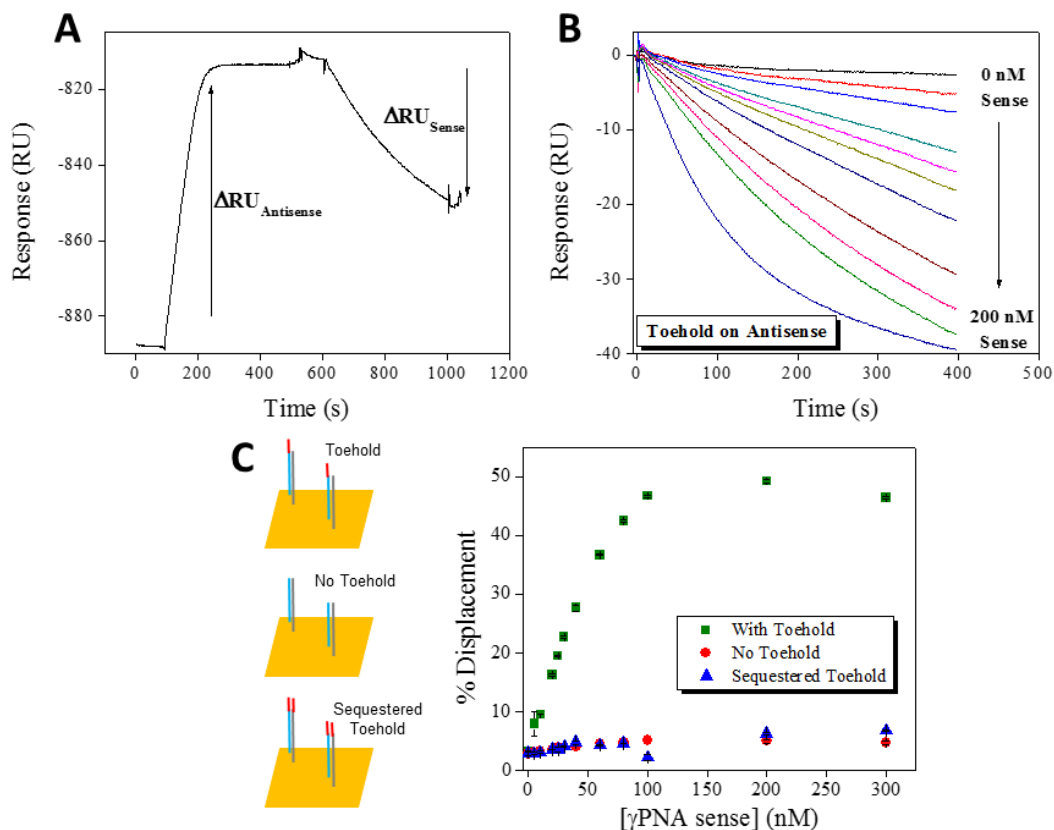
Figure 2.7 Surface plasmon characterization of γPNA displacement from complementary DNA. **(A.)** Calculation of percent displacement. The response unit change due to sense γPNA dissociation (ΔRU Sense) is divided by initially hybridized antisense γPNA (ΔRU Antisense). The experiments were conducted so that ΔRU antisense is constant for all runs. **(B.)** Dissociation of antisense γPNA through increasing sense γPNA concentrations over time. Every SPR run used a constant antisense concentration of 20 nM which was injected onto the SPR chip to hybridize the immobilized target DNA. Sense γPNA was then titrated (0-200 nM), to allow for displacement of the antisense γPNA from the chip. **(C.)** Various antisense conditions were considered including: toehold, no toehold and sequestered toehold (left). The total displacement achieved by the various conditions is shown (right). (All data in **C** is presented as average of n = 2 ± s.d.).

To try to further understand the displacement saturation, we tested the possibility of non-specific γPNA sense interactions on the SPR. First, we verified that sense γPNA does not interact with the streptavidin-functionalized chip alone, that is, without any immobilized DNA present on the chip. As expected, we saw no indication of a sense γPNA-streptavidin interaction (**Figure 2.8**).

50
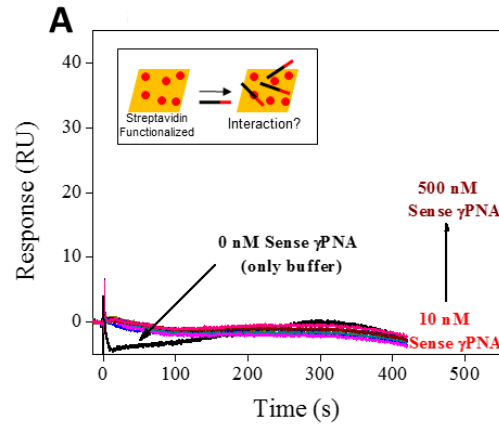
Figure 2.8 Non-specific interaction of increasing amounts of Sense γPNA (0-500 nM) flowed over a streptavidin-functionalized SPR chip (inset shows streptavidin (red dots) chip with introduced sense γPNA). We do not see any detectable levels of binding above background (0 nM sense).

Next, we tested if there is any non-specific binding between the sense γPNA and the homologous immobilized DNA target. We did indeed observe non-specific binding of the sense γPNA to the target strand particularly at concentrations above 200 nM sense γPNA (**Figure 2.9A**). We hypothesize that this non-specific interaction may be due to the formation of partial duplexes between the homologous sense γPNA and immobilized DNA. Interestingly, when we immobilize a longer DNA target having 5 additional bases that sequester the antisense toehold (Figure 2.7C), we observe little sense γPNA non-specific binding (**Figure 2.9B**). Clearly, further experiments are needed to better understand the origins of non-specific hybridization and lack of complete displacement. This can be tested in the future by studying different antisense/sense/DNA sequence combinations to investigate if off-target effects can be mitigated.
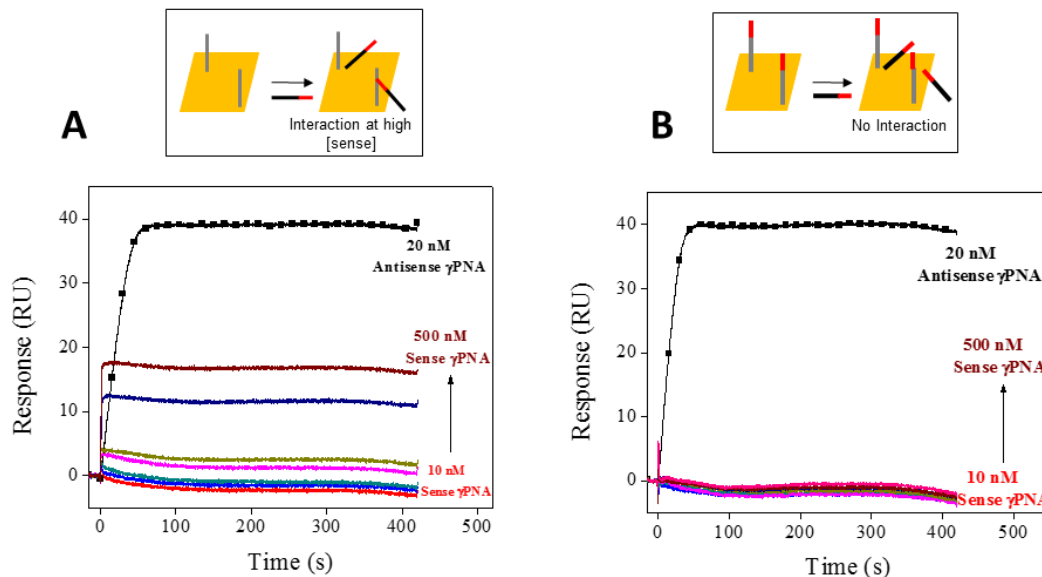
Figure 2.9 (A.) Non-specific binding of sense γPNA to an immobilized DNA target is evident at high concentration (> 200 nM) of sense γPNA (scheme above shows experiment, sense γPNA (black) and DNA (gray) have the same sequence). Above scheme shows experimental design. **(B.)** Immobilization of a DNA that contains 5-extra bases (designed to sequester antisense toehold) diminishes sense γPNA off-target sense binding. All data is presented as an average of two sample runs. In both cases, the antisense γPNA binding is shown (black curve) to indicate specific hybridization. The above scheme shows the experimental design (note, the longer DNA target).

To verify that the presence of the antisense toehold was necessary for displacement, we repeated the SPR displacement reaction by considering two separate experimental toehold-control conditions. The first control removed the toehold from the antisense γPNA to test if displacement driven by the sense γPNA can still proceed without proper toehold nucleation to the γPNA-10mer sequence. Here, we found that the removal of the antisense toehold gave no measurable displacement on the SPR (**Figure 2.7C**). The second control experiment utilized a longer immobilized target that completely base-pairs with the antisense γPNA toehold. When the longer target was applied, there was minimal detection of sense γPNA driven displacement (**Figure 2.7C**) presumably due to sequestering the antisense toehold.

After observing γPNA-driven displacement on the SPR, in vitro translation control studies were then conducted. The initial antisense γPNA probe was pre-annealed to the target mRNA (1 hour at 37 °C in 79 mM K$^+$ buffer). The sense γPNA was then introduced and allowed to interact with the antisense γPNA-mRNA complex over time. The total mixture (mRNA, antisense/sense γPNA) was subsequently added to the Rabbit Reticulocyte Lysate (RRL) and luciferase bioluminescence was measured using a TECAN plate reader after 90 minutes of translation. Following this approach, γPNA translation recovery was observed across a range of sense γPNA incubation times at equimolar sense-antisense (100 nM) concentrations in a time-dependent fashion (**Figure 2.10A**), with ca. 20% translation recovery observed in one hour, increasing to ca. 75% recovery in three hours.

The time dependence almost certainly indicates that our probe-driven reversibility has kinetic limitations. This is further supported by the SPR data, which demonstrated increase strand displacement as higher concentration sense γPNA was titrated. To ensure that the antisense γPNA does not knockdown an orthogonal luciferase, we incubated the toehold extended antisense γPNA at the high end of the dose range (100 nM) against a luciferase (10 nM mRNA) transcript with a scrambled target-binding site. We observed no knockdown of the luciferase expressed from the orthogonal transcript when compared to the 0 nM antisense γPNA control (**Figure 2.10B**). These results reflect the high degree of affinity and specificity antisense γPNA has for the target sequence of the transcript. Lastly, to show that the sense γPNA/mRNA interaction (no antisense present) does not cause elevated expression, the sense γPNA was incubated with the mRNA (100 nM sense, 2-hour incubation, 10 nM mRNA) and then added to the RRL. Again, the sense

γPNA showed no effect on protein expression levels when compared to the 0 nM γPNA control (**Figure 2.10B**).
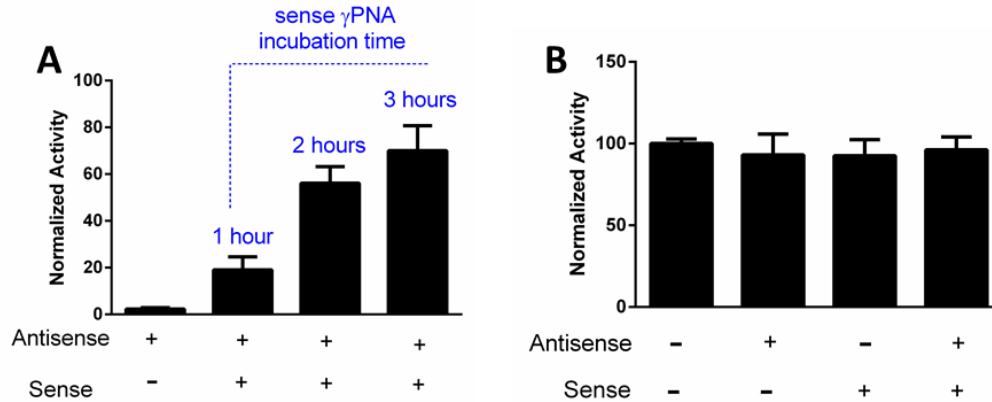
Figure 2.10 Time dependent translation recovery via γPNA-γPNA displacement. (**A.**) The amount of luciferase translation recovery observed was directly related to the sense γPNA incubation times. At 3-hour sense γPNA translation recovery approached ~75% activity opposed to only ~20% when 1-hour incubations were performed. Equimolar (100 nM) antisense γPNA/sense γPNA was used with 10 nM of target mRNA for all samples (Data is plotted as n=3 average ± s.d.). (**B.**) When the antisense γPNA alone or sense alone or both were incubated (1 hour at 37 °C) against an orthogonal mRNA transcript (scrambled antisense γPNA target site) we observed insignificant (p > .05) luciferase knockdown ([γPNA] = 100 nM, [mRNA] = 10 nM). (Data is plotted as n = 3 average ± s.d.).

The reversibility of an antisense γPNA that lacks the toehold domain was evaluated to determine if the increased γPNA-γPNA duplex stability alone was sufficient to reactivate translation. Initially, we annealed the "toehold-less" antisense γPNA to the luciferase mRNA at 37 °C. Next, we introduced the sense γPNA to the annealed mRNA/antisense γPNA and let the ternary mixture incubate for 2 hours before adding the entire mixture to the rabbit reticulocyte lysate (RRL) for translation. While the antisense-driven luciferase knockdown was conserved without the presence of a toehold domain, the sense-mediated reversibility was abolished completely (**Figure 2.11A**), indicating the importance of the antisense toehold as a nucleation site required to recover gene

translation. Furthermore, similar results were observed even at elevated temperatures (55 °C) applied over a 2-hour sense incubation time. Applying the same reaction conditions (sense incubation at 55 °C) to a toehold-containing antisense γPNA showed increased recovery of translation (**Figure 2.11B**) when compared to recovery values obtained at 37 °C sense incubation (70% versus 55%). Although operation of the strand displacement at 55 °C is not relevant for many biological applications, this is a useful experiment to explore the robustness of the strand displacement reaction and may be useful for in vitro experiments or methods.
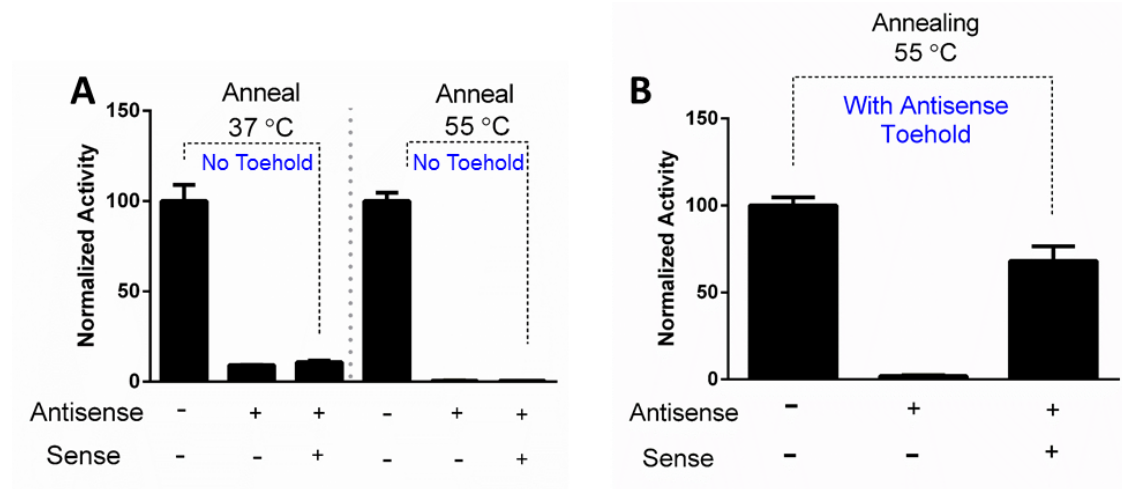
Figure 2.11 An antisense toehold is required to reverse γPNA-mediated translation inhibition. **(A.)** The absence of the antisense γPNA toehold domain eliminates any observed sense γPNA translation recovery (2-hour sense incubation [γPNA] = 100 nM, n = 3), however the toehold loss does not affect the antisense potency, see (+,-) bar. Additionally, the loss of the antisense γPNA toehold eliminates any observed translation recovery regardless of applying an elevated sense γPNA incubation temperature (55 °C) see (+,+) bar. (Data is plotted as n = 3 average ± s.d.). **(B.)** When the antisense γPNA toehold is available, applying an elevated temperature (55 °C) sense γPNA incubation yields high values of translational recovery (~70%) compared to the knockdown (p = .0002). (Data is plotted as n = 3 average ± s.d.).

An alternative to regulation of translation by exogenous sense γPNA is to utilize expressible RNA (e.g. miRNA, mRNA, or lncRNA) or exogenously supplied RNA (i.e. siRNA). Therefore, a sense RNA was tested for its ability to displace the antisense γPNA (**Figure 2.12A**). The sense RNA (200 nM) was incubated with pre-annealed antisense

γPNA/mRNA sample over the course of 2 hours. A two-fold excess (200 nM) of sense

RNA was required to obtain ~30% translation recovery (**Figure 2.12B**). This differs from

the sense γPNA experiments where 2-hour equimolar sense-antisense (100 nM)

incubations gave ~55% recovery. Furthermore, sense RNA concentrations that were 10-

fold higher (1 µM sense) than antisense γPNA yielded similar translation recovery results

to 200 nM sense RNA.
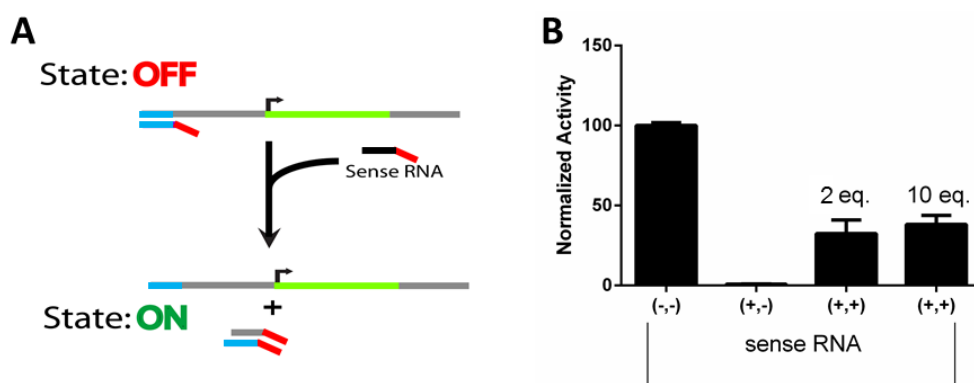
Figure 2.12 (A.) Reversible translation control with sense RNA in place of sense γPNA. The RNA probe replacement is the equivalent nucleotide sequence. **(B.)** Sense RNA displayed modest translation recovery (~30%, $p < .05$) at higher applied concentrations, specifically 200 nM (2 eq.) or 1000 nM (10 eq.) of sense RNA compared to 100 nM sense γPNA with a 2-hour displacement time. (Data is plotted as $n = 3$ average ± s.d.).

Additionally, we tested sense RNA driven-displacement on the SPR (**Figure**

2.13), however we did not observe antisense γPNA displacement, which could be due to

non-optimized toehold design (e.g. length, sequence, etc.) or the much shorter time scale

of the SPR experiment, where the sense RNA has only 400 seconds during which to

displace the antisense γPNA versus a two hour incubation prior to beginning in vitro

translation.
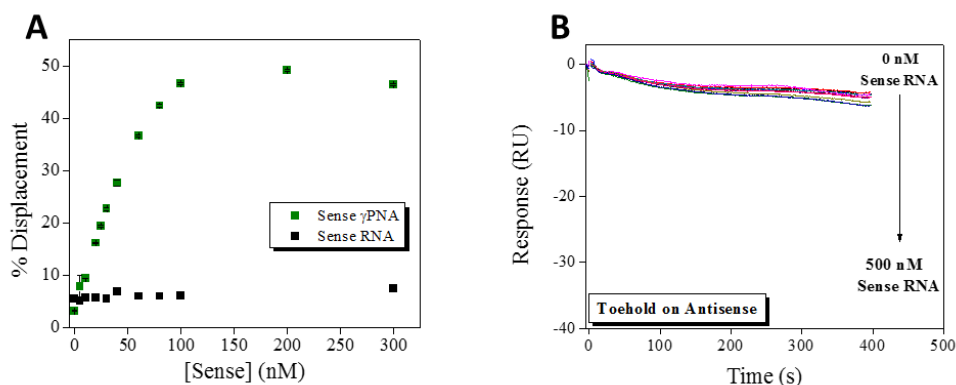
Figure 2.13 (A.) Dissociation of antisense γPNA through increasing sense RNA concentrations. Every SPR run used a constant antisense concentration of 20 nM to hybridize the immobilized target DNA. Sense RNA was titrated in (0-500 nM) to allow for displacement of the antisense γPNA. **(B.)** Percent displacement of antisense γPNA by sense RNA (black), also plotted in green is displacement from the sense γPNA experiment. (All data in **B** is presented as average of n = 2 ± s.d.).

To demonstrate translational control under physiological translation conditions, we tested sense γPNA reversal directly in a functional translation lysate system (**Figure 2.14A**). The sense γPNA was added at various concentrations to the RRL solution. These lysates were then charged with the antisense γPNA/mRNA complex (100 nM of antisense, 10 nM mRNA), and translation proceeded for 90 minutes. As expected, when no sense γPNA is present, ~98% of luciferase activity is blocked by the antisense strand (**Figure 2.14B**). Translation of luciferase is restored in a concentration-dependent manner, ultimately achieving ~90% recovery at a 20-fold (20X) excess of sense γPNA (**Figure 2.14B**). The excess sense is likely needed because of the constrained time-window (90 mins) and temperature (30 °C) the strand displacement reaction occurs in. Additionally, after strand displacement, protein expression is confined to this time and temperature window. Considering the antisense reversal in lysates, this suggests that such control may be possible in native physiological environments (e.g. cells), provided the excess sense strand does not exert significant off-target effects.
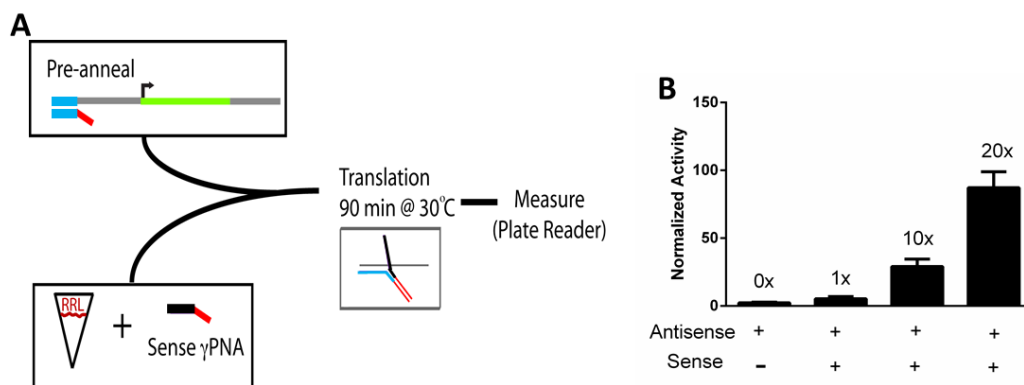
Figure 2.14 (A.) Reversible translation through addition of sense γPNA (1 – 20X) into rabbit reticulocyte lysate (RRL). The antisense γPNA (100 nM) is pre-annealed (1 hour at 37 °C) to the mRNA prior to the introduction into the RRL. The translation reaction then proceeds for 90 mins at 30 °C. Translation recovery as a function of sense γPNA concentration (N=3 for all concentrations). **(B.)** 0x represents 100 nM antisense γPNA (+,-), with no added sense γPNA. Significant (p < .05) translational recovery is seen at 10-fold and 20-fold sense concentration compared to antisense (100 nM) alone (~98% knockdown). (Data is plotted as n = 3 average ± s.d.).

2.4 Discussion

Reversible and selective translation control will provide a tool that is useful in the study of fundamental biological processes as well as in synthetic biology. Here, we demonstrated reversible translational regulation of a luciferase reporter in a cell-free system using γPNA strand displacement driven by toehold recognition.[39] Translation blocked by an antisense γPNA targeted to the 5′-terminus of the mRNA could be restored through addition of either a sense γPNA or a synthetic RNA designed to be fully complementary to the antisense γPNA. The latter result opens the door toward using endogenous sense molecules (e.g., miRNA) to reverse translational inhibition by an antisense γPNA, although further optimization of the toehold is needed to enhance the potency of reversal by RNA. In addition, successful demonstration of PNA as an inhibitor of transcription,[40] splicing[21,22,29] and miRNA function[28, 29] suggests that our

γPNA-based approach can be extended to allow reversible control over other steps in gene expression.

In addition to the luciferase reporter experiments, we developed a new SPR method to monitor strand displacement reactions in real time without the need for fluorescent labels.[41] This method should be useful for studying the kinetics of strand displacement for any other natural or synthetic nucleic acid. With growing interest in nucleic acid−based computing, SPR provides an attractive platform on which to study hybridization reactions in a label-free, automated, medium-throughput manner.

We anticipate that the γPNA displacement method may be useful in more elaborate cell-free experiments that include multiple gene targets, which are to be controlled discretely and independently, or to exert control over multiple open reading frames on a single transcript. Nevertheless, the simultaneous regulation of multiple genes will require careful sequence design of the γPNA system to limit off-target binding and maximize translation activation. Here, we directly synthesized the γPNAs to target the 5'-terminal UTR. However, if selectivity is a concern, additional focus can be placed on scanning the transcript for potential off-target sites, and shifting the γPNAs target site accordingly to limit the off-target binding potential. For example, shifting a few bases down from the 5'-terminal site may result in similar antisense potency, but improved selectivity. Future improvements upon the γPNA design, for instance by altering toehold sequence and length may lead to enhanced toehold nucleation and subsequent displacement in these types of reactions.

The next logical step in this work is to demonstrate reversible antisense effects in cell culture, which will require effective delivery of γPNAs into cells. Cell-penetrating

peptides,[42-44] cationic side chain modifications[31, 35, 45] or small molecule conjugates[46] have all been used to deliver PNAs into cells. In addition, a recent paper reported site-specific genome editing in vivo by γPNA delivered via a polymeric nanoparticle vehicle.[47] A similar nanoparticle formulation could be integrated with our technology to achieve intracellular translation recovery. In practice, this would involve delivering the antisense and sense γPNAs in separate transfections. Alternatively, a single nanoparticle bolus that delivers both γPNAs simultaneously could be used if the sense γPNA is prevented from hybridizing to the antisense γPNA, e.g., through introduction of a photoreleasable caging group.[48]

Another concern with moving our reversible translation inhibition to a cellular context is the possibility of off-target binding due to the exceptionally high affinity of γPNA,[37] which could lead to weaker antisense inhibition of the targeted mRNA and/or slower, less potent reversal due to competitive hybridization of one or both γPNAs to unintended sites. However, designing structure into the γPNAs, for example, in the form of a hairpin[49] or competitor strand,[50] could limit such off-target binding while preserving sufficient affinity to drive the key γPNA−γPNA hybridization reaction.

Finally, it could be anticipated that the cellular mRNA surveillance pathways would interfere with our approach by degrading the antisense-targeted transcript before the sense γPNA could be introduced. However, the activation of nonsense-mediated decay (NMD), nonstop-mediated decay (NSD), and no-go decay (NGD) mechanisms are dependent on the presence of a transcript-docked ribosome.[51] In the work presented here, we selected an mRNA target site (terminal 5′- UTR) that prevents 5′-UTR eukaryotic ribosomal initiation. Under this γPNA targeting strategy, we anticipate that little mRNA

will be lost due to ribosome-dependent degradation pathways. Similarly, RNaseH-mediated mRNA degradation is unlikely to occur due to the unnatural structure of γPNA. Thus, it should be possible, within cell culture, to trap a transcript using an antisense γPNA and then release it for translation at some later time through addition of the corresponding sense γPNA.

2.5   Conclusion

The results presented here demonstrate "toggling" an mRNA transcript from an OFF state to an ON state, using a complementary γPNA toehold-mediated strand displacement mechanism. Additionally, we developed a modified SPR method to verify the strand displacement phenomenon. In short, this project was a success, especially considering that this is the first PNA-based toehold-mediated strand displacement.

However, some difficulties were encountered. First, the explanation behind the 50% displacement saturation on SPR is still unclear, however the off-target sense binding was likely a part of the problem. As of this writing, I am exploring some potential mass transport limitations that may be the cause (especially after seeing the same displacement saturation in chapter 3 work). Additionally, there was some off-target knockdown (i.e., in the orthogonal FLUC sequence), however this likely comes with the territory when using such a high affinity oligonucleotide like γPNA. Nevertheless, careful attention to probe design (e.g., sequence, length, structure, etc.) may aid in improving the overall quality of the data.

2.6   Materials and Methods

2.6.1   (γ)PNA synthesis, purification, and characterization

PNA oligomers were synthesized and purified using common protocols. Mass

characterization was conducted by MALDI-TOF TOF (START PNA *m/z* found 4252.4

calcd 4255.0, TERM PNA *m/z* 4263.8 calcd 4263.0), and subsequently checked for purity

on a reverse phase HPLC (See Appendix for HPLC and MALDI-TOF data). **γPNA₁₀** and

γPNA₁₅ probes used in Figure 1.5 were HPLC purified and characterized by MALDI

TOF (**γPNA₁₀** *m/z* found 4041.6 calcd 4044.0, **γPNA₁₅** *m/z* 6019.1 calcd 6018) (See

Appendix for HPLC and MALDI-TOF data). γPNA oligomers used for reversible

translation experiments were obtained from PNA Innovations. PNA and γPNA stock

concentration was determined by measuring the oligomer absorption at 260 nm (collected

at 95°C) and dividing by the following respective molar extinction coefficients:

PNA START $\varepsilon = 146,700 \ M^{-1} \ cm^{-1}$

PNA 5' TERMINAL $\varepsilon = 155,800 \ M^{-1} \ cm^{-1}$

$\gamma PNA_{10} \ \varepsilon = 94,000 \ M^{-1} \ cm^{-1}$

$\gamma PNA_{15} \ \varepsilon = 155,800 \ M^{-1} \ cm^{-1}$

Antisense γPNA $\varepsilon = 150,700 \ M^{-1} \ cm^{-1}$

Sense γPNA $\varepsilon = 155,800 \ M^{-1} \ cm^{-1}$

(note: Sense γPNA extinction coefficient is indeed the same as PNA 5' TERMINAL and

γPNA_{15} although the sequences are different)

2.6.2 Luciferase plasmids for T7 RNA polymerase generation of RNA and in vitro protein synthesis in a rabbit reticulocyte lysate

The T7 Luciferase Control Plasmid, Promega part number L482A, was modified to remove alternate start codons, add the CMV transcription start sequence, a restriction site upstream of the Kozak-ATG and a restriction site at the start codon to enable luciferases to be inserted. The Promega plasmid was digested with BamHI and SacI and the luciferase was ligated into the Promega vector. This also introduced an NcoI site at the start codon. The firefly luciferase was PCR amplified digested and ligated into NcoI and SacI digested vector.

NcoFFlucF 5'-TATATACCATGGAAGACGCCAAAAACATAAAGAAAGG-3'

SacFFlucR 5'-TATATAGAGCTCGCCCCCTCGG-3'

This plasmid was then digested with HindIII and BamHI and annealed oligos were ligated to introduce an NheI site and CMV transcription start sequence.

HindCMVtransF 5-AGCTTTCAGATCCGCTAGCGCTACCGGG

BamCMVtransR 5'-GATCCCCGGTAGCGCTAGCGGATCTGAA

The firefly luciferase plasmid has the T7 promoter, CMV transcription start sequence and restriction sites, HindIII, NheI, BamHI and NcoI at the start codon. There is a SacI site 66 bases from the stop codon and a 30 base polyA sequence following the SacI site.

2.6.3 PCR amplification of the firefly luciferase plasmid

The firefly plasmid was digested (linearized) using an ApaL1 restriction site located downstream of the encoded poly A tail sequence. The linearized product was purified using the Thermo Scientific GeneJET Gel Extraction Kit protocol. The DNA was then PCR amplified using the NEB PCR Protocol for Phusion® High-Fidelity DNA Polymerase (cycled 35 times, PCR program 98 °C 2m, 98 °C 10s, 45 °C 15s, 72 °C, 2m, 72 °C 1m, hold at 4 °C).

Primer design: T7 transcription site 5'-TACGACTCACTATAGGG-3'

poly A tail site 5'-TTTTTTTTTTTTTTTTTTTTTTTTTTTTTT-3'

The products were purified using the Thermo Scientific Gel Extraction Kit protocol and verified using agarose gel electrophoresis (1.8 kB).

2.6.4 Transcription reaction and purification

The transcription reaction followed the Thermo Scientific conventional transcription protocol (50 μL final volume) and consistently gave high RNA product yield (~ 2.5 μM, determined via NanoDrop spectrophotometer). The transcription reaction was conducted at 37 °C for 2 hours. The transcription products were purified using the Thermo Scientific GeneJET RNA Cleanup and Concentration Micro Kit and concentration was measured using a NanoDrop spectrophotometer.

2.6.5 γPNA/mRNA annealing

The γPNA and RNA were annealed together in the presence of 79 mM potassium chloride (designed to match the K^+ concentration in the rabbit reticulocyte lysate, RRL source) and DEPC-treated water. The RNA concentration for all translation experiments is set at 10 nM in the final translation reaction. The probe concentration varies depending on the desired final concentration of probe. The initial antisense probe is annealed at 37 °C for 1 hour. In the case of the reversible translation experiments, an additional pre-incubation time (1-3 hours) is given for sense γPNA displacement at 37 °C being careful to maintain the incubation salt concentration (79 mM).

2.6.6 Translation conditions and luciferase read out

The translation reaction was conducted using the Promega Luciferase Assay System (E1500) (rabbit reticulocyte lysate). The PNA concentration was determined by considering the 50 μL final translation reaction volume. The translation reaction is conducted at 37 °C for 2 hours. Immediately after, the samples are stored in ice to quench any further protein synthesis. Following the Promega Rabbit Reticulocye Lysate System technical manual, 5 μL lysate solution is mixed into 50 μL Promega Luciferase Assay Reagent (E1483) added to a Thermo Scientific Nunc 96 well plate (flat white). The bioluminescent reading was collected on a TECAN Infinite M1000 plate reader.

2.6.7 Surface plasmon resonance (SPR)

All SPR experiments were performed on a Biacore T100 instrument (GE Healthcare) equipped with a four-channel sensor chip. The commercially available chip is

coated with a carboxylmethyl dextran matrix that allows further functionalization with streptavidin via a standard NHS-EDC coupling procedure.[52] Immobilization of streptavidin was continued until 7000 response units (RU) of the protein were captured on each of the four channels (flow cells). The final step of the sensor design involved non-covalent capture of the 5'-biotinylated DNA targets (~150 RU) on the respective flow cells bearing immobilized streptavidin.

Each experiment was preceded by injection of a solution containing 20 nM of the antisense γPNA oligomer for 400 s (flow rate = 30 μL/min). A dissociation time of 200 s was incorporated after the injection to allow for diffusion of unbound antisense oligomers from the sensor surface. The subsequent displacement assay was then performed by injecting a solution containing a fixed concentration of either the sense γPNA/RNA oligomer (flow rate = 30 μL/min) and monitoring the sensor response over 400 s. Each displacement cycle was ended by introducing a pulse of a regeneration cocktail (1 M NaCl, 10 mM NaOH) for 30 s at a flow rate of 50 μL/min. The cocktail serves to release any residual antisense/sense oligomers and is followed by a buffer injection (150 s, flow rate = 30 μL/min) to reestablish a baseline prior to the next displacement cycle.

The attenuation in response units following introduction of the sense oligomer was taken as evidence of displacement of the antisense γPNA from the sensor surface. Therefore, we established a quantitative estimate of the displacement reaction by the ratio of signal attenuation upon introduction of the sense γPNA, ΔRU (sense), to enhancement upon introduction of the complementary antisense γPNA, ΔRU (antisense) (Eqn. 1).

$$\% \text{ Displacement} \quad = \quad \frac{\Delta RU \text{ (sense)}}{\Delta RU \text{ (antisense)}} \quad \text{x} \quad 100 \qquad (1)$$

2.7   Appendix

2.7.1   PNA START HPLC & MALDI-TOF

PNA START *m/z* found 4252.4 calcd 4255.0
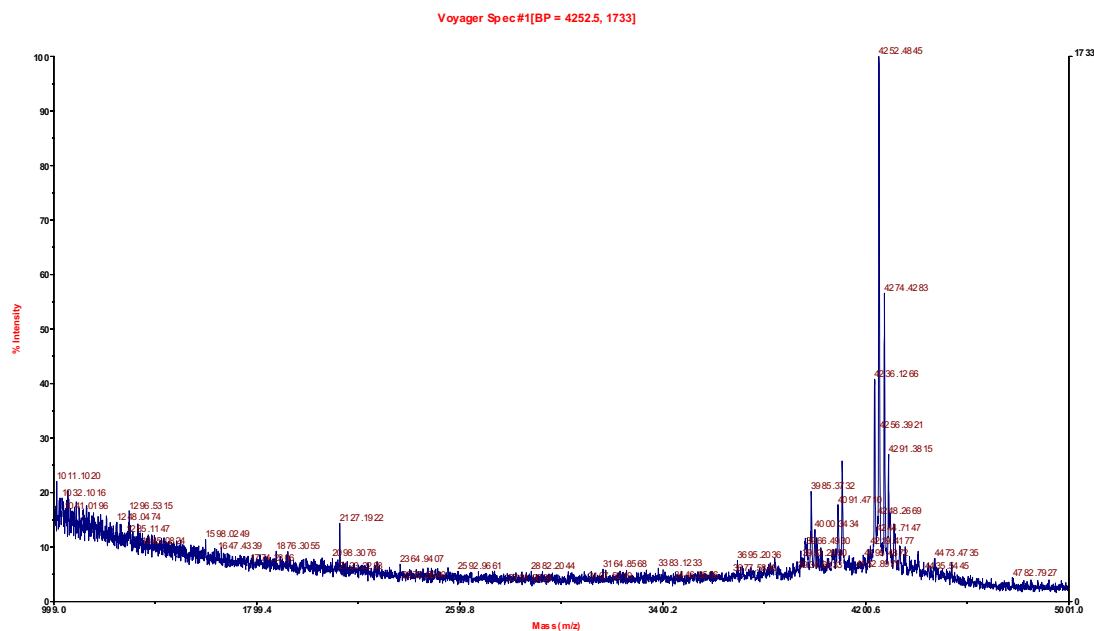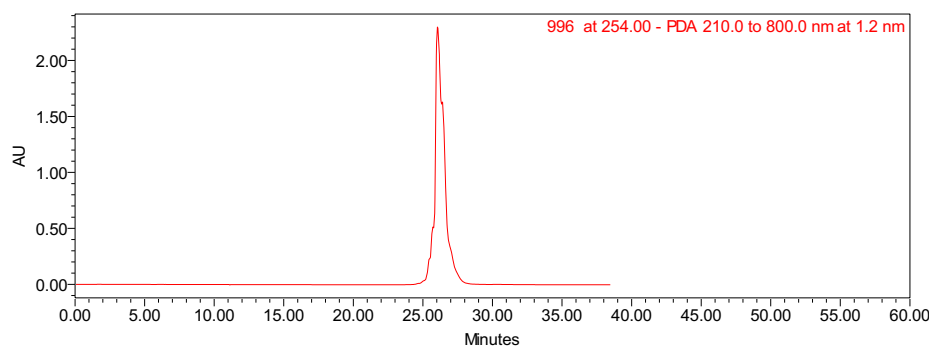
2.7.2 PNA 5' TERMINAL HPLC & MALDI-TOF

PNA 5' TERM *m/z* found 4263.8 calcd 4263.0
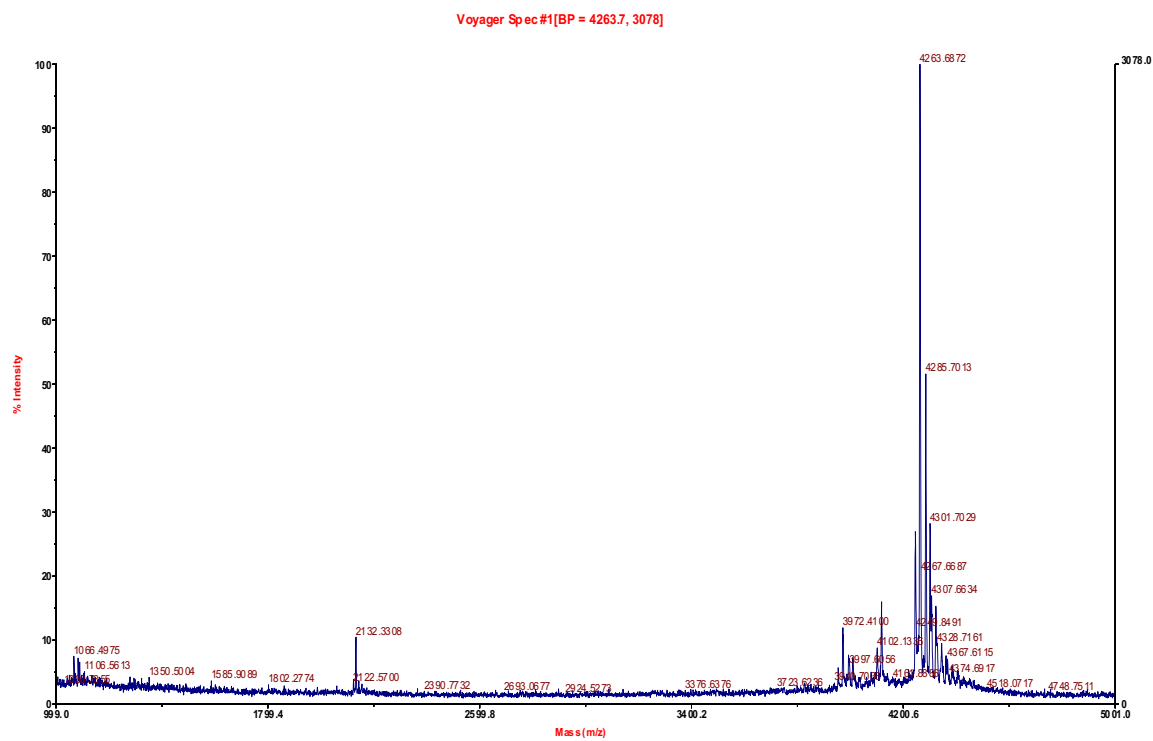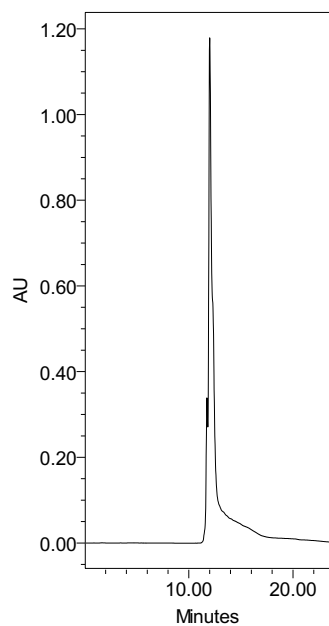
2.7.3 γPNA₁₀ HPLC & MALDI-TOF

γPNA$_{10}$ *m/z* found 4041.6 calcd 4044.0
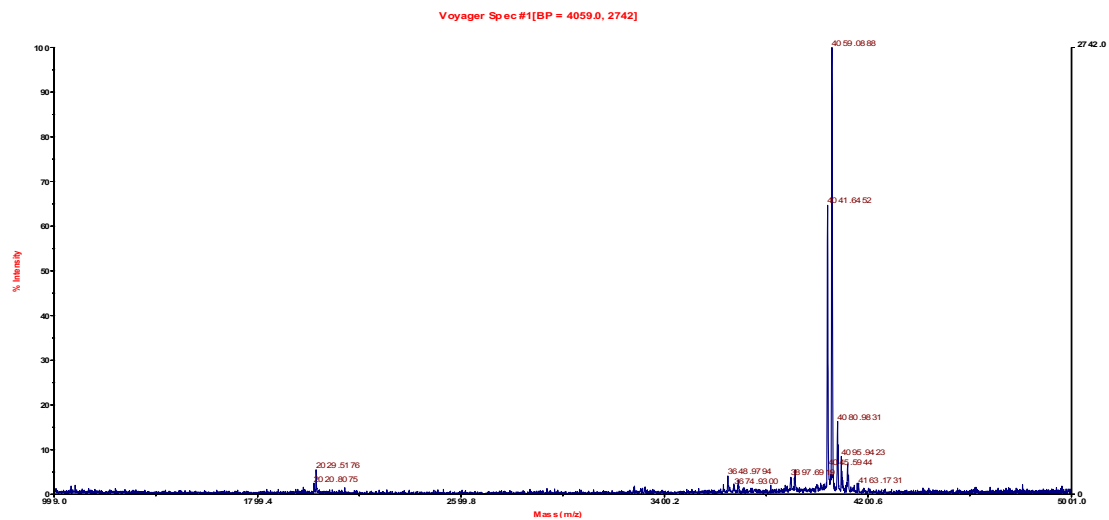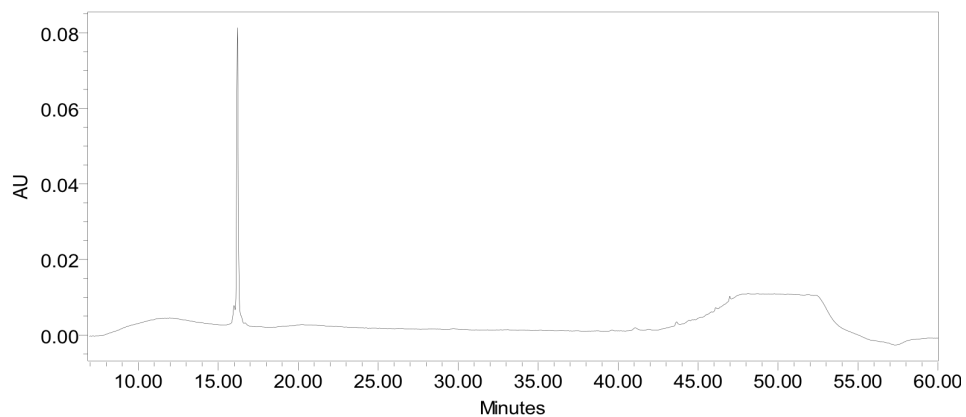
2.7.4 γPNA₁₅ HPLC & MALDI-TOF

, **γPNA₁₅** found *m/z* 6019.1 calcd 6018
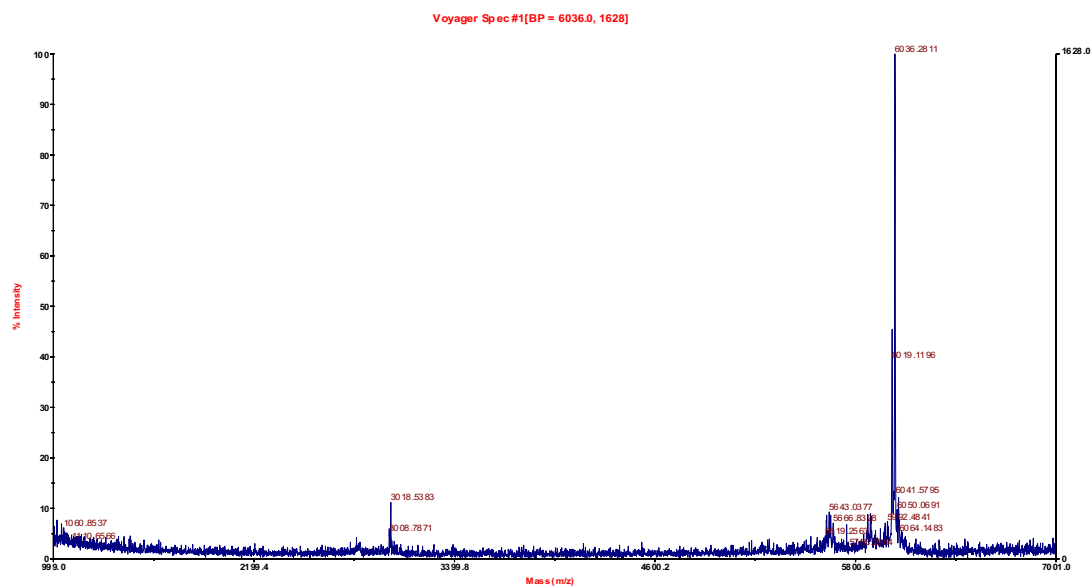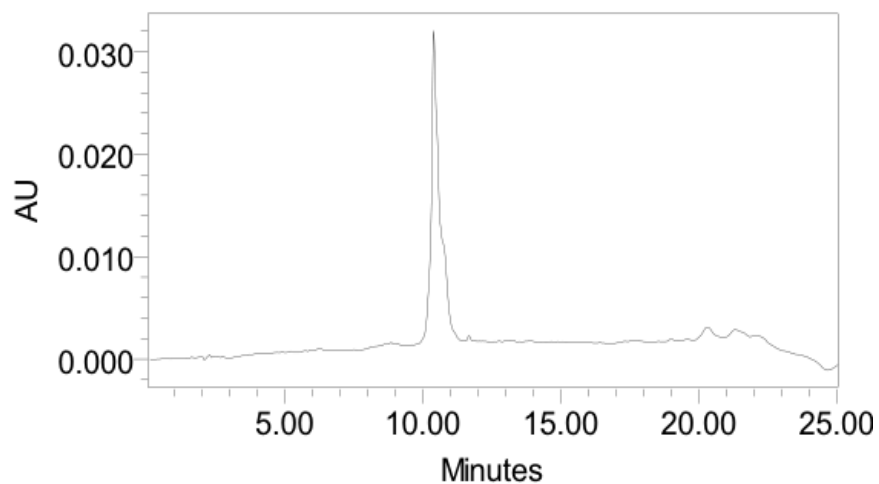
2.8   References

1.   Mutalik, V. K.; Qi, L.; Guimaraes, J. C.; Lucks, J. B.; Arkin, A. P., Rationally designed families of orthogonal RNA regulators of translation. *Nature Chemical Biology* **2012,** *8* (5), 447-454.

2.   Chappell, J.; Takahashi, M. K.; Meyer, S.; Loughrey, D.; Watters, K. E.; Lucks, J., The centrality of RNA for engineering gene expression. *Biotechnology Journal* **2013,** *8* (12), 1379-1395.

3.   Van Der Kelen, K.; Beyaert, R.; Inze, D.; De Veylder, L., Translational control of eukaryotic gene expression. *Critical Reviews in Biochemistry and Molecular Biology* **2009,** *44* (4), 143-168.

4.   Jackson, R. J.; Hellen, C. U. T.; Pestova, T. V., The mechanism of eukaryotic translation initiation and principles of its regulation. *Nature Reviews Molecular Cell Biology* **2010,** *11* (2), 113-127.

5.   Jackson, R. J.; Hellen, C. U.; Pestova, T. V., The mechanism of eukaryotic translation initiation and principles of its regulation. *Nature Reviews Molecular Cell Biology* **2010,** *11* (2), 113-127.

6.   Lundin, K. E.; Gissberg, O.; Smith, C. I. E., Oligonucleotide Therapies: The Past and the Present. *Human Gene Therapy* **2015,** *26* (8), 475-485.

7.   Suess, B.; Fink, B.; Berens, C.; Stentz, R.; Hillen, W., A Theophylline Responsive Riboswitch Based on Helix Slipping Controls Gene Expression *in Vivo*. *Nucleic Acids Research* **2004,** *32*, 1610-1614.

8.   Mutalik, V. K.; Guimaraes, J. C.; Cambray, G.; Lam, C.; Christoffersen, M. J.; Mai, Q. A.; Tran, A. B.; Paull, M.; Keasling, J. D.; Arkin, A. P.; Endy, D., Precise and reliable gene expression via standard transcription and translation initiation elements. *Nature Methods* **2013,** *10* (4), 354-360.

9.   Valencia-Sanchez, M. A.; Liu, J. D.; Hannon, G. J.; Parker, R., Control of translation and mRNA degradation by miRNAs and siRNAs. *Genes & Development* **2006,** *20* (5), 515-524.

10.   Hochrein, L. M.; Schwarzkopf, M.; Shahgholi, M.; Yin, P.; Pierce, N. A., Conditional Dicer substrate formation via shape and sequence transduction with small conditional RNAs. *Journal of the American Chemical Society* **2013,** *135* (46), 17322-17330.

11.   Isaacs, F. J.; Dwyer, D. J.; Ding, C. M.; Pervouchine, D. D.; Cantor, C. R.; Collins, J. J., Engineered riboregulators enable post-transcriptional control of gene expression. *Nature Biotechnology* **2004,** *22* (7), 841-847.

12.   Green, A. A.; Silver, P. A.; Collins, J. J.; Yin, P., Toehold switches: de-novo-designed regulators of gene expression. *Cell* **2014,** *159* (4), 925-39.

13.   Young, D. D.; Lively, M. O.; Deiters, A., Activation and Deactivation of DNAzyme and Antisense Function with Light for the Photochemical Regulation of Gene Expression in Mammalian Cells. *Journal of the American Chemical Society* **2010,** *132* (17), 6183-6193.

14.   Nielsen, P. E.; Egholm, M.; Berg, R. H.; Buchardt, O., Sequence-Selective Recognition of DNA by Strand Displacement with a Thymine-Substituted Polyamide. *Science* **1991,** *254*, 1498-1500.

15.   Egholm, M.; Buchardt, O.; Christensen, L.; Behrens, C.; Freier, S. M.; Driver, D. A.; Berg, R. H.; Kim, S. K.; Nordén, B.; Nielsen, P. E., PNA Hybridizes to

Complementary Oligonucleotides Obeying the Watson-Crick Hydrogen-Bonding Rules. *Nature* **1993,** *365*, 566-568.

16.   Sahu, B.; Sacui, I.; Rapireddy, S.; Zanotti, K. J.; Bahal, R.; Armitage, B. A.; Ly, D. H., Synthesis and characterization of conformationally preorganized, (R)-diethylene glycol-containing gamma-peptide nucleic acids with superior hybridization properties and water solubility. *Journal of Organic Chemistry* **2011,** *76* (14), 5614-27.

17.   Nielsen, P. E., Gene targeting and expression modulation by peptide nucleic acids (PNA). *Current Pharmaceutical Design* **2010,** *16*, 3118-3123.

18.   Liu, B.; Han, Y.; Ferdous, A.; Corey, D. R.; Kodadek, T., Transcription Activation by a PNA-Peptide Chimera in a Mammalian Cell Extract. *Chemical Biology* **2003,** *10*, 909-916.

19.   Møllegaard, N. E.; Buchardt, O.; Egholm, M.; Nielsen, P. E., Peptide Nucleic Acid. DNA Strand Displacement Loops as Artificial Transcription Promoters. *Proceedings of the National Academy of Sciences of the United States of America* **1994,** *91*, 3892-3895.

20.   Janowski, B. A.; Kaihatsu, K.; Huffman, K. E.; Schwartz, J. C.; Ram, R.; Hardy, D.; Mendelson, C. R.; Corey, D. R., Inhibiting Transcription of Chromosomal DNA with Antigene Peptide Nucleic Acids. *Nature Chemical Biology* **2005,** *1*, 210-215.

21.   Sazani, P.; Gemignani, F.; Kang, S.-H.; Maier, M. A.; Manoharan, M.; Persmark, M.; Bortner, D.; Kole, R., Systemically Delivered Antisense Oligomers Upregulate Gene Expression in Mouse Tissues. *Nature Biotechnology* **2002,** *20*, 1228-1233.

22.   Ivanova, G. D.; Arzumanov, A.; Abes, R.; Yin, H.; Wood, M. J. A.; Lebleu, B.; Gait, M. J., Improved Cell-Penetrating Peptide-PNA Conjugates for Splicing Redirection in HeLa Cells and Exon Skipping in mdx Mouse Muscle. *Nucleic Acids Research* **2008,** *36*, 6418-6428.

23.   Yin, H.; Lu, Q.; Wood, M., Effective Exon Skipping and Restoration of Dystrophin Expression by Peptide Nucleic Acid Antisense Oligonucleotides in mdx Mice. *Molecular Therapy* **2008,** *16*, 38-45.

24.   Bai, H.; You, Y.; Yan, H.; Meng, J.; Xue, X.; Hou, Z.; Zhou, Y.; Ma, X.; Sang, G.; Luo, X., Antisense Inhibition of Gene Expression and Growth in Gram-Negative Bacteria by Cell-Penetrating Peptide Conjugates of Peptide Nucleic Acids Targeted to *rpoD* Gene. *Biomaterials* **2012,** *33*, 659-667.

25.   Doyle, D. F.; Braasch, D. A.; Simmons, C. G.; Janowski, B. A.; Corey, D. R., Inhibition of Gene Expression Inside Cells by Peptide Nucleic Acids: Effect of mRNA Target Sequence, Mismatched Bases, and PNA Length. *Biochemistry* **2001,** *40*, 53-64.

26.   Kaihatsu, K.; Huffman, K. E.; Corey, D. R., Intracellular uptake and inhibition of gene expression by PNAs and PNA-peptide conjugates. *Biochemistry* **2004,** *43* (45), 14340-14347.

27.   Knudsen, H.; Nielsen, P. E., Antisense Properties of Duplex- and Triplex-Forming PNAs. *Nucleic Acids Research* **1996,** *24*, 494-500.

28.   Torres, A. G.; Fabani, M. M.; Vigorito, E.; Williams, D.; Al-Obaidi, N.; Wojciechowski, F.; Hudson, R.; Seitz, O.; Gait, M. J., Chemical structure requirements and cellular targeting of microRNA-122 by peptide nucleic acids anti-miRs. *Nucleic Acids Research* **2012,** *40*, 2152-2167.

29.   Cheng, C. J.; Bahal, R.; Babar, I. A.; Pincus, Z.; Barrera, F.; Liu, C.; Svoronos, A.; Braddock, D. T.; Glazer, P. M.; Engelman, D. M.; Saltzman, W. M.; Slack, F. J.,

MicroRNA silencing for cancer therapy targeted to the tumor microenvironment *Nature* **2015,** *518*, 107-110.

30.   Dragulescu-Andrasi, A.; Rapireddy, S.; Frezza, B. M.; Gayathri, C.; Gil, R. R.; Ly, D. H., A simple gamma-backbone modification preorganizes peptide nucleic acid into a helical structure. *Journal of the American Chemical Society* **2006,** *128* (31), 10258-10267.

31.   Delgado, E.; Bahal, R.; Yang, J.; Lee, J. M.; Ly, D. H.; Monga, S. P., β-Catenin knockdown in liver tumor cells by a cell permeable gamma guanidine-based peptide nucleic acid. *Current Cancer Drug Targets* **2013,** *13* (8), 867-878.

32.   Ly, D. H., Personal communication.

33.   Demidov, V. V.; Potaman, V. N.; Frank-Kamanetskii, M. D.; Egholm, M.; Buchardt, O.; Sönnichsen, S. H.; Nielsen, P. E., Stability of Peptide Nucleic Acids in Human Serum and Cellular Extracts. *Biochemical Pharmacology* **1994,** *48*, 1310-1313.

34.   Good, L.; Awasthi, S. K.; Dryselius, R.; Larsson, O.; Nielsen, P. E., Bactericidal Antisense Effects of Peptide-PNA Conjugates. *Nature Biotechnology* **2001,** *19*, 360-364.

35.   Dragulescu-Andrasi, A.; Rapireddy, S.; He, G.; Bhattacharya, B.; Hyldig-Nielsen, J. J.; Zon, G.; Ly, D. H., Cell-permeable peptide nucleic acid designed to bind to the 5'-untranslated region of E-cadherin transcript induces potent and sequence-specific antisense effects. *Journal of the American Chemical Society* **2006,** *128* (50), 16104-16112.

36.   Kozak, M., An analysis of 5'-noncoding sequences from 699 vertebrate messenger RNAs. *Nucleic Acids Research* **1987,** *15* (20), 8125-8148.

37.   Sahu, B.; Sacui, I.; Rapireddy, S.; Zanotti, K. J.; Bahal, R.; Armitage, B. A.; Ly, D. H., Synthesis and Characterization of Conformationally Preorganized, (R)-Diethylene Glycol-Containing γ-Peptide Nucleic Acids with Superior Hybridization Properties and Water Solubility. *Journal of Organic Chemistry* **2011,** *76*, 5614-5627.

38.   Zhang, D. Y.; Winfree, E., Control of DNA Strand Displacement Kinetics Using Toehold Exchange. *Journal of the American Chemical Society* **2009,** *131* (47), 17303-17314.

39.   Srinivas, N.; Ouldridge, T. E.; Sulc, P.; Schaeffer, J. M.; Yurke, B.; Louis, A. A.; Doye, J. P.; Winfree, E., On the biophysics and kinetics of toehold-mediated DNA strand displacement. *Nucleic Acids Research* **2013,** *41* (22), 10641-58.

40.   Hu, J. X.; Corey, D. R., Inhibiting gene expression with peptide nucleic acid (PNA)-peptide conjugates that target chromosomal DNA. *Biochemistry* **2007,** *46* (25), 7581-7589.

41.   Chang, A. L.; McKeague, M.; Liang, J. C.; Smoke, C. D., Kinetic and Equilibrium Binding Characterization of Aptamers to Small Molecules using a Label-Free, Sensitive, and Scalable Platform. *Analytical Chemistry* **2014,** *86* (7), 3273-3278.

42.   Koppelhus, U.; Nielsen, P. E., Cellular delivery of peptide nucleic acid (PNA). *Advanced Drug Delivery Reviews* **2003,** *55* (2), 267-280.

43.   Abes, S.; Ivanova, G. D.; Abes, R.; Arzumanov, A. A.; Williams, D.; Owen, D.; Lebleu, B.; Gait, M. J., Peptide-based delivery of steric-block PNA oligonucleotides. *Methods in Molecular Biology* **2009,** *480*, 85-99.

44.   Deuss, P. J.; Arzumanov, A. A.; Williams, D. L.; Gait, M. J., Parallel synthesis and splicing redirection activity of cell-penetrating peptide conjugate libraries of a PNA cargo. *Organic & Biomolecular Chemistry* **2013,** *11* (43), 7621-30.

45.   Zhou, P.; Wang, M.; Du, L.; Fisher, G. W.; Waggoner, A.; Ly, D. H., Novel binding and efficient cellular uptake of guanidine-based peptide nucleic acids (GPNA). *Journal of the American Chemical Society* **2003,** *125* (23), 6878-9.

46.   Shiraishi, T.; Nielsen, P. E., Nanomolar cellular antisense activity of peptide nucleic acid (PNA) cholic acid ("umbrella") and cholesterol conjugates delivered by cationic lipids. *Bioconjugate Chemistry* **2012,** *23* (2), 196-202.

47.   Bahal, R.; McNeer, N. A.; Quijano, E.; Liu, Y. F.; Bhunia, D. C.; Ly, D. H.; Saltzman, W. M.; Glazer, P. M., Site-Specific Genome Editing of Hematopoietic Stem Cells for Beta Thalassemia Gene Therapy. *Molecular Therapy* **2014,** *22*, S290-S291.

48.   Liu, Q. Y.; Deiters, A., Optochemical Control of Deoxyoligonucleotide Function via a Nucleobase-Caging Approach. *Accounts of Chemical Research* **2014,** *47* (1), 45-55.

49.   Bonnet, G.; Tyagi, S.; Libchaber, A.; Kramer, F. R., Thermodynamic basis of the enhanced specificity of structured DNA probes. *Proceedings of the National Academy of Sciences of the United States of America* **1999,** *96* (11), 6171-6176.

50.   Zhang, D. Y.; Chen, S. X.; Yin, P., Optimizing the specificity of nucleic acid hybridization. *Nature Chemistry* **2012,** *4* (3), 208-214.

51.   Schweingruber, C.; Rufener, S. C.; Zund, D.; Yamashita, A.; Muhlemann, O., Nonsense-mediated mRNA decay - Mechanisms of substrate mRNA recognition and degradation in mammalian cells. *Biochimica Et Biophysica Acta-Gene Regulatory Mechanisms* **2013,** *1829* (6-7), 612-623.

52.   Nguyen, B.; Tanious, F. A.; Wilson, W. D., Biosensor-surface plasmon resonance: Quantitative analysis of small molecule-nucleic acid interactions. *Methods* **2007,** *42* (2), 150-161.

Chapter 3: Translation Control Using Chimeric γPNA Strand Displacement

3.1 Introduction

The renewed focus in the last 15 years on nucleic acid hybridization kinetics and thermodynamics has provided an impressive set of Watson-Crick nanotechnologies.[1-5] The resultant nucleic acid systems often demonstrate a stimulus-dependent re-distribution of molecular species, which in turn yields a detectable output. Characteristically, well-designed *dynamic* systems can (1) receive and autonomously (non-enzymatically) (2) process a nucleic acid input, that in turn, drives a molecular and/or mechanical (3) output. The output species, which is often a nucleic acid, may directly report on the presence of a disease marker or be used to alter the genetic information behind the disease.[6, 7] Additionally, multiple nucleic acid devices can be "wired" together, in a cascading or parallel manner, to form gate circuits which are layered for higher order computation.[8, 9] The internal structure of the nucleic acid device itself and the recognition event between the device and the input, are all programmed by Watson-Crick base pairs.[10] Thus, given the well-understood nature of DNA base-pairing, the nucleic acid interactions are engineered to achieve agreement between user design and the resultant device performance.[11] Furthermore, computational tools, such as NUPACK web application, are readily available and can be used to design and simulate nucleic acids systems.[12]

The central component in dynamic nucleic acid nanotechnology is the single stranded toehold domain.[13] The toehold domain allows for kinetically fast molecular

rearrangements (processing and output generation) between a mix of Watson-Crick cognate molecules.[14] Furthermore, without the presence of an exposed toehold domain, new duplex combinations are kinetically discouraged, regardless of any potential thermodynamic gain upon duplex rearrangement.[15] Thus, the toehold domain accelerates the reaction by providing a "docking" domain to initiate the strand displacement reaction. The strand displacement reaction is largely governed by the coupling between toehold thermodynamics and displacement kinetics. For example, modifying the toehold length or increasing the G-C content can increase the binding strength between complementary pairs and accelerate the rate of the overall displacement reaction.[13, 14]

However, binding selectivity is also important in toehold driven hybridization reactions.[16] The need for high affinity (sensitivity), but without compromised selectivity, presents an interesting challenge in the design and implementation of hybridization probes.[17, 18] To strike a balance between affinity and selectivity, nucleic acid systems are designed to contain regions that impart binding affinity (toehold), but also contain structural regions that minimize "off-target" events by introducing a discriminatory competing intramolecular architecture.[19, 20] Indeed, the incorporation of competitive internal structure to improve target selectivity is a design feature that has been implemented in several nucleic acid designs for some time now, including triplex forming oligonucleotides and molecular beacons, to name a few.[21-23]

It should be noted, that much of the strand displacement work has involved DNA/RNA only, whereas demonstrations that employ analog systems (e.g., PNA or LNA) are sparse.[24, 25] Similar to DNA/RNA, PNA/LNA rely on the same Watson-Crick base-pairing rules and are dictated, in large part, by nearest-neighbor thermodynamics in

target recognition.[26, 27] Thus, to a first approximation, DNA/RNA computational tools may also be used reliably to design analog hybridization nanotechnologies. However, due to PNA having a drastically different backbone (chemical makeup and lack of charge), application of these tools should be used cautiously.

The analog nucleic acids demonstrate heightened affinity/selective properties and enhanced bio-stability, thus giving them several potential contextual advantages in dynamic nucleic acid technology compared to DNA/RNA.[28, 29] Specific to PNA, several backbone modifications have recently been explored to improve the physiochemical properties and cellular compatibility. For example, PNA modified at the γ-position with solubilizing agents has improved water solubility, improved target binding affinity, and, enhanced cellular delivery of the PNA molecule class.[30-32] In short, the unique features of non-natural nucleic acids present interesting opportunities to create more robust DNA/RNA hybrid or orthogonal technologies.

Besides demonstrating improved physiochemical or binding properties, nucleic acid analogs can also be made to "play" by different rules than the natural nucleic acids. For example, recent work with γ-modified peptide nucleic acids (γPNA, γ = methyl) demonstrated orthogonal bimolecular recognition of right- *and* left-handed probes.[33] Specifically, depending on which amino acid stereoisomer (D or L) was used in γPNA synthesis, the probe can adopt either right- or left-handed pre-organization. To this end, successful γPNA-γPNA duplex formation is a function of sequence *and* helical complementarity. Although left-handed γPNA does not bind DNA/RNA, left-handed domains can be conjugated to right-hand domain containing probes to interface with the natural nucleic acid class. The construction of this type of "chimeric" molecule allows for

bi-helical and orthogonal interactions among complementary pairs. For example, recent work by Winssinger and coworkers demonstrated DNA template-driven turnover enhancement of a ruthenium functionalized chimeric γPNA (γ = methyl). The chimeric γPNA has a hairpin architecture that is composed of three connected domains; L-γPNA domain, followed by an achiral unmodified PNA domain that is internally hybridized to a connected D-γPNA domain.[34] Moreover, the D-γPNA domain is terminally functionalized with a ruthenium complex that is catalytically enhanced upon a DNA-mediated (target) structural rearrangement. This work presents an interesting *in vitro* example of chiral γPNA for improved nucleic acid catalysis, however the application of helically orthogonal γPNA which confers bioactivity has not been achieved yet.

To address the gap in strand displacement mediated nucleic acid nanotechnology using PNA, we recently designed a toehold-mediated strand displacement system using γ-modified peptide nucleic acid (γPNA, γ = diethylene glycol).[35] In brief, this work demonstrated toehold-mediated reversible γPNA antisense control of a reporter gene and characterized the strand displacement reaction biophysically. However, due to the high binding affinity of γPNA some concerns with selectivity were noted, thereby leaving room for design improvement.

In this work, we demonstrate orthogonal recognition and reversible translation control using γPNA designed with concatenated left- and right-handed domains. The right-handed domain is designed to bind to DNA and mRNA, whereas the downstream left-handed domain is designed to function as a toehold domain. The left-handed toehold domain initiates helical and sequence compatible γPNA-γPNA strand displacement.

Additionally, the chimeric strand displacement reaction is characterized directly using surface plasmon resonance.

3.2 Results

As mentioned above, *in vitro* reversible translation control of a reporter gene was shown using a complementary probe system composed of an antisense γPNA and a complementary sense γPNA. In this work, we investigated a helically chimeric γPNA system for mediating reversible translation control. The two chimeric γPNA probes, which are referred to antisense γPNA$_{CH}$ and sense γPNA$_{CH}$, contain a 10-mer right-handed domain, a diethylene glycol (miniPEG) linker, which is attached to a 6-mer left-handed toehold domain. The miniPEG linker functions to separate the two helical domains within probe(s). Specifically, we speculated that directly connecting the chimeric domains may lead to unwanted backbone conformational distortions, which in turn, could potential complicate any hybridization reactions. Furthermore, the sense γPNA$_{CH}$ and antisense γPNA$_{CH}$ are sequence *and* helical complements in the 10-mer and 6-mer domains (**Table 3.1**).

Table 3.1 mRNA (target) and γPNA used in cell-free and biophysical experiments[a]

mRNA (FLUC) Target	5'-AGACCCAAGC-3'
Chimeric Antisense γPNA$_{CH}$	H2N-K-TCTGGGTTCG-miniPEG-*ATATTA*-H
Chimeric Sense γPNA$_{CH}$	H-AGACCCAAGC-miniPEG-*TATAAT*-K-NH2
Right-Handed Sense γPNA$_{RH}$	H-AGACCCAAGC-miniPEG-TATAAT-K-NH2

[a]Toehold domains are indicated in red and italics indicate left-handed monomers. K = lysine.

3.2.1   Translation inhibition and recovery by chimeric γPNA

Guided by our recent demonstration of firefly luciferase (FLUC) knockdown using γPNA$_{RH}$, we designed the antisense γPNA$_{CH}$ to bind to FLUC mRNA at the terminal end to the 5'-UTR via the 10-base right-handed domain. In brief, the reversible translation experiments are conducted as shown below (**Figure 3.1**).
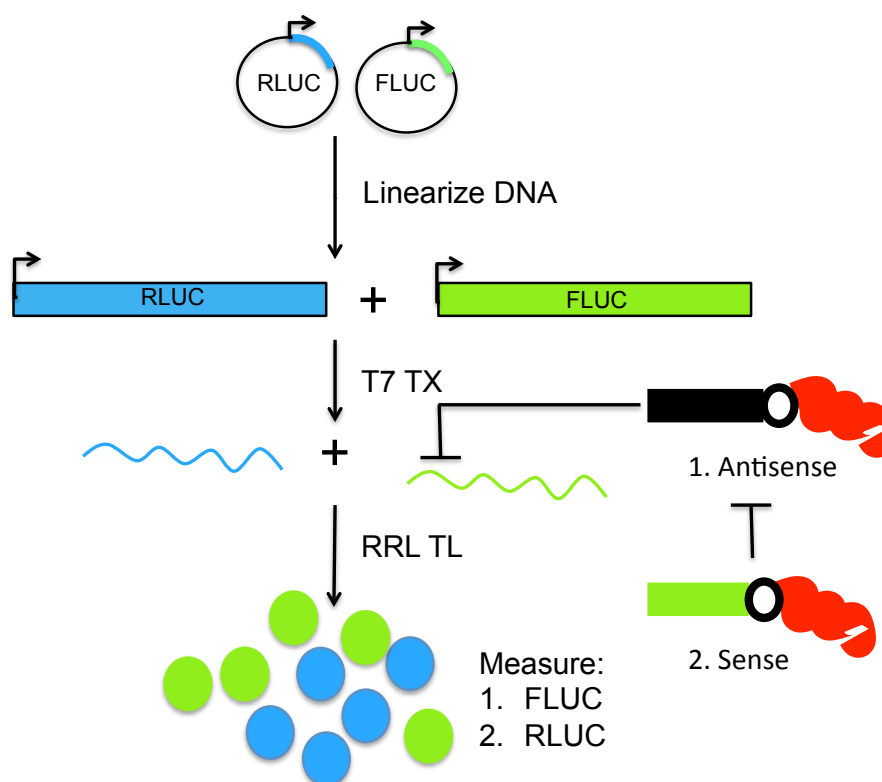
Figure 3.1 General workflow of reversible translation control using chimeric γPNA in cell-free lysate (RRL). Following linearization of plasmid firefly (FLUC) and *Renilla* (RLUC) DNA and transcription, chimeric γPNA (γPNA$_{CH}$) probes are pre-annealed with mRNA prior to translation (RRL TL). The antisense γPNA$_{CH}$ and sense γPNA$_{CH}$ both contain right- and left-handed domains, which are separated by a diethlyene glycol (miniPEG) spacer (black disk). The antisense γPNA$_{CH}$ right-handed domain (black) is complementary to the 5'-terminal end of FLUC mRNA, preventing downstream translation. Strand displacement of the antisense γPNA$_{CH}$ is toehold-mediated (toehold shown in red) by a sense γPNA$_{CH}$ input. After antisense displacement, FLUC mRNA is available for downstream translation. Input of a sense γPNA$_{CH}$ is unable to displace antisense γPNA$_{RH}$ due to helically orthogonal toeholds. RLUC signal is measured to quantitate off-target binding of the γPNA$_{CH}$ probes.

To test γPNA$_{CH}$ antisense inhibition of FLUC expression, we pre-annealed 100 nM antisense γPNA$_{CH}$ to 10 nM FLUC target for 1.0-hr at 37 °C. Additionally, to investigate the specificity of γPNA$_{CH}$ right-handed domains we performed the annealing and translation reactions in the presence of 10 nM *Renilla* luciferase (RLUC). The annealed γPNACH/mRNA (FLUC and RLUC) mixture was then added to rabbit reticulocyte lysate (RRL) for translation (90 mins at 30 °C). After translation, the amount of knockdown was qualitatively determined by the amount of bioluminescence signal, which was measured on a TECAN plate reader. Here, we observed ~90% and ~5% antisense γPNA$_{CH}$ inhibition of FLUC and RLUC, respectively (**Figure 3.2**, (**A**, case +, -)).

Next, we investigated if the sense γPNA$_{CH}$ can recover FLUC expression to levels comparable to untreated (0 nM) γPNA$_{CH}$ samples. Specifically, annealing sense γPNA$_{CH}$ to the antisense γPNA$_{CH}$/mRNA (pre-annealed) mixture, we expected to observe increased FLUC expression due to γPNA$_{CH}$-γPNA$_{CH}$ strand displacement. When incubating 100 nM sense γPNA$_{CH}$ for 1.0-hr before adding the total mixture to RRL, we observed ~50% FLUC signal (compared to untreated FLUC expression), representing a 5-fold increase in expression compared to the antisense alone treatment (**Figure 3.2**, (**A**, case +, +)). Furthermore, increasing the sense annealing time to 3.0-hr we observed ~80% FLUC expression, which represents an 8-fold increase relative to the untreated control (**Figure 3.2**, (**B**, case +, +)). Unfortunately, upon the addition of sense γPNA$_{CH}$ we observe a 20% and ~55% off-target knockdown of RLUC signal, at 1.0-hr and 3.0-hr sense annealing times respectively. The reduced RLUC signal is likely due to off-target

binding of the right-handed sense domain. Thus, future designs may try different target

sites which would thus change the sequences of the probes to try and improve selectivity.
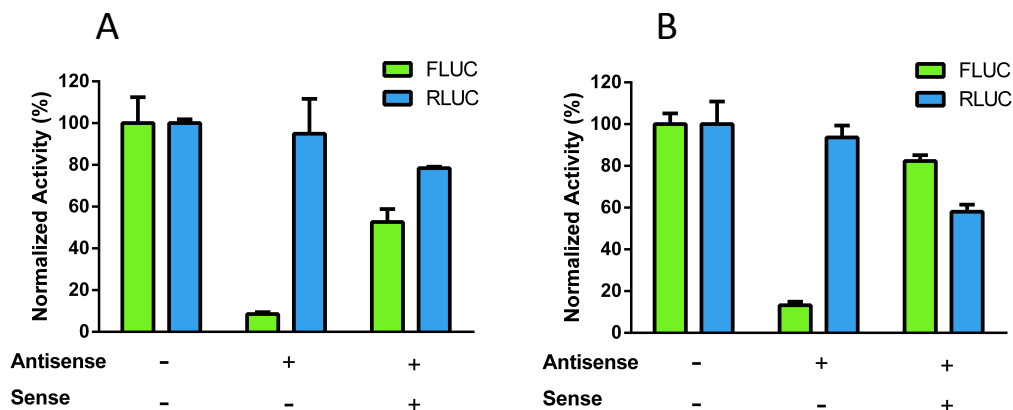
Figure 3.2 Chimeric γPNA reversible translation in cell free lysate. (**A.**) The addition of the antisense γPNA$_{CH}$ (100 nM, annealed 1.0-hr at 37 °C) inhibits ~90% firefly luciferase (FLUC) expression and ~5% *Renilla* luciferase (RLUC), see case (+, -). By sequentially incubating an equimolar amount of the sense γPNA$_{CH}$, for an additional 1.0-hr, ~50% FLUC and ~80% RLUC (~20% off-target knockdown) expression is observed, see case (+, +). (**B.**) Doubling the sense γPNA$_{CH}$ annealing time to 3.0-hr allows for >80% FLUC and ~55% RLUC expression respectively, see case (+, +). All annealing steps were performed at 37 °C with 10 nM of FLUC and RLUC, respectively. Data is plotted as n = 2 average ± SD.

3.2.2   Helical toehold-dependent reversible translation

We additionally investigated the dependence of the strand displacement reaction

on the chirality of the sense toehold. Sense γPNA$_{RH}$ contains the exact sequence

composition (including the miniPEG linker) as the sense γPNA$_{CH}$, but contains a right-

handed toehold (see **Table 3.1**). Although the antisense γPNA$_{CH}$ and the sense γPNA$_{RH}$

probes have 10-bases of helical and sequence complementarity, this complementary

domain is expected to be masked in the incumbent mRNA-antisense γPNA$_{CH}$ duplex

structure. Therefore, we hypothesized that the overall γPNA$_{CH}$-γPNA$_{RH}$ displacement

would be kinetically limited and dependent on a cognate toehold interaction. To test this,

we subsequently incubated either sense γPNA$_{CH}$ (helical and sequence complement) or a

control γPNA, named sense γPNA_{RH}, after pre-annealing to the antisense γPNA_{CH} (same

conditions as above) to the luciferase mRNA. After annealing, we introduced the entire

probe/mRNA (three components) mixture into the RRL translation cocktail to translate

over 90-minutes at 30 °C. After translation, we measured the total luciferase knockdown

of an antisense γPNA_{CH} only tube and the luciferase expression from the two sense cases

(chimeric or right-handed). To quantify the total recovery for the sense probes, we

calculated the fold-increase of luciferase activity relative to the knockdown in the

antisense γPNA_{CH} only tube. Unfortunately, and surprisingly, both sense probes

demonstrated similar levels of luciferase recovery across all sense annealing time tested

(**Figure 3.3**). Specifically, a similar level of translation recovery was observed,

irrespective of the toehold chirality (match or mismatch) and sense annealing times

applied (30-mins, 1.0-hr, and 3.0-hr). It may be that the annealing incubation time (even

at 30-minutes) coupled to the translation conditions (90-mins at 30 °C) may not allow

kinetic discrimination between sense γPNA_{CH} and sense γPNA_{RH}.
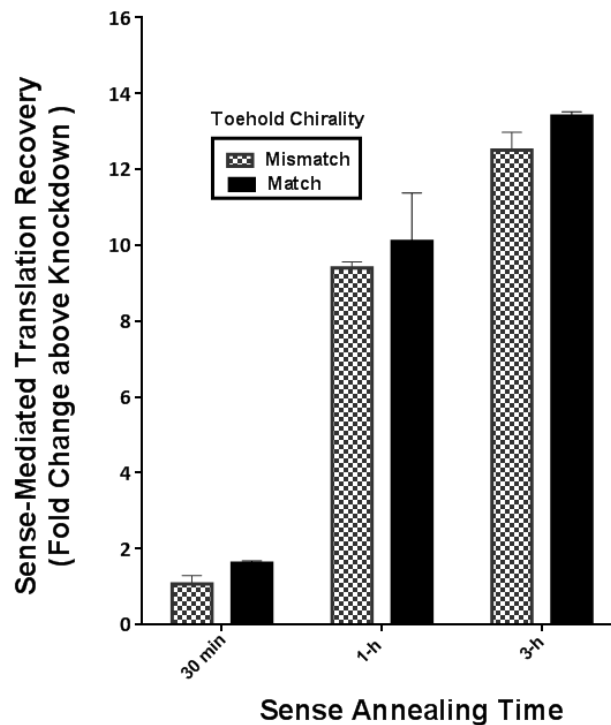
Figure 3.3 Translation recovery as a function of toehold chirality and annealing time. After antisense γPNA$_{CH}$ is annealed to the FLUC transcript (1.5-hr), either the sense γPNA$_{CH}$, which has the helically complementary toehold (black bar), or the toehold non-cognate sense γPNA$_{RH}$ (crosshatch bar) is introduced to the mixture, respectively. The sense strand incubation time is 30-min, 1-hr, or 3-hr. The sense annealing step was conducted on the bench top (room temperature). After the sense annealing step, the probe/mRNA mixture was placed into the RRL media for translation for 1.5-hr at 30 °C. Data is plotted as n = 3 average ± SD.

3.2.3   Analysis of γPNA$_{CH}$ strand displacement by SPR

Recently, we demonstrated a label-free method to measure toehold-mediated strand displacement using surface plasmon resonance (SPR). Here, the SPR method was applied to characterize both the γPNA$_{CH}$-γPNA$_{CH}$ and the orthogonal γPNA$_{RH}$-γPNA$_{CH}$ strand displacement. First, the antisense γPNA$_{CH}$ is injected over a biotinylated-DNA chip to measure the on-chip association of the antisense probe (measured in response units). The biotinylated-DNA is complementary to right-handed antisense γPNA$_{CH}$ domain and represents the same sequence as the FLUC mRNA target site. After duplex formation, the

antisense γPNA_{CH} left-handed toehold is unbound and provides access to downstream strand displacement (**Figure 3.4**, Chimeric Antisense). Strand displacement is mediated initially through a left-handed toehold nucleation, and then a right-handed branch migration. After a completed branch migration, strand displacement results in measurable antisense γPNA_{CH} mass loss from the chip (**Figure 3.4**, Branch Migration and Strand Displacement).
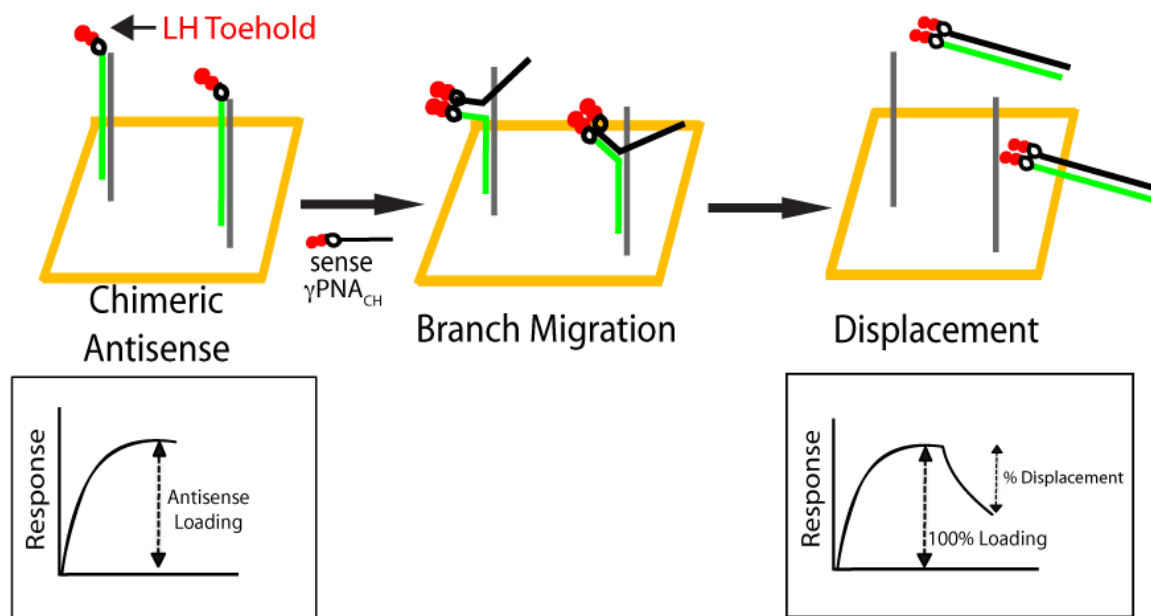
Figure 3.4 Surface plasmon resonance (SPR) method to measure γPNA_{CH}-γPNA_{CH} displacement. Step I (association phase): antisense γPNA_{CH} is loaded onto the SPR chip by binding surface DNA (grey). The left-handed toehold (red) is not bound. Step II (branch migration): The addition sense γPNA_{CH} (DNA protecting strand shown in grey) initiates toehold-mediated γPNA_{CH}-γPNA_{CH} branch migration (unresolvable by SPR) and completes strand displacement (Step III). After strand displacement, the DNA protector is displaced and the γPNAs are duplexed. The ratio of γPNA association versus mass loss due to displacement is calculated as the percent displacement.

The initial injection of 3 nM antisense γPNA_{CH} into the flow cell, followed by a titrated concentration (0-400 nM) of sense γPNA_{CH} resulted in a clear association and γPNA_{CH} -γPNA_{CH} dissociation signal (**Figure 3.5A**). The total sense-driven displacement (calc. % displacement) is calculated by dividing the displacement signal change (ΔRU S:CH) by the antisense γPNA_{CH} association signal (ΔRU AS:CH). The percent displacement increases as a function of sense γPNA_{CH} in a dose-dependent manner (**Figure 3.5B**). For example, at the 400 nM sense γPNA_{CH} injection, we observed ~45% antisense displacement. To demonstrate strand displacement as a function of toehold chirality, we again injected antisense γPNA_{CH} (3 nM) to bind to the surface displayed DNA target. The subsequent injection of a titrated concentration (0-400 nM) of sense γPNA_{RH} did not yield any measurable antisense strand displacement off the chip. We interpret the lack of antisense γPNA_{CH} displacement by sense γPNA_{RH} as indicative of a chiral mismatch between probes. Additionally, this result may support the above hypothesis that the required conditions (temperature) in the cell-free experiments are not ideal for observing the toehold-binding preferences.

Given the antisense γPNA_{CH} displacement has not completely saturated at 400 nM sense γPNA_{CH}, we presumed there may be some competitive off-target binding between the sense strand and immobilized DNA, thus saturating the total displacement amount near 50%, as seen in a prior set of γPNA SPR displacement experiments. However, when we directly injected the sense γPNA_{CH} over the immobilized DNA (no antisense hybridized to the DNA), we did not observe any measurable binding (**Figure 3.5**, **blue triangles**). Currently, the reason behind the 50% displacement saturation is unknown, but mass transport effects may be possible. For example, it may be that during the sense

injection there is limited mass transport (after displacement) of the γPNA-γPNA duplex away from the chip into the buffer flow. The rate of transport of the γPNA-γPNA duplex (in bulk) away from the chip is dictated by the flow geometry and the molecular diffusion coefficient of the duplex.[36] The rate of diffusion of a substance (γPNA-γPNA) is inversely proportionally to the molecular weight (radius of gyration), and, considering the γPNA-γPNA duplex molecular weight is ~13,000 g/mol, the diffusion for the duplex is slower than a single stranded γPNA. However, diffusion is inversely proportional to the cube root of the molecular weight, thus the diffusion coefficient difference between a single stranded γPNA and a γPNA-γPNA is small. Additionally, we considered if the flow velocity was limiting the rate of transport. Specifically, the rate of transport goes by the cube root of the flow velocity, thus very large changes in flow rate are required to increment the transport rate (e.g. a 2x increase in the rate of transport requires a 8x increase in flow velocity). Nevertheless, we conducted our SPR experiments at a relatively high flow rate (30 μL/min) to ensure the rate of transport was not the limiting factor in the displacement measurement. It is more likely that the saturation of displacement signal is an effect of weak (off-target) interactions between the injected sense strand and the chip surface and/or the immobilized DNA, thereby retaining mass at the chip surface. To test if the sense strand interacts with the chip, we directly titrated the sense γPNA$_{CH}$ over the immobilized DNA. Here, we did observe non-specific binding of the sense γPNA$_{CH}$ at the higher sense concentrations tested (**Figure 3.6**). We interpret that this non-specific interaction may be due to the formation of weak interactions between the homologous sense γPNA and immobilized DNA. Considering this, it should be possible to measure higher levels of percent displacement by performing the reaction

at higher temperature or simply by introducing a buffer wash step after the sense strand

injection to remove any weakly bound sense-chip interactions and the γPNA-γPNA

duplexes. This latter hypothesis is currently under investigation.
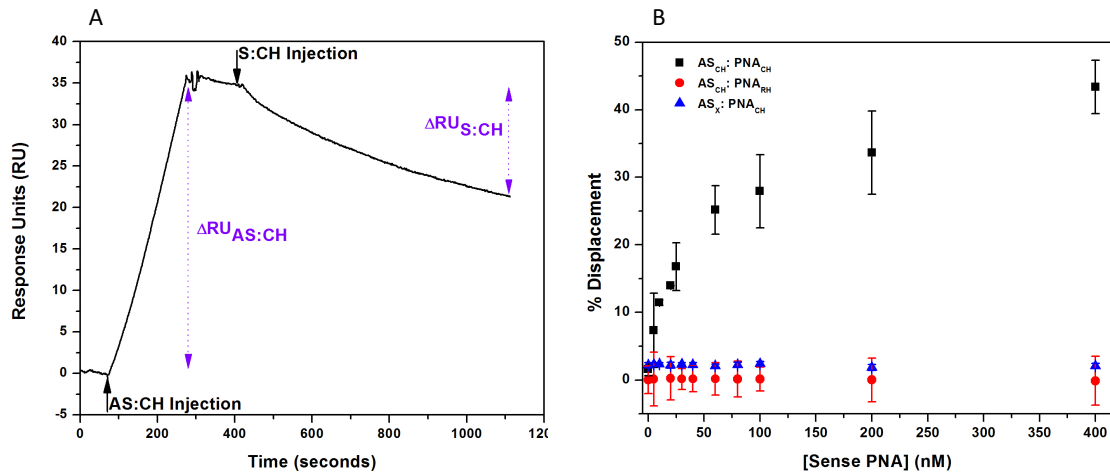
Figure 3.5 Quantifying chimeric strand displacement by SPR. (**A.**) Raw SPR data showing the initial association antisense γPNA$_{CH}$ ($\Delta RU_{antisense}$) and subsequent strand displacement by sense γPNA$_{CH}$ (ΔRU_{sense}). Calculation of percent displacement is performed by dividing ΔRU_{sense} by $\Delta RU_{antisense}$ (double head purple arrows). (**B.**) Dose response dependent antisense γPNA$_{CH}$ strand displacement by sense γPNA$_{CH}$. Calculated percent displacement from complementary γPNA$_{CH}$-γPNA$_{CH}$ pairs (black squares) is compared to percent displacement of antisense γPNA$_{RH}$ by sense γPNA$_{CH}$ (red circles). Data in B is plotted as n = 3 average ± SD.
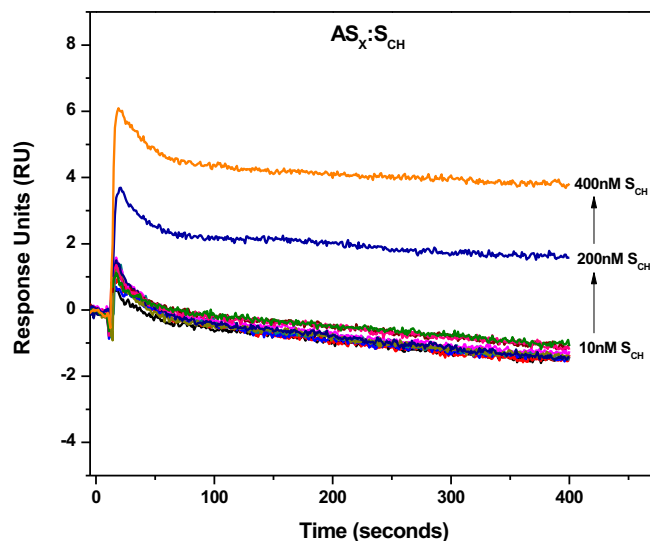
Figure 3.6 Non-specific binding of sense γPNA to an immobilized DNA target is evident at high concentration of sense γPNA.

3.2.4 Analysis of the γPNA$_{CH}$ probes by UV-vis and CD spectroscopy

γPNA$_{CH}$-γPNA$_{CH}$ (1:1 at 2.5 μM) duplex formation was analyzed by UV-vis melting. Given that there are two discrete helical domains within the chimeric probes, connected by a diethylene glycol linker, we hypothesized that the melting profile of the γPNA$_{CH}$-γPNA$_{CH}$ duplex may contain two melting transitions. Nevertheless, we did not observe a resolved sigmoidal melting transition(s) with the chimeric duplex. However, a monotonically increasing change in absorbance across increasing temperatures was observed (**Figure 3.7**). Specifically, we interpret the ~0.1 absorbance change to be evidence of chimeric duplex formation and not just due to the intramolecular melting of base stacking.
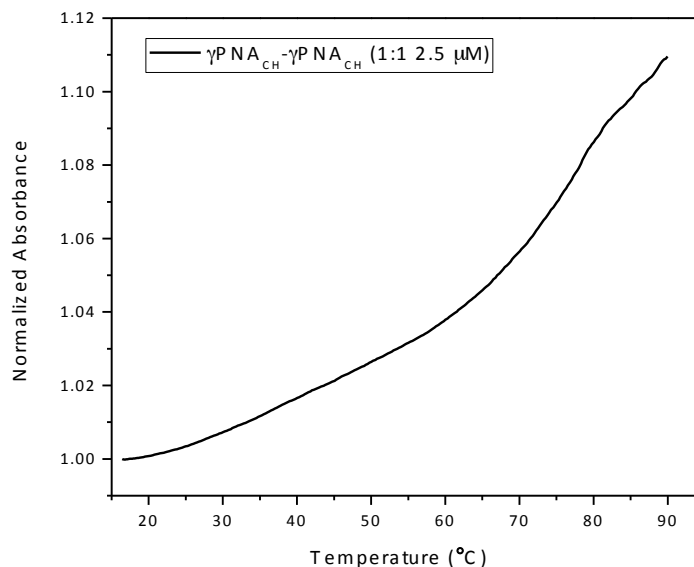
Figure 3.7 Thermal melting analysis of the γPNA$_{CH}$-γPNA$_{CH}$ duplex (1:1 at 2.5 µM).

Additionally, we analyzed the γPNA$_{CH}$-γPNA$_{CH}$ (1:1 at 2.5 µM) using circular dichroism (CD) to verify chimeric duplex formation. Although the chimeric probe design includes both a right- and left-handed domain, the right-handed domain contains 10-bases total, compared to the 6-left handed bases in the toehold domain, we expected to observe an overall right-handed CD signal for both the monomeric and duplex structures. The duplex demonstrated an attenuated exciton pattern with a minimum peak at ~280 nm, a crossover at ~260 nm, and a maximum at 265 nm, with, all of which are characteristic of a right-handed duplex (**Figure 3.8**). However, the duplex signal amplitude is quite attenuated and not well defined at lower wavelengths (<250 nm).
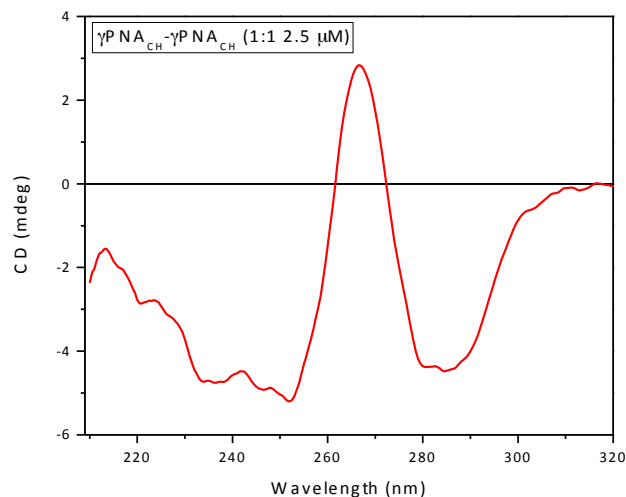
Figure 3.8 Circular dichroism of the γPNA$_{CH}$-γPNA$_{CH}$ duplex (1:1 at 2.5 µM).

To simply the analysis, we also investigated the CD profile of the monomeric antisense and sense γPNA$_{CH}$ probes. As expected, CD analysis of the individual antisense γPNA$_{CH}$ yielded an overall right-handed exciton pattern, with a maximum at ~268 nm and a minimum at ~245 nm (**Figure 3.9**). Unexpectedly, however, the sense γPNA$_{CH}$ yielded a slightly attenuated left-handed exciton pattern (**Figure 3.9)**. The left-handed sense γPNA$_{CH}$ chirality observed may be because the left-handed toehold domain is on the C-terminal end of the probe, thereby allowing for the sterically-mediated C-to-N helical transduction of the left-handed domain into the right-handed domain (i.e., the "sergeants-and-soldiers effect").[37] However, this process would require communication through the intervening diethylene glycol spacer, which seems unlikely.
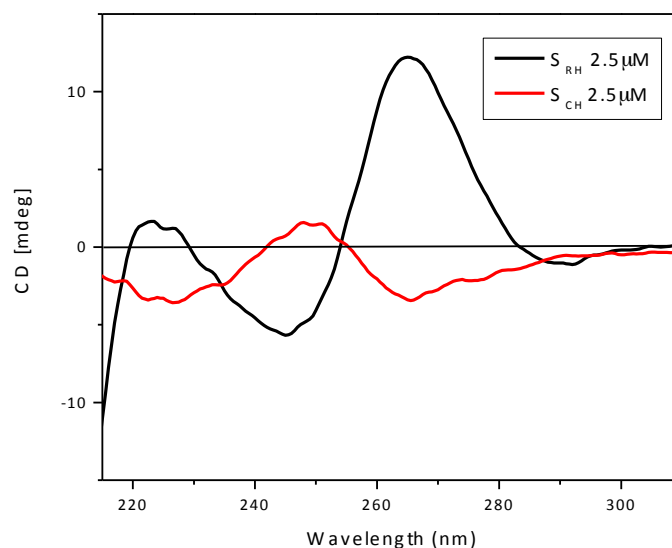
Figure 3.9 Circular dichroism of the antisense γPNA_{CH} (black) and sense γPNA_{CH} (red) tested at 2.5 μM.

To further investigate the sense γPNA_{CH} properties, we investigated the individual 10-mer right-handed "domain" and the individual 6-mer left-handed "toehold" within the sense γPNA_{CH}. To this end, we obtained a 10-mer γPNA with the same sequence and γ–substitution pattern as found in the sense γPNA_{CH} right-handed domain. Additionally, we studied a left-handed 6-mer γPNA with the same sequence and γ–substitution amount found in the sense γPNA_{CH} toehold handed domain. The analysis of the right handed 10-mer γPNA domain alone yielded an overall right handed signal on CD as expected (**Figure 3.10A**). Furthermore, the 6-mer left-handed γPNA also demonstrated the expected helicity, however the signal was jagged. As a control, we also investigated a right-handed γPNA 6-mer with the identical sequence and γ–substitution as the left-handed 6-mer γPNA. The 6-mer right-handed γPNA demonstrated a proportionally enantiomeric CD signal compared to the left-handed 6-mer, however, again, the signal is quite jagged (**Figure 3.10B**).
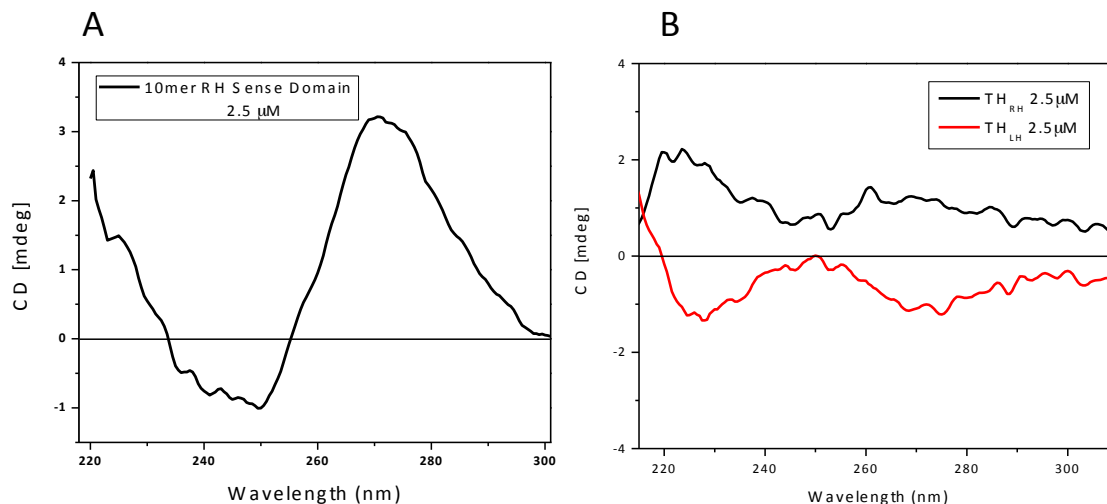
Figure 3.10 Circular dichroism of the γPNA chiral domains. (**A.**) Analysis of the right-handed 10-mer domain alone. (**B.**) Analysis of the 6-mer left- and right-handed domains individually. All probes concentrations are 2.5 μM.

3.3   Discussion

The construction of programmed bimolecular hybridizations, which depend on both sequence and helical complementarity, is an exciting expansion of nucleic acid recognition.[38] For example, the administration of left-handed probes can be used for unambiguous and selective interactions. Moreover, orthogonal recognition would be useful in improving the hybridization selectivity in complex settings (e.g., cells) where the potential of off-target binding is high. Given that the toehold-mediated strand displacement mechanism is leveraged in many *in vitro* and *in vivo* nucleic acid dynamic applications, we first wanted to show that the chimeric γPNA probes were capable of antisense knockdown and strand displacement-mediated recovery. To this end, we did observe potent firefly luciferase knockdown when applying antisense γPNA$_{CH}$ and

translation recovery through sense-mediated displacement (**Figure 3.2**). Furthermore, this result demonstrates that the presence of two helically chimeric internal domains is not a drastic impediment to intermolecular binding reactions.

However, our main objective in this project was to demonstrate strand displacement that depends on sequence *and* chiral complementarity, which we were unable to show in our cell free translation assay. Given that the sense-mediated strand displacement reaction should be kinetically limited by the incumbent structure (i.e., mRNA/antisense γPNA_{CH} duplex) it was expected that the helically-cognate toehold pairs should interact faster than the helical mismatch pairs, thus demonstrating kinetic discrimination within the expression recovery assay. Unfortunately, we observed a similar level of translation recovery irrespective of input sense toehold chirality and the total sense annealing time. The sense γPNA_{RH} does contain 10-bases of perfect sequence and helical complementarity to the antisense γPNA_{CH}, which suggests that duplex formation is thermodynamically favorable, and thus, is likely driving the displacement reaction forward. It is possible, that the antisense γPNA_{CH} is not stably bound to the mRNA target and is in a configurational-unstable duplex state, potentially due to the chimeric nature of the probe, thereby allowing for either of the two sense probes to achieve similar levels of displacement. The observation of all-around poor CD results, specifically the lack of clear signal and amplitude, demonstrates that the probe quality (e.g., monomer purity) is questionable. Nevertheless, moving forward with this project a complete re-order/re-design, with monomer optical purity verified, is warranted here. Additionally, given that we observed a left-handed CD signal with the sense γPNA_{CH}, it is worthwhile to investigate the role of the linker and domain placement in chimeric

designs, specifically as it relates to the overall helical structure and downstream bioactivity applications.

Fortunately, we achieved kinetic helical discrimination using SPR. The difference between the SPR and the cell free results may be due to the differences in the experimental conditions. Specifically, even with applying an abridged sense time annealing (the shortest used here is 30 minutes), the cell-free translation requires a 90-minute 30 °C incubation time, whereas the SPR is performed at room temperature. The time and temperature parameters used in the cell-free experiments may allow for indiscriminate antisense displacement and subsequent protein expression. This suggests that all hope is not lost on building chimeric probes in the future, however experimental conditions and probe quality should be closely considered to avoid ambiguous results.

3.4   Conclusion

In this chapter, we presented a different approach to achieve bimolecular strand displacement, which considered above all else, implementing a left-handed toehold domain to initiate the reaction. Some of the data contained in this chapter, specifically the SPR results, demonstrate that the "chimeric probe" strategy can indeed work. Nevertheless, there were some unexpected results that confounded the overall interpretation of the results. For example, the left-handed CD signal for the sense γPNA$_{CH}$ was unexpected of course, but also it is difficult to rationally account for. The CD measurement of the individual sense γPNA$_{CH}$ domains showed their expected signal (i.e., right or left), however the signals were particularly jagged. Thus, taking these factors into account, future chimeric work will likely need to "start fresh" with a new set

of probes for one, but also consider exploring different design implementations of the chimeric probe. For example, exploration of different linker lengths or compositions may be worthwhile to explore if this feature has any bearing on the CD signals and strand displacement selectivity. Ensuring the optical purity of the monomer batch, which is used in oligomer synthesis, is key for any future chimeric project. Additionally, adding/deleting or changing the chemical composition of the intervening linker should be considered and characterized on UV-vis/CD.

Although achieving a bioactive demonstration is important, it is not essential for the first demonstration of the chimeric probe system. The novelty is in the left-handed mediated strand displacement. Thus, if a future project revisits this work, I would advise shifting the focus to understand the biophysics of the displacement reaction. For example, the construction of a γPNA_{CH} complementary set that contained a quencher/dye pair to report on the strand displacement reaction would be beneficial. Employing this type fluorescent probe design would allow for an easier experimental platform to explore different probe composition effects (e.g., altering sequence, length, etc.). In short, once some of the basic "rules" for building and using chimeric PNAs are established, then research around bioactivity is appropriate.

3.5 Materials and Methods

3.5.1 γPNA probes and characterization

γPNA oligomers were obtained from PNA Innovations with HPLC purification. γPNA stock concentration was determined by measuring the oligomer absorption at 260 nm (collected at 95°C) and dividing by the following respective molar extinction coefficients:

Antisense γPNA_{CH} $\varepsilon = 161{,}300$ M^{-1} cm^{-1}

Sense γPNA_{CH} $\varepsilon = 171{,}500$ M^{-1} cm^{-1}

Sense γPNA_{RH} $\varepsilon = 171{,}500$ M^{-1} cm^{-1}

Right-handed 10-mer domain of Sense γPNA_{CH} $\varepsilon = 104{,}600$ M^{-1} cm^{-1}

Left-handed 6-mer domain of Sense γPNA_{CH} $\varepsilon = 66{,}900$ M^{-1} cm^{-1}

Right-handed 6-mer domain of Sense γPNA_{RH} $\varepsilon = 66{,}900$ M^{-1} cm^{-1}

3.5.2 Generation of RNA and in vitro protein synthesis in a rabbit reticulocyte lysate

The Renilla luciferase plasmid was ordered from Promega (pRL-CMV). The firefly luciferase plasmid was prepared following previously published technique.[35] The transcription reaction followed the Thermo Scientific conventional transcription protocol (50 μL final volume) and consistently gave high RNA product yield (~ 2.5 μM, determined via NanoDrop spectrophotometer). The transcription reaction was conducted at 37 °C for 2 hours. The transcription products were purified using the Thermo Scientific GeneJET RNA Cleanup and Concentration Micro Kit and concentration was measured using a NanoDrop spectrophotometer.

3.5.3 γPNA/mRNA annealing

The *γ*PNA (antisense and sense) and RNA were annealed together in the presence of 79 mM potassium chloride (designed to match the K^+ concentration in the rabbit reticulocyte lysate, RRL source) and DEPC-treated water. The RNA concentration for all translation experiments is set at 10 nM in the final translation reaction. The probe concentration varies depending on the desired final concentration of probe. The initial antisense probe is annealed at 37 °C for a user-defined duration. In the case of the reversible translation experiments, an additional pre-incubation time is given for sense γPNA displacement at 37 °C being careful to maintain the incubation salt concentration (79 mM).

3.5.4 Translation conditions and luciferase read out

The translation reaction was conducted using the Promega Luciferase Assay System (E1500) (rabbit reticulocyte lysate). The PNA concentration is determined by considering the 50 μL final translation reaction volume. The translation reaction is conducted at 37 °C for 2 hours. Immediately after, the samples are stored in ice to quench any further protein synthesis. Following the Promega Rabbit Reticulocye Lysate System technical manual, 5 μL lysate solution is mixed into 50 μL Promega Luciferase Assay Reagent (E1483) added to a Thermo Scientific Nunc 96 well plate (flat white). The bioluminescent reading was collected on a TECAN Infinite M1000 plate reader.

3.5.5 Surface plasmon resonance (SPR) analysis of the chimeric probes

All SPR experiments were performed on a Biacore T100 instrument (GE Healthcare) equipped with a four-channel sensor chip and all displacement data is presented in triplicate average. The commercially-available chip is coated with a carboxylmethyl dextran matrix that allows further functionalization with streptavidin via a standard NHS-EDC coupling procedure. Immobilization of streptavidin was continued until 6000 response units (RU) of the protein were captured on each of the four channels (flow cells). The final step of the sensor design involved non-covalent capture of the 5'-biotinylated DNA targets (~120 RU) on the respective flow cells bearing immobilized streptavidin.

Each experiment was preceded by injection of a solution containing 3 nM of the chimeric antisense γPNA oligomer for 400 s (flow rate = 30 μL/min). A dissociation time of 100 s was incorporated after the injection to allow for diffusion of unbound antisense oligomers from the sensor surface. The subsequent displacement assay was then performed by injecting a solution containing a fixed concentration of either the chimeric sense γPNA or the right handed sense control (flow rate = 30 μL/min) and monitoring the sensor response over 600 s. Each displacement cycle was ended by introducing a pulse of a regeneration cocktail (1 M NaCl, 10 mM NaOH) for 30 s at a flow rate of 50 μL/min. This cocktail serves to release any residual antisense/sense oligomers and is followed by a buffer injection (150 s, flow rate = 30 μL/min) to reestablish a baseline prior to the next displacement cycle. The sensogram data includes chip density and probe molecular weight corrections to allow for direct comparisons of the multiple runs. We established a quantitative estimate of the displacement reaction by the ratio of signal attenuation upon

introduction of the sense γPNA, ΔRU (sense), to enhancement upon introduction of the

complementary antisense γPNA, ΔRU (antisense) (Eqn. 1).

$$\% \text{ Displacement} \quad = \quad \frac{\Delta RU \text{ (sense)}}{\Delta RU \text{ (antisense)}} \quad \text{x } 100 \qquad (1)$$

3.6 References

1.   Chen, Y. J.; Groves, B.; Muscat, R. A.; Seelig, G., DNA nanotechnology from the test tube to the cell. *Nature Nanotechnology* **2015,** *10* (9), 748-760.
2.   Rudchenko, M.; Taylor, S.; Pallavi, P.; Dechkovskaia, A.; Khan, S.; Butler, V. P.; Rudchenko, S.; Stojanovic, M. N., Autonomous molecular cascades for evaluation of cell surfaces. *Nature Nanotechnology* **2013,** *8* (8), 580-586.
3.   Delebecque, C. J.; Lindner, A. B.; Silver, P. A.; Aldaye, F. A., Organization of Intracellular Reactions with Rationally Designed RNA Assemblies. *Science* **2011,** *333* (6041), 470-474.
4.   Douglas, S. M.; Bachelet, I.; Church, G. M., A logic-gated nanorobot for targeted transport of molecular payloads. *Science* **2012,** *335* (6070), 831-4.
5.   Yurke, B.; Turberfield, A. J.; Mills, A. P.; Simmel, F. C.; Neumann, J. L., A DNA-fuelled molecular machine made of DNA. *Nature* **2000,** *406* (6796), 605-608.
6.   Levesque, M. J.; Ginart, P.; Wei, Y.; Raj, A., Visualizing SNVs to quantify allele-specific expression in single cells. *Nature Methods* **2013,** *10* (9), 865-7.
7.   Hochrein, L. M.; Schwarzkopf, M.; Shahgholi, M.; Yin, P.; Pierce, N. A., Conditional Dicer substrate formation via shape and sequence transduction with small conditional RNAs. *Journal of the American Chemical Society* **2013,** *135* (46), 17322-30.
8.   Seelig, G.; Soloveichik, D.; Zhang, D. Y.; Winfree, E., Enzyme-free nucleic acid logic circuits. *Science* **2006,** *314* (5805), 1585-8.
9.   Frezza, B. M.; Cockroft, S. L.; Ghadiri, M. R., Modular multi-level circuits from immobilized DNA-based logic gates. *Journal of the American Chemical Societ* **2007,** *129* (48), 14875-9.
10.   Chen, X.; Ellington, A. D., Shaping up nucleic acid computation. *Current Opinion in Biotechnology* **2010,** *21* (4), 392-400.
11.   SantaLucia, J.; Hicks, D., The thermodynamics of DNA structural motifs. *Annual Review of Biophysics and Biomolecular Structure* **2004,** *33*, 415-440.
12.   Zadeh, J. N.; Steenberg, C. D.; Bois, J. S.; Wolfe, B. R.; Pierce, M. B.; Khan, A. R.; Dirks, R. M.; Pierce, N. A., NUPACK: Analysis and Design of Nucleic Acid Systems. *Journal of Computational Chemistry* **2011,** *32* (1), 170-173.
13.   Zhang, D. Y.; Seelig, G., Dynamic DNA nanotechnology using strand-displacement reactions. *Nature Chemistry* **2011,** *3* (2), 103-113.
14.   Zhang, D. Y.; Winfree, E., Control of DNA Strand Displacement Kinetics Using Toehold Exchange. *Journal of the American Chemical Society* **2009,** *131* (47), 17303-17314.
15.   Simmel, F. C.; Yurke, B., Using DNA to construct and power a nanoactuator. *Physical Review E* **2001,** *63* (4).
16.   Zhang, D. Y.; Chen, S. X.; Yin, P., Optimizing the specificity of nucleic acid hybridization. *Nature Chemistry* **2012,** *4* (3), 208-214.
17.   Wu, L. R.; Wang, J. S.; Fang, J. Z.; Evans, E. R.; Pinto, A.; Pekker, I.; Boykin, R.; Ngouenet, C.; Webster, P. J.; Beechem, J.; Zhang, D. Y., Continuously tunable nucleic acid hybridization probes. *Nature Methods* **2015,** *12* (12), 1191-+.
18.   Khodakov, D.; Wang, C. Y.; Zhang, D. Y., Diagnostics based on nucleic acid sequence variant profiling: PCR, hybridization, and NGS approaches. *Advanced Drug Delivery Reviews* **2016,** *105*, 3-19.

19. Vieregg, J.; Pierce, N. A., Selective Nucleic Acid Capture with Shielded Covalent Probes. *Biophysical Journal* **2014,** *106* (2), 617a-617a.

20. Dirks, R. M.; Pierce, N. A., Triggered amplification by hybridization chain reaction. *Proceedings of the National Academy of Sciences of the United States of America* **2004,** *101* (43), 15275-15278.

21. Roberts, R. W.; Crothers, D. M., Specificity and Stringency in DNA Triplex Formation. *Proceedings of the National Academy of Sciences of the United States of America* **1991,** *88* (21), 9397-9401.

22. Tsourkas, A.; Behlke, M. A.; Rose, S. D.; Bao, G., Hybridization kinetics and thermodynamics of molecular beacons. *Nucleic Acids Research* **2003,** *31* (4), 1319-1330.

23. Bonnet, G.; Tyagi, S.; Libchaber, A.; Kramer, F. R., Thermodynamic basis of the enhanced specificity of structured DNA probes. *Proceedings of the National Academy of Sciences of the United States of America* **1999,** *96* (11), 6171-6176.

24. Ackermann, D.; Famulok, M., Pseudo-complementary PNA actuators as reversible switches in dynamic DNA nanotechnology. *Nucleic Acids Research* **2013,** *41* (8), 4729-4739.

25. Wang, Z. H.; Zhang, K.; Shen, Y. F.; Smith, J.; Bloch, S.; Achilefu, S.; Wooley, K. L.; Taylor, J. S., Imaging mRNA expression levels in living cells with PNA center dot DNA binary FRET probes delivered by cationic shell-crosslinked nanoparticles. *Organic & Biomolecular Chemistry* **2013,** *11* (19), 3159-3167.

26. Ratilainen, T.; Norden, B., Thermodynamics of PNA interactions with DNA and RNA. *Methods in Molecular Biology* **2002,** *208*, 59-88.

27. Bruylants, G.; Boccongelli, M.; Snoussi, K.; Bartik, K., Comparison of the thermodynamics and base-pair dynamics of a full LNA:DNA duplex and of the isosequential DNA:DNA duplex. *Biochemistry* **2009,** *48* (35), 8473-82.

28. Jepsen, J. S.; Sorensen, M. D.; Wengel, J., Locked nucleic acid: A potent nucleic acid analog in therapeutics and biotechnology. *Oligonucleotides* **2004,** *14* (2), 130-146.

29. Nielsen, P. E., Peptide nucleic acid. A molecule with two identities. *Accounts of Chemical Research* **1999,** *32* (7), 624-630.

30. Dragulescu-Andrasi, A.; Rapireddy, S.; Frezza, B. M.; Gayathri, C.; Gil, R. R.; Ly, D. H., A simple gamma-backbone modification preorganizes peptide nucleic acid into a helical structure. *Journal of the American Chemical Societ* **2006,** *128* (31), 10258-67.

31. Sahu, B.; Chenna, V.; Lathrop, K. L.; Thomas, S. M.; Zon, G.; Livak, K. J.; Ly, D. H., Synthesis of conformationally preorganized and cell-permeable guanidine-based gamma-peptide nucleic acids (gammaGPNAs). *Journal of Organic Chemistry* **2009,** *74* (4), 1509-16.

32. Delgado, E.; Bahal, R.; Yang, J.; Lee, J. M.; Ly, D. H.; Monga, S. P., beta-Catenin knockdown in liver tumor cells by a cell permeable gamma guanidine-based peptide nucleic acid. *Current Cancer Drug Targets* **2013,** *13* (8), 867-78.

33. Sacui, J.; Hsieh, W. C.; Manna, A.; Sahu, B.; Ly, D. H., Gamma Peptide Nucleic Acids: As Orthogonal Nucleic Acid Recognition Codes for Organizing Molecular Self-Assembly. *Journal of the American Chemical Society* **2015,** *137* (26), 8603-8610.

34. Chang, D.; Lindberg, E.; Winssinger, N., Critical Analysis of Rate Constants and Turnover Frequency in Nucleic Acid-Templated Reactions: Reaching Terminal Velocity. *Journal of the American Chemical Society* **2017,** *139* (4), 1444-1447.

35.   Canady, T. D.; Telmer, C. A.; Oyaghire, S. N.; Armitage, B. A.; Bruchez, M. P., In Vitro Reversible Translation Control Using gammaPNA Probes. *Journal of the American Chemical Society* **2015,** *137* (32), 10268-75.

36.   Schuck, P.; Zhao, H., The role of mass transport limitation and surface heterogeneity in the biophysical characterization of macromolecular binding processes by SPR biosensing. *Methods in Molecular Biology* **2010,** *627*, 15-54.

37.   Green, M. M.; Peterson, N. C.; Sato, T.; Teramoto, A.; Cook, R.; Lifson, S., A Helical Polymer with a Cooperative Response to Chiral Information. *Science* **1995,** *268* (5219), 1860-1866.

38.   Manicardi, A.; Corradini, R., Effect of chirality in gamma-PNA: PNA interaction, another piece in the picture. *Artifical DNA PNA XNA* **2014,** *5* (3), e1131801.

Chapter 4: Improved Kinetic Target Discrimination by a Structured γPNA

4.1 Introduction

High affinity recognition and accurate discrimination of nucleic acids can provide clinical utility in the form of diagnosis, monitored prognosis, and guided treatment.[1-5] In addition to clinical applications, nucleic acid technologies are commonly used to profile[6, 7] or perturb[8, 9] gene expression in single cells or blood, providing the researcher with genotype or mechanism related information. Nevertheless, the construction and application of a hybridization method which operates robustly under physiological conditions and can discriminate between closely related sequences remains a challenge.[10] Appling temperature or chemical denaturing stringency methods can be an effective way to increase probe-target selectivity, but the results are not always consistent and this method is limited to *in vitro* systems.[11]

An attractive probe demonstrates high selectivity while yielding a sufficient (beyond a defined diagnostic threshold) on-target binding. To maximize selectivity, an ideal free energy change for the probe-perfect match target would be small ($\Delta G \approx 0$), to ensure a positive free energy change in the probe-mismatch, even for the less (~1-2 kcal/mol) destabilizing T-G, G-G, and G-A mismatches.[12, 13] Designing probe systems that meet these thermodynamic requirements can be challenging, especially when considering factors such as solution salinity, temperature and target concentration can all effect the hybridization thermodynamics. Additionally, considering sensitivity is

paramount in low-copy target identification, the researcher can face a difficult balance between selectivity and affinity.

In addition to the application of nanomaterials[14] (e.g., nanoparticles, DNA nanostructures, nanowires, and surface electrodes) in nucleic acid detection, a promising approach in hybridization technology has been to engineer the molecular probe directly through the incorporation thermodynamic parameters in probe design.[15] The incorporation of intra- or intermolecular probe structure serves to lower the free energy change of all possible hybridization reactions. Consequently, targets are discriminated by an impeding thermodynamic barrier within the probe, which can only be overcome by the perfect match complement. For example, in molecular beacons, and stringency-clamped triplex forming oligonucleotides, a portion of the target complementary sequence within the probe is "masked" by an *intramolecular* stem structure that serves to mitigate the hybridization free energy change to both perfect and mismatch targets.[16-18] The molecular beacon is structurally engineered to increase the reaction free energy difference between the probe-perfect match and probe-mismatch targets ($\Delta\Delta G$) by incorporating an internal competitor domain.[19, 20]

Additionally, probes with *intermolecular* structure that can rearrange upon target binding, resulting in a single strand dissociation event (dissociative probes), have also been used to increase hybridization selectivity.[12, 21, 22] In general, dissociative probes are composed of two partially-complementary single strands that form a duplex with a single-stranded overhang domain. The internal duplex domain (branch migration region) confers enhanced target discrimination properties through thermodynamic gating/screening of invading base-pairs. The overhang (toehold) domain serves to

recognize the target and initializes the strand displacement of the competitor strand. This strand output can serve as an input to downstream a dissociative probe(s) to perform programmed or "sensed" molecular computation, mechanical actuation, and biomolecule amplification.[23] The length and sequence of the overhang can be tuned to alter the hybridization kinetics over a factor of 10^6 (1 M^{-1s-1} to $10^6\,M^{-1s-1}$).[21, 24] These features, in combination with computational tools[25] which allow for performing design-test cycles *in silico*, have allowed for the engineering of DNA probes with defined thermodynamic and kinetic behavior.[21]

The same molecular engineering principles detailed above have also be applied to 'non-natural' nucleic acids probes, such as peptide nucleic acid (PNA). For example, self-complementary PNA hairpin formation with subsequent PNA single-stranded and stem-loop DNA recognition has been confirmed.[26, 27] Additionally, stem-containing[28] and stem-less[29, 30] PNA-based molecular beacons studies have demonstrated improved (relative to DNA molecular beacons) binding selectivity and affinity. In the case of stemless PNA molecular beacons, target selectivity is achieved through the energetic cost of transitioning the PNA structure from a collapsed globular state (via PNA neutral backbone and hydrophobic bases) to a linear duplex state. In addition, toehold-mediated DNA-PNA and PNA-PNA dissociative probes have been constructed for mRNA imaging *in vivo* and *in vitro* translation control.[31, 32] In short, the above examples, do incorporate structure and toehold elements into PNA, however these studies were either not designed to understand/stdudy PNA selectivity directly or lack a clear description of design rules to achieve high PNA selectivity. Nevertheless, given PNAs broad use in molecular diagnostics (e.g. FISH,[33, 34] PCR clamping,[35, 36] sandwich hybridization,[37, 38] and

electrochemical readout[39, 40]) and as a bioactive probe (e.g., antigene,[41, 42] antisense,[43-45], antisplice,[46] antimiR,[47] and gene editing[48]), providing a highly tunable method to enhance PNA selectivity would be beneficial.

PNA confers several advantages over DNA/RNA systems which encourage its continued research and application in biotechnology. PNA is highly stable against proteases and nucleases due to its non-natural backbone.[49] Furthermore, due to its uncharged backbone, PNA demonstrates high DNA/RNA affinity.[49, 50] In addition, a newer generation of γ–modified PNA derivatives (γPNA), developed by Ly and coworkers, has demonstrated additional physiochemical enhancements.[51,52] γPNA is preorganized into a rigid helix (B-form like), which confers a lower entropic penalty during hybridization to helical DNA/RNA, thus improving affinity. Furthermore, γPNA displays enhanced selectivity (relative to PNA), likely due to the limited configurational freedom of the backbone, which is a necessary feature to enable mismatch tolerance.[13, 53] However, as observed previously,[37] γPNA selectivity is dependent on the target mutation placement, thus for all but the most centrally located target mutations (e.g., distal mutations on the target strand are difficult to discriminate against) the necessary γPNA design to achieve high target discrimination can be obscure.

To this end, we aimed to improve γPNA binding selectivity by incorporating competing internal structure, which has conferred high selectivity in molecular beacons and dissociative probes. In a proof-of-concept approach, we developed a γPNA probe with intramolecular stem-loop and an overhang domain and characterized the binding selectivity to single mismatched targets. Thus, we combined structural features found in DNA molecular beacons and dissociative probes into γPNA design. Importantly, our

chosen method to increase γPNA selectivity relies on already established principles, and

as such, this strategy can be easily generalized to any γPNA-target interaction.

4.2 Results

In this work, we demonstrate improved binding selectivity of γPNA by introducing

the intramolecular structure. Furthermore, we investigated γPNA selectivity in several

contexts. First, using surface plasmon resonance (SPR), we investigated the

thermodynamic and kinetic relationship between γPNA structure and single mismatch

discrimination. Moreover, we considered different mutation types and placement relative

to the structured γPNA binding domain (overhang). Subsequently, we compared the

selectivity of a linear unstructured γPNA to a structured γPNA in an antisense assay, an

application where PNA is commonly applied.

4.2.1 γPNA binding discrimination on SPR

To improve the binding selectivity between perfect and mismatch targets, we

designed a γPNA probe with a 10-mer target complementary domain, an internal ethylene

glycol repeating loop, and a 5-mer unmodified PNA domain that forms a 5-mer

intramolecular stem 'mask' (**Table 4.1**, struc_γPNA). We specifically chose to construct

the stem to be composed of γPNA-PNA because we wanted to increase the likelihood

that this domain would be displaced by the invading DNA target. We speculated that if

we used a γPNA-γPNA stem, the affinity would be too high for efficient DNA-mediated

invasion. We additionally tested an unstructured 10-mer γPNA (**Table 4.1**, unstruc_γPNA)

to compare the struc_γPNA binding and selectivity. We distinguished two targeting

domains within the γPNAs: a 5-mer overhang domain (also called a "toehold") and a

concatenated 5-mer stem domain. Struc_γPNA has a stem-loop, whereas the

unstruc_γPNA does not. The hybridization between the struc_γPNA and target initiates at

the 5-base overhang domain. Permitting a stable overhang interaction, the target bases

invade into the struc_γPNA 5-base stem structure. In short, the intramolecular stem

functions to introduce a thermodynamic competitor to the invading target sequence.

Table 4.1 γPNAs and target sequences used in SPR experiments[a]

Sequence Name	Sequence[a]	Mismatch
Structured γPNA (struc_γPNA)	NH2-K-TCTGGGTTCG-eg8-cgaac-H	
Unstructured γPNA (unstruc_γPNA)	NH2-K-TCTGGGTTCG-H	
Perfect Match (PM)	5'-AGACCCAAGC-3'	
Stem Mismatch (S-MM-7T)	5'-AGACCC**T**AGC-3'	(**T**-T)
Stem Mismatch (S-MM-6A)	5'-AGACC**A**AAGC-3'	(**A**-G)
Stem Mismatch (S-MM-7G)	5'-AGACCC**G**AGC-3'	(**G**-T)
Overhang Mismatch (O-MM-4A)	5'-AGA**A**CCAAGC-3'	(**A**-G)
Overhang Mismatch (O-MM-3T)	5'-AG**T**CCCAAGC-3'	(**T**-T)
Overhang Mismatch (O-MM-4T)	5'-AGA**T**CCAAGC-3'	(**T**-G)

a. Mutations are in bold.

We anticipated the overhang and stem mutations would lead to decreased probe

binding (relative to the perfect match) by struc_γPNA because of mismatch-mediated

destabilization. However, the loss in struc_γPNA affinity is compensated for in the gain

of selectivity against mismatched targets. In contrast, we hypothesized that unstruc_γPNA would demonstrate increased binding affinity (relative to struc_γPNA) due to the lack of any competing internal structure, however at the cost of selectivity.

We designed a series of single mismatch targets to investigate unstruc_γPNA and struc_γPNA binding selectivity using surface plasmon resonance (SPR) (**Figure 4.1**). The biotinylated-DNA targets are immobilized onto a streptavidin-functionalized chip and the γPNAs are injected at a single concentration. Specifically, by measuring the γPNA rate of association (i.e., probe on-rate) to a series of mutation targets, unstruc_γPNA and struc_γPNA kinetic discrimination can be compared to each other. The DNA targets to contain single mutations, which correspond to the overhang or stem binding domain of struc_γPNA (**Table 4.1**). Furthermore, to compare the effect of the overhang and stem mutations on binding selectivity, we designed mutated target pairs which contain the same mutation, but placed in either the overhang or stem binding domain. For example, O-MM-3T and S-MM-7T both result in a T-T mismatch with the γPNA's, but occur in the overhang or stem domain, respectively.
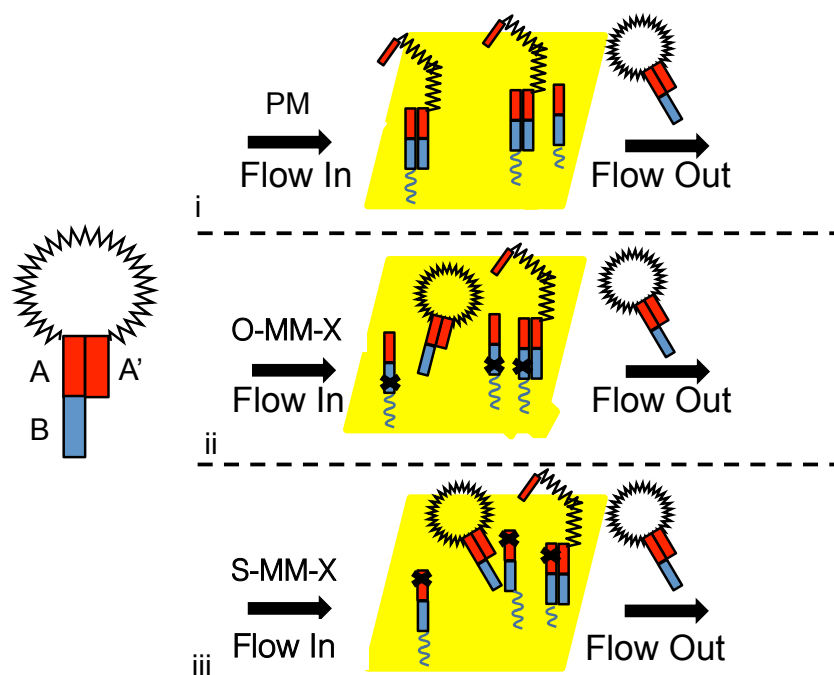
Figure 4.1 Direct binding of γPNA-target measured by surface plasmon resonance (SPR). Structured γPNA shown on left with overhang (B, blue), stem (A, red) and complementary stem (A', red) domains shown. Unstructured γPNA (not shown) is composed of the overhang (B) and stem (A) domains only. To characterize probe-target binding, the γPNAs (individually) are injected over the immobilized perfect match (PM), overhang mismatch (O-MM-X), or stem mismatch (S-MM-X) targets.

Following the above SPR procedure, struc_γPNA demonstrated slower target association relative to unstruc_γPNA (**Figure 4.2**). The slow association kinetics was evidenced across a range of struc_γPNA concentrations and quantified by measuring the on-rate slope (time span: 80s-100s) at each probe concentration (10, 15, 20, and 25 nM). Considering struc_γPNA initiates target hybridization through the 5-base overhang, a mutation placed in this domain is likely to discourage stable binding. In contrast, unstruc_γPNA can bind the target through any subset of its single stranded 10-bases. Moreover, after overhang domain "nucleation", the downstream stem structure further

impedes the struc_γPNA/target association kinetics. Compared to the perfect match, all

the mutations studied attenuated struc_γPNA and unstruc_γPNA binding (as measured by

the max SPR response).
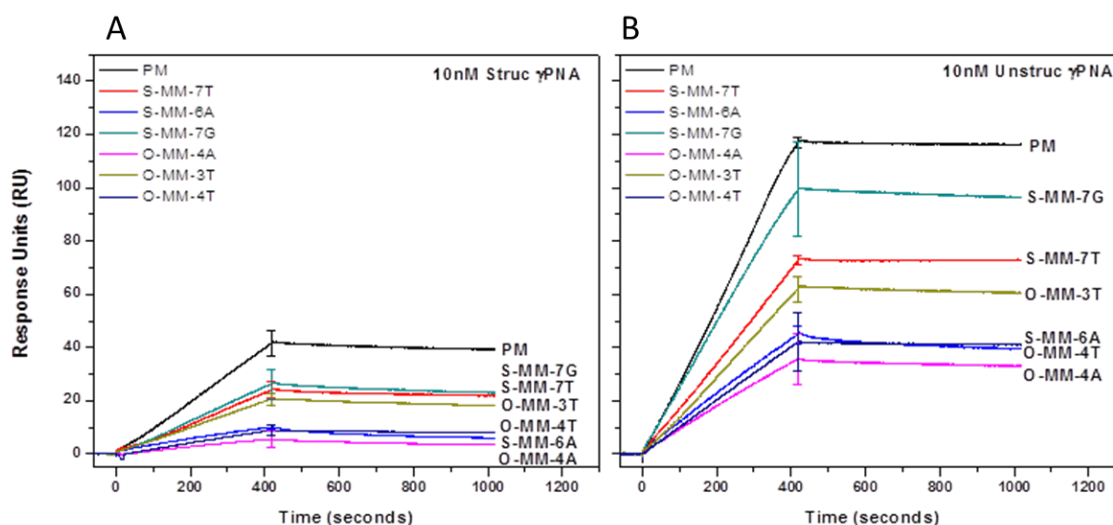
Figure 4.2 Direct binding SPR sensograms for (**A.**) struc_γPNA (10 nM) and (**B.**) unstruc_ γPNA (10 nM). DNA target sequences are given in Table 1.1. All data is plotted as n = 3 average ± SD.

Struc_γPNA demonstrated higher target discrimination compared to

unstruc_γPNA. Specifically, we divided the perfect match association by the individual

mutation target association (measured in response units and taken at the highest

association amount), to calculate the fold-difference in binding discrimination of the

struc_γPNA and unstruc_γPNA, respectively. Here, we observed O-MM-4A is the

highest discriminated target, demonstrating a steady ~7.5-fold selectivity ratio, when

using struc_γPNA across a range of concentrations (**Figure 4.3A**). Unstruc_γPNA also

discriminated against O-MM-4A at lower probe concentrations (~3.5-fold at

[Unstruc_γPNA] = 10 nM) as well, but the selectivity ratio declines as the probe

concentration increases (**Figure 4.3B**). For example, at 25 nM unstruc_γPNA displays

~1.5-fold selectivity against O-MM-4A. In addition, struc_γPNA maintained high

selectivity against S-MM-6A and O-MM-4T, with calc. >2.5-fold selectivity at all probe

concentrations. In contrast, unstruc_γPNA demonstrated ~2.75-fold discrimination

against S-MM-6A and O-MM-4T at the lowest probe concentration tested (10 nM), but

the selectivity fell to ~1.25-fold at 25 nM. Besides the ~1.25-fold selectivity of the

struc_γPNA at 25 nM against O-MM-3T, struc_γPNA demonstrated at least 1.5-fold

selectivity across all targets and probe concentrations. In contrast, unstruc_γPNA displays

less than 2.0-fold mutation selectivity against all targets (at 25 nM).
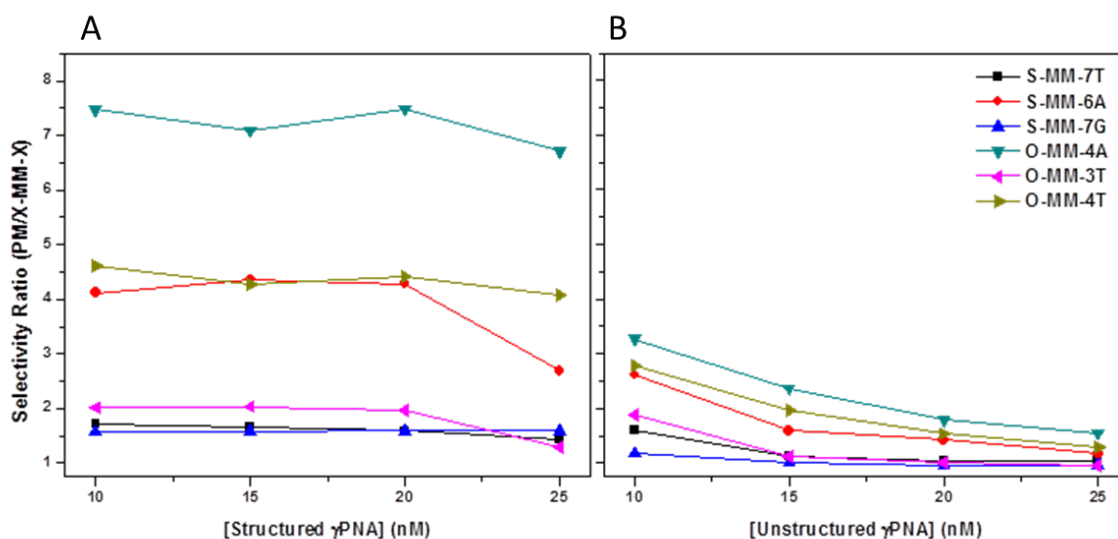
Figure 4.3 Selectivity ratio of (**A.**) struc_γPNA and (**B.**) unstruc_γPNA as determined by dividing the association max (max response units (RU) in Figure 1.2) of the perfect match to each respective target mutant association max.

The kinetic discrimination potential of struc_γPNA is further supported by comparing

the probe-target on-rate slopes (time span: 80s-100s) (**Figure 4.4**). Here, by dividing the

probe/perfect match on rate by the on rate relative to the probe/mutation case, the binding

selectivity (kinetic) can be compared as well. At 20 nM struc_γPNA displayed ~6.25 fold

on-rate difference between O-MM-4A and PM (**Figure 4.5A**). The same mutation

comparison relative to unstruc_γPNA (20 nM) represents only ~3.0-fold change (**Figure

4.5B**). The discrimination achieved against O-MM-4A seems to be related to the

mutation placement central within the overhang. Indeed, O-MM-4T, which contains the

identical mutation placement demonstrated high discrimination as well. In addition,

struc_γPNA did not achieve similar levels of discrimination against S-MM-7G, which

like O-MM-4T, leads to a wobble mutation base pair. Although these results demonstrate

the advantage of using structured probes to improve selectivity, they also suggest careful

consideration of mutational placement should be considered in structure probe design.

For example, it appears that building probes which can "process" (e.g., discriminate) the

mutation directly at the overhang (toehold) domain is likely a faithful design heuristic to

achieve high selectivity.
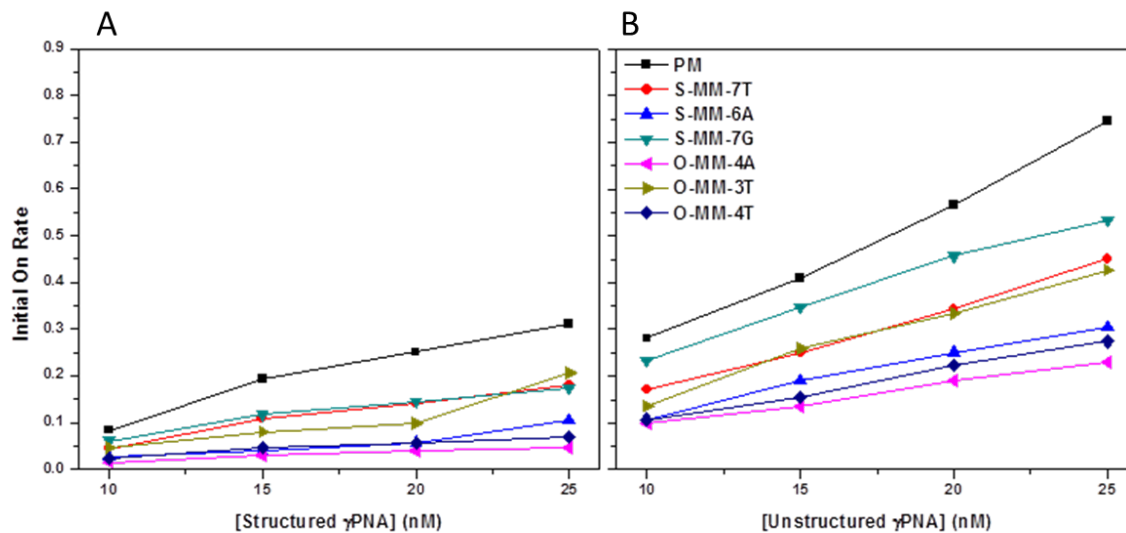
Figure 4.4 Rate of probe-targe association (on-rate) of (**A.**) struc_γPNA and (**B.**) unstruc_γPNA to the various target sequences. On-rate is value is determined by calculating the slope of probe-target association between 80-100s. All data is plotted as $n = 3$ average ± SD.
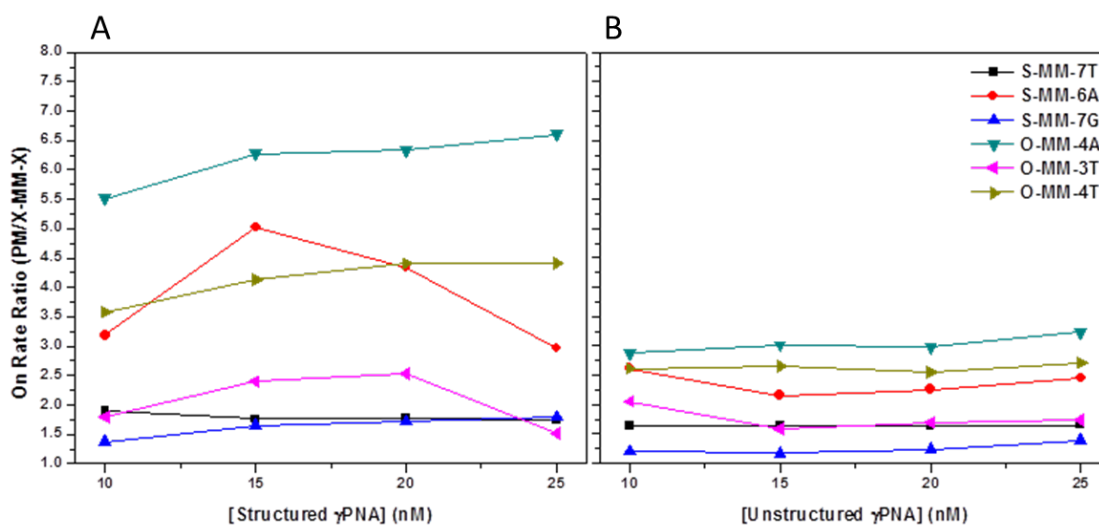
Figure 4.5 Selectivity ratio of (**A.**) struc_γPNA and (**B.**) unstruc_γPNA as determined by dividing the on rate of the perfect match to each respective target on rate.

4.2.2 γPNA-target melting analysis

We analyzed the thermal binding stability of O-MM-4A and O-MM-4T to unstruc_γPNA and unstruc_γPNA, respectively, to further investigate the difference in binding selectivity observed on SPR. These targets are interesting to study because they have the same mutation placement, but of course, different mutation type. We observed both mutation targets generated a decrease in melting temperature (T_m), measured at 260 nm, relative to the perfect match (**Figure 4.6**). Furthermore, an ~24 °C T_m difference was observed between unstruc_γPNA/O-MM-4A and unstruc_γPNA/PM, whereas unstruc_γPNA/O-MM-4T and unstruc_γPNA/PM had an ~16 °C T_m difference.
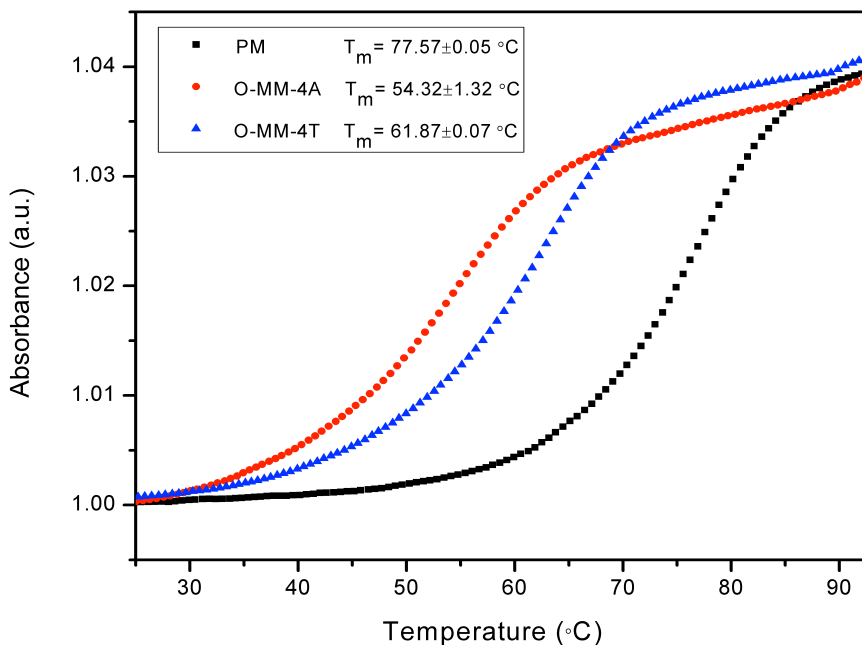
Figure 4.6 UV-vis melting analysis of unstruc_γPNA/O-MM-4T and unstruc_γPNA/O-MM-4A, and unstruc_γPNA/PM. All samples contained 2 μM DNA and 2 μM unstruc_γPNA in 100 mM NaCl, 10 mM Tris-HCL (pH = 7.4), and 0.1 mM Na_2EDTA. Absorbance was measured at 260 nm.

We also analyzed the hybridization stability of struc_γPNA to the O-MM-4A, O-MM-4T, and PM targets. Struc_γPNA/O-MM-4A demonstrated ~7 °C lower melting stability than struc_γPNA/O-MM-4T. However, both mutation cases resulted in at least ~24 °C decrease in melting temperature relative to the struc_γPNA/PM case. Additionally, we analyzed the melting temperature of the stem-loop structure within struc_γPNA. Specifically, given the relatively large G-C content of stem-loop structure with struc_γPNA, we monitored the temperature denaturation process at 275 nm (cytosine shifts the maximum absorption to 280 nm[27]). The melting temperature transition was found to be independent of struc_γPNA concentration over a 10-fold concentration range (**Figure 4.8**). Moreover, the melting transition of the stem-loop structure within struc_γPNA is below the bimolecular melting temperature of both struc_γPNA/O-MM-4A and struc_γPNA/O-MM-4T, thus we only observe a single transition in the melting plots shown in **Figure 4.7**.
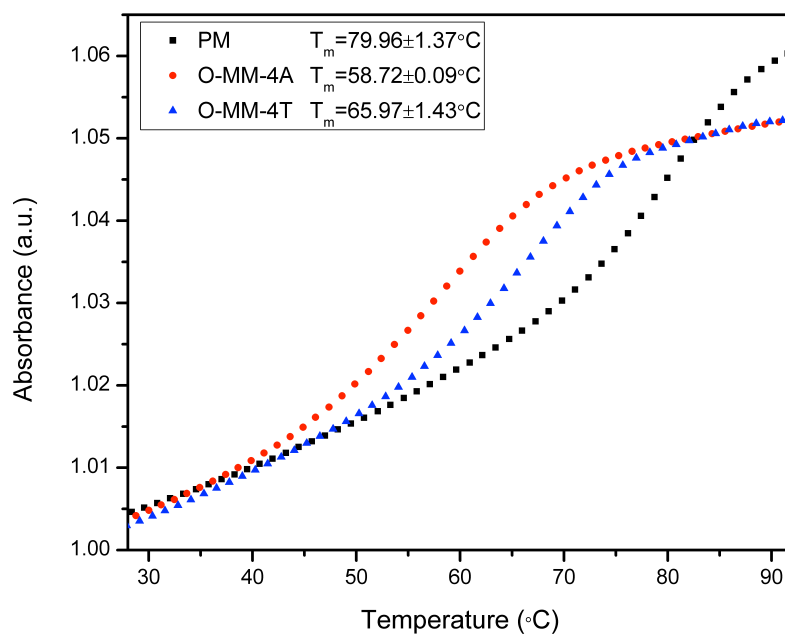
Figure 4.7 UV-vis melting analysis of struc_γPNA/O-MM-4T, struc_γPNA/O-MM-4A, and struc_γPNA/PM. All samples contained 2 µM DNA and 2 µM unstruc_γPNA in 100 mM NaCl, 10 mM Tris-HCL (pH = 7.4), and 0.1 mM Na$_2$EDTA. Absorbance was measured at 260 nm.
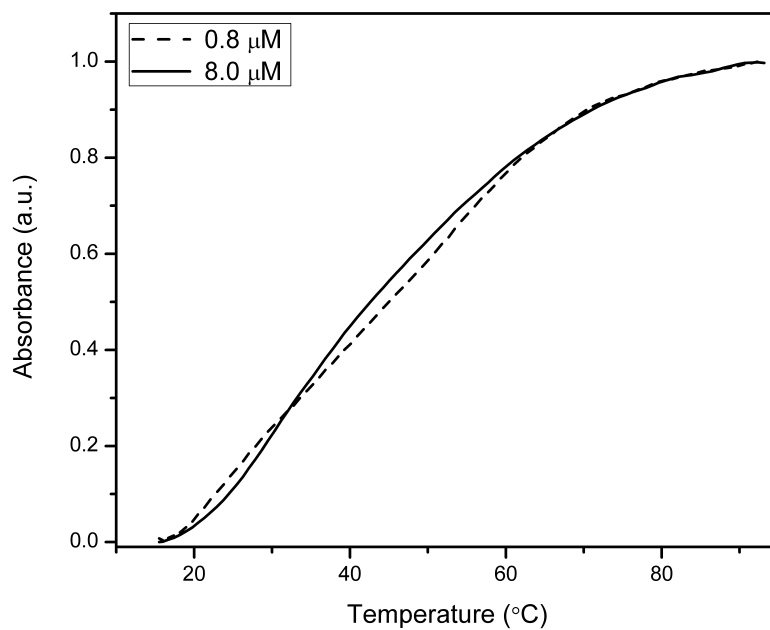
Figure 4.8 UV-vis melting analysis of struc_γPNA. Samples were measured in 100 mM NaCl, 10 mM Tris-HCL (pH = 7.4), and 0.1 mM Na$_2$EDTA. Absorbance was measured at 275 nm.

4.2.3 γPNA antisense knockdown and target selectivity

Both γPNAs are complementary to a 10-mer site at the 5'-UTR terminal end of a firefly luciferase (Fluc) mRNA, which has previously been shown to be a potent antisense target site. Additional to the perfect match target, we introduced an overhang mutation (**Table 4.2**, O-MM-4A) and a stem mutation (**Table 4.2**, S-MM-7U) to the luciferase transcript to test γPNA selectivity.

Table 4.2 Firefly luciferase mRNA targets[a]

Sequence Name	Sequence[a]	Mismatch Type
Perfect Match (PM)	5'-AGACCCAAGC-3'	
Stem Mismatch (S-MM-7U)	5'-AGACCC**U**AGC-3'	(**U**-T)
Overhang Mismatch (O-MM-4)	5'-AGA**A**CCAAGC-3'	(**A**-G)

a. Mutations are in bold.

To compare the antisense activity of the γPNAs, we annealed titrating amounts of unstruc_γPNA and struc_γPNA to the Fluc mRNA targets (individually) for 1-hour at 37 °C prior to luciferase expression in rabbit reticulocyte lysate (RRL) (**Figure 4.9A**). As expected unstruc_γPNA had higher antisense activity (IC_{50} = 45 nM), compared to struc_γPNA (IC_{50} = 131 nM) (**Figure 4.9B**). We interpret the ~3-fold difference in antisense potency to be the result of the decreased affinity of struc_γPNA. The two independent mutations in the mRNA decreased antisense knockdown for both probes relative to the perfect match. In the case of the stem mutation (S-MM-7U), both unstruc_γPNA (IC_{50} = 78 nM) and struc_γPNA (IC_{50} = 239 nM) demonstrated a ~2-fold

decrease in antisense efficacy, as compared to the perfect match. A further decrease in the antisense potency was observed for the overhang mutation in both struc_γPNA (IC_{50} = 340 nM) and unstruc_γPNA (IC_{50} = 84 nM). We did not observe a pronounced difference in unstruc_γPNA antisense efficiency against the two mismatched targets, as compared to struc_γPNA, likely due to the same probe/mRNA duplex length allowed (6 bases can bind the probe beyond the mutation) in both the O-MM-4A and S-MM-7U cases.
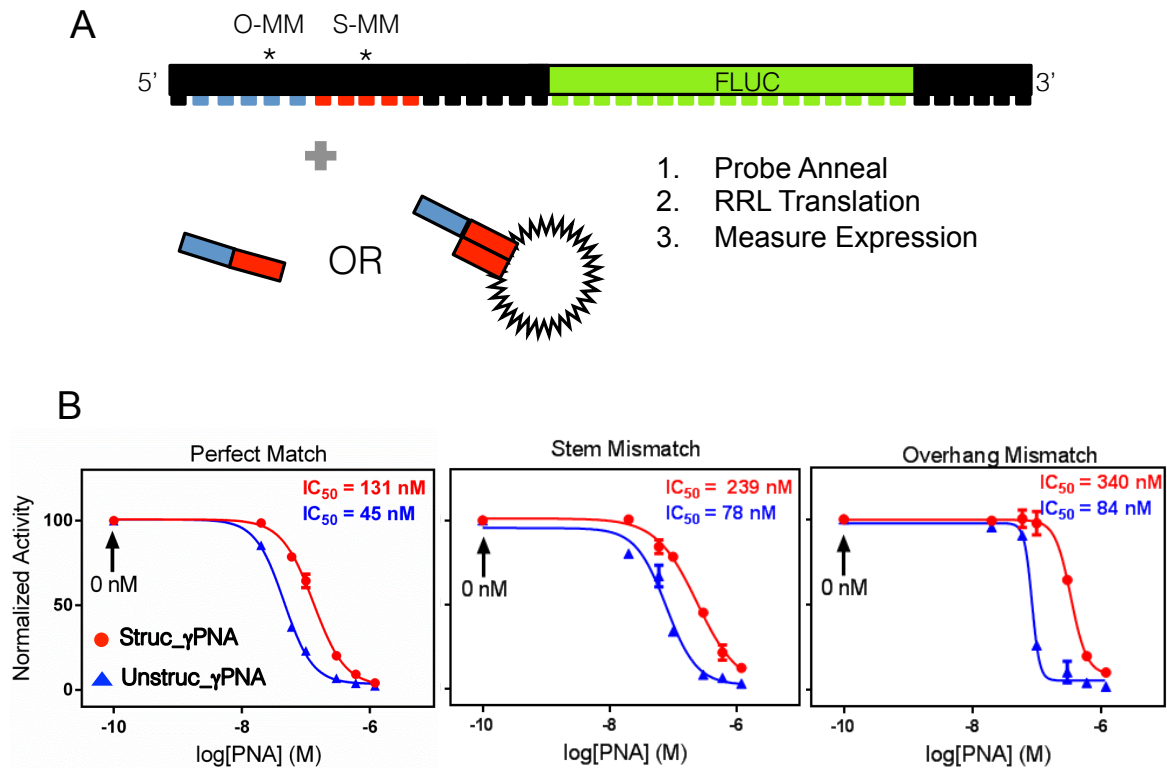
Figure 4.9 Comparison of sturc_γPNA and unstruc_γPNA antisense knockdown against perfect and mismatched targets. (**A.**) Compared to the perfect match (PM) firefly transcript, the overhang (O-MM-4A) and stem (S-MM-7U) mismatch have single mutations in the luciferase 5'-UTR (near terminal-end of transcript). Both unstruc_γPNA and struc_γPNA each contain an overhang (blue) and stem (red) binding domains, however the struc_γPNA contains an ethylene glycol loop (black jagged line) connected to a 5-mer PNA stem-forming domain. The probes are (1) annealed to the targets transcripts prior to (2) translation in RRL and (3) plate reader quantification of luminescence. (**B.**) Overlay of struc_γPNA and unstruc_γPNA antisense titration curves (both tested at n = 3) with 1-hour probe preannealed (in buffered solution to match RRL salt concentration of 79 mM K^+ in DEPC-treated H_2O) to the PM, S-MM-7U and O-MM-4A targets.

Considering the γPNA was annealed for 1-hour in the prior dose-response experiments we hypothesized further annealing to 3-hours would lead to increased struc_γPNA perfect match knockdown and selectivity. We annealed unstruc_γPNA and struc_γPNA to the three target cases for 1-hour and 3-hours, translated the transcripts and measured the overall luciferase inhibition (**Figure 4.10**).

To compare the target selectivity of the γPNAs, we divided the mutation knockdown amount by the perfect match knockdown amount, computed at a γPNA concentration of 100 nM. For struc_γPNA, we observed a 1.5-fold antisense difference between the overhang and perfect match at 1-hour annealing. Applying a 3-hour annealing increased the overhang-to-perfect match selectivity to 1.7-fold. In terms of antisense inhibition, the struc_γPNA knockdown the overhang mismatch ~10% compared to ~50% knockdown of the perfect match case (1.7-fold difference). In the case of the stem mutation case, struc_γPNA yielded a 1.2- and 1.3-fold difference between the mutation and perfect match knockdown, for the 1-hour and 3-hour annealing times, respectively (**Table 4.3**). Interestingly, unstruc_γPNA demonstrated a 1.5-fold difference between the stem mutation and perfect match at 1-hour annealing. However, the fold change was no longer statistically significant (student t-test) using a 3-hour annealing time due to the further knockdown of the stem mutation target. Further increasing annealing times may lead to more pronounced fold-differences between perfect and mismatch targets due to the binding reactions nearing equilibrium. However, by 3-hours we can easily observe antisense differences between the target transcripts.
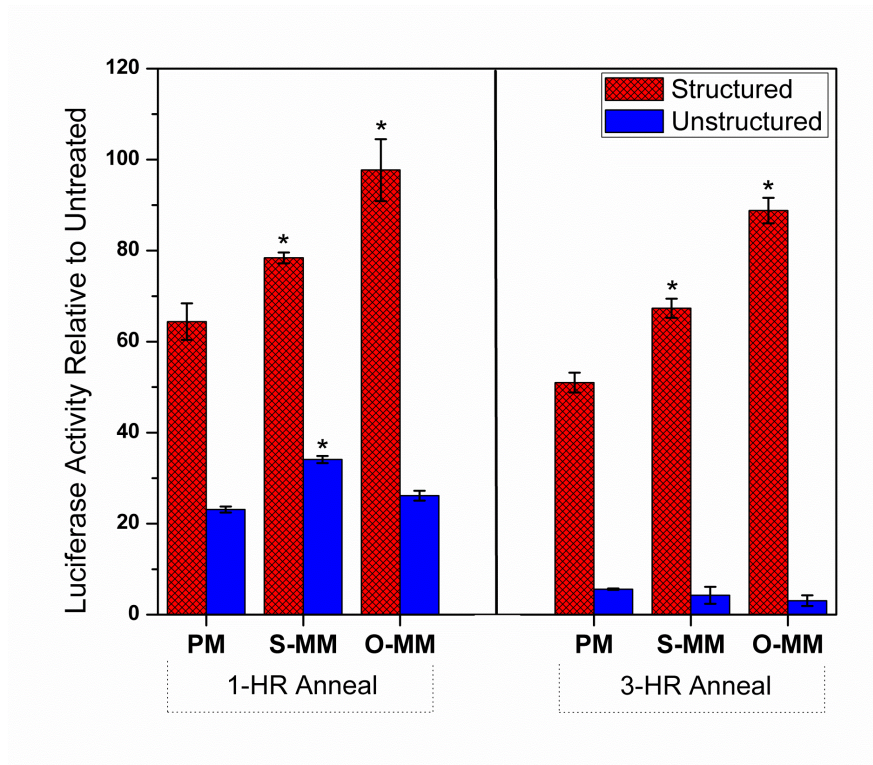
Figure 4.10 Improved antisense target discrimination by increasing annealing times. We compared (by ratio) the percent luciferase inhibition of PM to the mutation cases (S-MM-7U and O-MM-4A), as a function of probe-target annealing time, at either 1-hour or 3-hours, of the struc_γPNA and unstruc_γPNA. At a 1-hour annealing time (left panel), the struc_γPNA demonstrated a statistically significant (* = $p < 0.05$) difference in luciferase inhibition between the PM and S-MM-7U and the PM and O-MM-4A, whereas the unstruc_γPNA only showed a significant difference between the S-MM-7U. At a 3-hour annealing time (right panel) there is no inhibition difference ($p > 0.05$) amongst the three targets when using the unsturc_γPNA, however the sturc_γPNA demonstrated increasing, compared to the 1-hour annealing time, discrimination of the mismatched to perfect match targets. All data shown is presented as an average of $n = 3 \pm SD$.

Table 4.3 Cell-free antisense selectivity ratio[a]

1-HR Selectivity Ratio	Structured γPNA	Unstructured γPNA
O-MM-4A	1.5	N.S.
S-MM-7U	1.2	1.5
3-HR Selectivity Ratio	Structured γPNA	Unstructured γPNA
O-MM-4A	1.7	N.S.
S-MM-7U	1.3	N.S.

a. N.S. = not statistically significant.

4.3 Discussion

We aimed to expand the selectivity of γPNA using a general method which can be easily adapted to other target sequences. Struc_γPNA binding was particularly sensitive to mutations in the overhang (toehold) domain, as evidence by the ~7-fold on-rate difference between O-MM-4A and PM (at 25 nM). In comparison, O-MM-4T, which contains the same mutation placement as O-MM-4A, but consists of an T-T mismatch, yielded ~4-fold selectivity (at 25 nM). The difference in selectivity observed against O-MM-4A and O-MM-4T may be due to several factors. For one, it may be that the A-base mutation in O-MM-4 leads to a favorable staking interaction with the 5'-proximal A-base (e.g., purine-purine stacking), thereby placing the target into a biased helical conformation prior to γPNA interaction. This presumed helical bias by O-MM-4A may be unfavorable to the γPNA interaction, which would lead to higher selectivity. The fact that O-MM-4T can form a potentially "mutation compensating" wobble (G-T) pair, yet is still suitably discriminated against, demonstrates the influence the surrounding bases have on the hybridization reaction.

We also demonstrated the benefits of incorporating internal structure for increased antisense selectivity. Here, we observed a drastic decrease in the antisense knockdown when the target mRNA contained a single mutation. After annealing the probes for 3-hours under physiological conditions, we measured struc_γPNA achieved ~10% knockdown of the O-MM-4A Fluc transcript, whereas the perfect match Fluc gave ~50% knockdown. In contrast, unstruc_γPNA demonstrated no selectivity between O-MM-4A and the perfect match transcripts (expression knockdown was >90% for both) with 3-hour annealing.

In general, we employed two central design elements from current hybridization probe technologies to improve γPNA selectivity. First, we incorporated intramolecular stem-loop structure to improve binding selectivity. Second, the stem-loop γPNA (struc_γPNA) contains an extended arm (overhang) to accelerate the target binding interaction, as conducted in dissociative (strand displacement) probe design. Struc_γPNA incorporates the thermodynamic benefits of molecular beacons, however the mechanism of target recognition is not initialized at the loop domain (struc_γPNA has an ethylene glycol loop) but through a single stranded overhang (toehold) domain. This latter feature is attractive because it allows for control over the hybridization kinetics by tuning the sequence content and length.

It is perfectly rational to estimate that with the proper probe modeling (i.e. probe design to achieve $\Delta G \approx 0$) many of these challenges can be overcome. To a first approximation, the use of established design tools that incorporate DNA/DNA nearest-neighbor parameters is a good starting point for γPNA hybridization probe design. However, because of structural preorganization and lack of backbone charge on γPNA hybridization energetics, these DNA/RNA tools can be misleading in γPNA design. Thus, an investigator who wants to use γPNA in a selectivity assay is encouraged to test several structured probes (e.g. different toehold and stem/branch migration lengths and sequence content) to discover which design gives the best results.

Looking ahead, the application of highly selective (γ)PNA probes is still underexplored, but presents a promising chassis to develop further. Besides the attractive biophysical characteristics, the nuclease and protease resistance exhibited by PNA may also be useful for *in situ* or unprocessed sample detection of nucleic acid targets.

Importantly, γPNA improves retains these features as well as expands on the properties available (e.g., cell delivery,[52] duplex DNA invasion,[54] and orthogonal recognition[55]). The pre-arranged helical structure of γPNA gives higher binding affinities through exhibiting both shape- and base-complementarity. This may allow for the use of relatively short toeholds (3-5 bases) that also demonstrate fast binding kinetics, in comparison to analogous DNA probes. γPNA helical preorganization also leads to higher selectivity by increasing the free-energy difference between the perfect and mismatched targets. Thus, γPNA demonstrates a desirable anti-correlative relationship between affinity and selectivity. Furthermore, although γPNA does demonstrate high selectivity, especially against central mutations, the additional incorporation of intra or intermolecular structure is anticipated to lead to unbiased mutation discrimination.

4.4   Conclusion

In this chapter, we demonstrated a structure-incorporation method to increase γPNA selectivity. We applied a hybrid approach to do so. First, we incorporated stem-loop intramolecular structure, as seen in molecular beacon design. Second, we used an extended overhang (toehold) domain to initialize the target-probe interaction, as seen in dissociative probe design. The enhanced selectivity of this probe was tested on SPR and measured in a cell-free assay. At the time of writing we are still performing SPR experiments to obtain equilibrium constant data.

Although this project is not complete it is/was a fun project to think about and conduct. I truly think that this method (structuring a γPNA) has plenty of research potential and promise to warrant further exploration. Here, we designed a probe around a

"fixed" target sequence (due to that sequence occurring in the fluc gene). However, future work could explore additional target/probe combinations. For example, a mutation placed at the distal end of a target may be sufficiently discriminated against by shifting the overhang domain to coincide with the distal end bases. The discrimination of alternatively placed mutations is achieved by similar means. Specifically, to discriminate against a target mutation, the probe design should "shift" the overhang domain to coincide with the target mutation placement. Additional questions around overhang length as it relates to binding rate and selectivity are interesting as well. For example, the comparison of a probe set with either varying overhang lengths (i.e., 3,5,6), all targeting the same target sequence will allow for an investigator to compare the binding rate and selectivity among the probe set. Lastly, the loop domain within the structured γPNA used here is a simple hydrocarbon linker, however alternate chemical groups may be substituted instead. For example, a peptide loop may extend or promote the cellular capability (e.g., delivery, protein substrate, etc.) of the structured γPNA.

4.5 Materials and Methods

4.5.1 γPNA/DNA oligomers

All γPNA oligomers reported here were purchased from PNA Innovations Inc. (www.pnainnovations.com). Concentrations of struc_γPNA ($\varepsilon = 146{,}700\ M^{-1}\ cm^{-1}$) and unstruc_ γPNA ($\varepsilon = 94{,}400\ M^{-1}\ cm^{-1}$) were determined by UV-vis absorption on a Varian Cary 300 spectrophotometer. Sequences of all biotinylated target DNA oligonucleotides used in SPR direct binding experiments are also given below. DNA oligonucleotides were ordered from Integrated DNA Technologies (idtdna.com)

4.5.2 Surface plasmon resonance (SPR)

SPR experiments were performed using a Biacore T100 instrument (GE Healthcare) and four-channel carboxymethyl dextran matrix sensor chips. This commercially available CM5 chips (GE Healthcare) were further functionalized with streptavidin (approximately 5000 RUs) via NHS-EDC coupling. 5′ biotinylated DNA targets (all oligonucleotide DNA targets used are shown in table below) were individually immobilized (approximately 120 RUs) to the streptavidin labeled surface and chips were finalized for PNA injections by priming five times with buffer. Buffer used for chip preparation and all subsequent SPR experiments is 10 mM HEPES pH 7.4, 100 mM NaCl, 3 mM Na_2EDTA, and 0.005% v/v polysorbate 20 (HBS-EP Buffer).

DNA Sequence	Sequence[a]
Perfect Match (PM)	5'- BT-TTTTTAGACCCAAGC-3'
Stem Mismatch (S-MM-7T)	5'- BT-TTTTTAGACCCTAGC-3'
Stem Mismatch (S-MM-6A)	5'- BT-TTTTTAGACCAAAGC-3'
Stem Mismatch (S-MM-7G)	5'- BT-TTTTTAGACCCGAGC-3'
Overhang Mismatch (O-MM-4A)	5'- BT-TTTTTAGAACCAAGC-3'
Overhang Mismatch (O-MM-3T)	5'- BT-TTTTTAGTCCCAAGC-3'
Overhang Mismatch (O-MM-4T)	5'- BT-TTTTTAGATCCAAGC-3'

a. BT = Biotinylated

Direct binding experiments were conducted in triplicate (sensorgrams provided are an average of all three experiments with a standard deviation shown at 418 sec) as well as background subtracted for streptavidin and buffer backgrounds. Various concentrations (10, 15, 20, or 25 nM) of structured or unstructured γPNA were injected over the prepared sensor chip for 400 sec (flow rate = 30 μL/min). This was followed by a dissociation cycle via buffer injection for 600 sec (flow rate = 30 μL/min). Finally, a regeneration cycle was conducted to wash any residual γPNA from the sensor chip (30 sec injection of 1M NaCl, 10mM NaOH flow rate = 50 μL/min), followed by a buffer injection to reestablish a baseline for subsequent injections (150 sec injection of buffer flow rate = 30 μL/min).

On-Rates were calculated using the slopes of the raw sensorgrams between 80-100 sec.

$$On \; Rate = \frac{RU_{80 \; sec} - RU_{100 \; sec}}{20 \; sec}$$

On Rate Ratios were calculated by dividing the PM on rate by each mismatch.

$$On \; Rate \; Ratio = \frac{PM_{On \; Rate}}{X - MM - XX_{On \; Rate}}$$

Selectivity Ratios were calculated for all mismatch DNAs using the maximum at 418 sec. Max RUs of the PM were divided between that of the mismatches in order to compare the penalty each mismatch imposed on γPNA binding.

$$Selectivity \; Ratio = \frac{PM_{MAX}}{X - MM - XX_{MAX}}$$

4.5.3 Mutation Fluc template production and *in vitro* transcription

A previously cloned firefly luciferase template (T7 promoter) was used as the 'perfect match' template (Fluc-PM) and used to create the additional O-MM-4 (Fluc-O-MM) and S-MM-7 (Fluc-S-MM) firefly templates. To create the mutant subclones Fluc-PM was digested at a PvuII (upstream of T7 promoter) and HindIII (downstream of T7 promoter) cut site. The digested Fluc vector was then purified using agarose gel electrophoresis (0.4%). The O-MM-4 and S-MM-7 forward and reverse sequences were ordered from Integrated DNA Technologies (idtdna.com) and contained the PvuII and HindIII overhangs. The O-MM-4 and S-MM-7 oligonucleotides were pre-annealed into duplex formation prior to T4-ligation.

O-MM-4A insert sequences:

5'-CTG GCT TAT CGA AAT TAA TAC GAC TCA CTA TAG GGA GAA CCA

5'-AGC TTG GTT CTC CCT ATA GTG AGT CGT ATT AAT TTC GAT AAG CCA G

S-MM-7U insert sequences:

5'-CTG GCT TAT CGA AAT TAA TAC GAC TCA CTA TAG GGA GAC CCT

5'-AGC TAG GGT CTC CCT ATA GTG AGT CGT ATT AAT TTC GAT AAG CCA G

After ligation, the plasmid was transfected (Mach1/T1 *E. coli*) and plated (plasmid confers ampicillin resistance) over night. The resultant colonies were selected and sent for sequencing for verification.

4.5.4 PCR amplification of the firefly luciferase plasmid

The firefly plasmids were PCR amplified using the NEB PCR Protocol for Phusion High-Fidelity DNA Polymerase (cycled 35 times, PCR program 98 °C, 2 min; 98 °C, 10 s; 45 °C, 15 s; 72 °C, 2 min; 72 °C, 1 min; hold at 4 °C).

Primer design: T7 transcription site 5′-TACGACTCACTATAGGG

poly A tail site: 5′-TTTTTTTTTTTTTTTTTTTTTTTTTTTTTT

The products were purified using the Thermo Scientific Gel Extraction Kit protocol and verified using agarose gel electrophoresis (1.8 kB). Transcription Reaction

and Purification. The transcription reaction followed the Thermo Scientific conventional transcription protocol (50 μL final volume) and consistently gave high RNA product yield (~2.5 μM, determined via NanoDrop spectrophotometer). The transcription reaction was conducted at 37 °C for 2 h. The transcription products were purified using the Thermo Scientific GeneJET RNA Cleanup and Concentration Micro Kit and concentration was measured using a NanoDrop spectrophotometer.

4.5.5   γPNA/mRNA annealing

The γPNA (struc_ γPNA or unstruc_ γPNA) and mRNA were annealed together in the presence of 79 mM potassium chloride (designed to match the K+ concentration in the rabbit reticulocyte lysate, RRL Promega) and DEPC-treated water. The RNA concentration for all translation experiments is set at 10 nM in the final translation reaction at a final volume of 15 μL. The probe concentration varies depending on the desired dose. The probe/mRNA is annealed at 37 °C for 1 h.

4.5.6   Translation conditions and luciferase readout

The translation reaction was conducted using the Promega Luciferase Assay System (E1500) (rabbit reticulocyte lysate). The entire 15 μL of annealing solution (above) is mixed into 20 μL lysate. The γPNA concentration is determined by considering the 35 μL final translation reaction volume. The translation reaction is conducted at 30 °C for 1.5 h. 15 μL of lysate solution is mixed into 15μL of Promega Luciferase Assay Reagent (E1483) added to a Thermo Scientific Nunc 96 well plate (flat

white). The bioluminescence reading was collected on a TECAN Infinite M1000 plate

reader.

4.6   Appendix

4.6.1   On-rate tables for γPNAs

Table 4.4A-1 On-rates for unstructured γPNA (slope 80-100 secs)

Concentration	10nM	15nM	20nM	25nM
PM	0.26327 $\pm$0.0284	0.40611$\pm$0.02393	0.54476$\pm$0.03014	0.70474$\pm$0.03838
S-MM-6A	0.10412$\pm$0.02782	0.22585$\pm$0.07809	0.26221$\pm$0.05839	0.35285$\pm$0.05713
S-MM-7T	0.16337$\pm$0.01545	0.25335$\pm$0.02606	0.33557$\pm$0.02699	0.44316$\pm$0.03688
S-MM-7G	0.23773$\pm$0.12872	0.33784$\pm$0.17916	0.43515$\pm$0.0926	0.52684$\pm$0.01848
O-MM-3T	0.1098$\pm$0.02348	0.23799$\pm$0.07381	0.28556$\pm$0.04332	0.39695$\pm$0.05713
O-MM-4A	0.10753$\pm$0.01667	0.17615$\pm$0.02166	0.23501$\pm$0.01849	0.31309$\pm$0.02625
O-MM-4T	0.06394$\pm$0.05462	0.09464$\pm$0.07294	0.14782$\pm$0.04355	0.1873$\pm$0.01665

Table 4.5A-2 On-rates for structured γPNA (slope 80-100 secs)

Concentration	10nM	15nM	20nM	25nM
PM	0.07815$\pm$0.02295	0.17964$\pm$0.0285	0.23795$\pm$0.03121	0.30186$\pm$0.01366
S-MM-6A	0.0269$\pm$0.0135	0.05467$\pm$0.02092	0.06239$\pm$0.02202	0.14391$\pm$0.01449
S-MM-7T	0.02917$\pm$0.0314	0.09723$\pm$0.02118	0.1387$\pm$0.03758	0.16352$\pm$0.01575
S-MM-7G	0.04948$\pm$0.05674	0.10213$\pm$0.11543	0.12762$\pm$0.00761	0.16346$\pm$0.02175
O-MM-3T	0.03932$\pm$0.01071	0.07261$\pm$0.02672	0.09206$\pm$0.0225	0.19957$\pm$0.02158
O-MM-4A	0.00794$\pm$0.02494	0.03845$\pm$0.01194	0.0617$\pm$0.02433	0.07471$\pm$0.01182
O-MM-4T	N/A (Negative)	0.00652$\pm$0.04139	0.00604$\pm$0.01282	0.01114$\pm$0.01115

4.6.2 γPNA direct binding sensograms

Figure 4.11A Direct binding SPR sensograms for (A) struc_γPNA (10 nM) and (B) unstruc_ γPNA (15 nM). DNA target sequences are given in Table 1.1. All data is plotted as *n* = 3 average ± SD.

Figure 4.12A Direct binding SPR sensograms for (A) struc_γPNA (10 nM) and (B) unstruc_ γPNA (20 nM). DNA target sequences are given in Table 1.1. All data is plotted as *n* = 3 average ± SD.
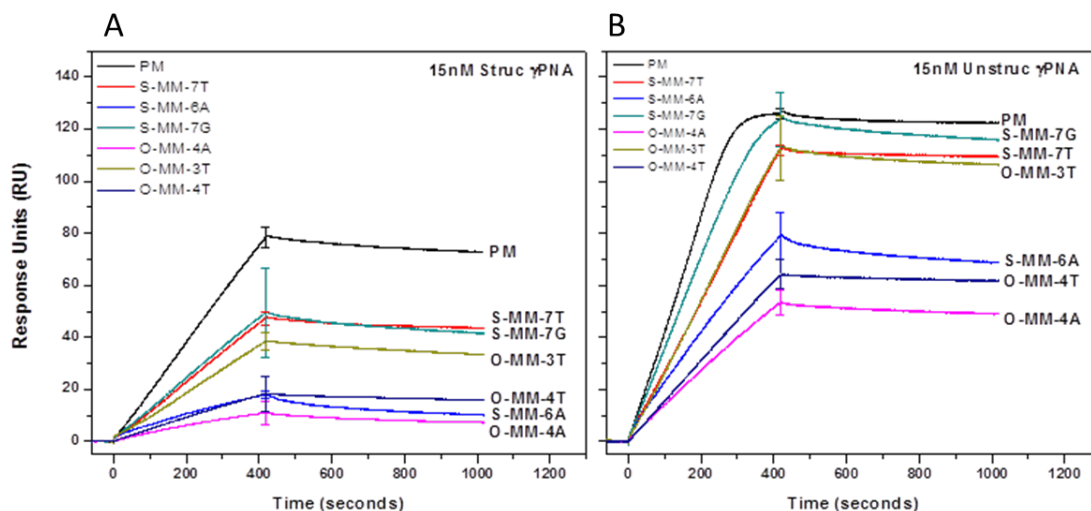
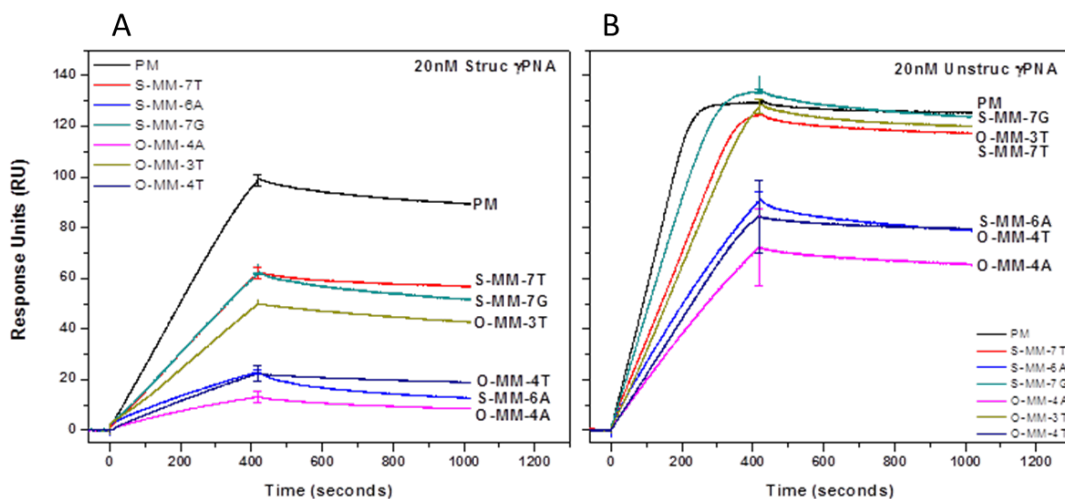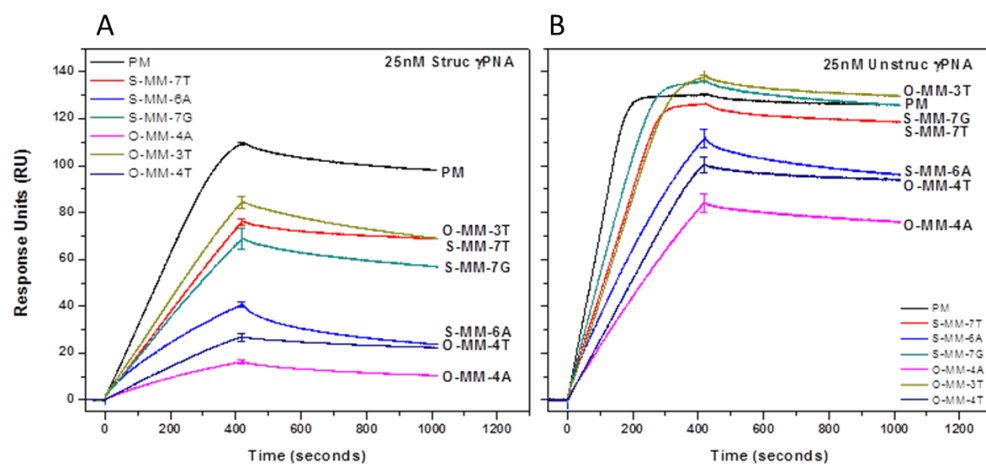**Figure 4.13A** Direct binding SPR sensograms for (A) struc_γPNA (10 nM) and (B) unstruc_ γPNA (25 nM). DNA target sequences are given in Table 1.1. All data is plotted as *n* = 3 average ± SD.

4.7   References

1.   Niemz, A.; Ferguson, T. M.; Boyle, D. S., Point-of-care nucleic acid testing for infectious diseases. *Trends in Biotechnology* **2011,** *29* (5), 240-50.
2.   Hung, E. C.; Chiu, R. W.; Lo, Y. M., Detection of circulating fetal nucleic acids: a review of methods and applications. *Journal of Clinical Pathology* **2009,** *62* (4), 308-13.
3.   Wan, J. C.; Massie, C.; Garcia-Corbacho, J.; Mouliere, F.; Brenton, J. D.; Caldas, C.; Pacey, S.; Baird, R.; Rosenfeld, N., Liquid biopsies come of age: towards implementation of circulating tumour DNA. *Nature Reviews Cancer* **2017,** *17* (4), 223-238.
4.   Diehl, F.; Schmidt, K.; Choti, M. A.; Romans, K.; Goodman, S.; Li, M.; Thornton, K.; Agrawal, N.; Sokoll, L.; Szabo, S. A.; Kinzler, K. W.; Vogelstein, B.; Diaz, L. A., Jr., Circulating mutant DNA to assess tumor dynamics. *Nature Medicine* **2008,** *14* (9), 985-90.
5.   Khodakov, D.; Wang, C.; Zhang, D. Y., Diagnostics based on nucleic acid sequence variant profiling: PCR, hybridization, and NGS approaches. *Advanced Drug Delivery Reviews* **2016,** *105* (Pt A), 3-19.
6.   Epstein, J. R.; Biran, I.; Walt, D. R., Fluorescence-based nucleic acid detection and microarrays. *Analytica Chimica Acta* **2002,** *469* (1), 3-36.
7.   Levesque, M. J.; Ginart, P.; Wei, Y.; Raj, A., Visualizing SNVs to quantify allele-specific expression in single cells. *Nature Methods* **2013,** *10* (9), 865-7.
8.   Deleavey, G. F.; Damha, M. J., Designing Chemically Modified Oligonucleotides for Targeted Gene Silencing. *Chemistry & Biology* **2012,** *19* (8), 937-954.
9.   Roth, C. M.; Yarmush, M. L., Nucleic acid biotechnology. *Annual Review of Biomedical Engeering* **1999,** *1*, 265-97.
10.   Zhang, D. Y.; Chen, S. X.; Yin, P., Optimizing the specificity of nucleic acid hybridization. *Nature Chemistry* **2012,** *4* (3), 208-14.
11.   Urakawa, H.; El Fantroussi, S.; Smidt, H.; Smoot, J. C.; Tribou, E. H.; Kelly, J. J.; Noble, P. A.; Stahl, D. A., Optimization of single-base-pair mismatch discrimination in oligonucleotide microarrays. *Applied Environmental Microbiology* **2003,** *69* (5), 2848-56.
12.   Zhang, D. Y.; Chen, S. X.; Yin, P., Optimizing the specificity of nucleic acid hybridization. *Nature Chemistry* **2012,** *4* (3), 208-214.
13.   Kool, E. T., Hydrogen bonding, base stacking, and steric effects in DNA replication. *Annual Review of Biophysics and Biomolecular Structure* **2001,** *30*, 1-22.
14.   Smith, S. J.; Nemr, C. R.; Kelley, S. O., Chemistry-Driven Approaches for Ultrasensitive Nucleic Acid Detection. *Journal of the American Chemical Society* **2017,** *139* (3), 1020-1028.
15.   Demidov, V. V.; Frank-Kamenetskii, M. D., Two sides of the coin: affinity and specificity of nucleic acid interactions. *Trends in Biochemical Sciences* **2004,** *29* (2), 62-71.
16.   Bonnet, G.; Tyagi, S.; Libchaber, A.; Kramer, F. R., Thermodynamic basis of the enhanced specificity of structured DNA probes. *Proceedings of the National Academy of Sciences of the United States of America* **1999,** *96* (11), 6171-6176.
17.   Tyagi, S.; Kramer, F. R., Molecular beacons: Probes that fluoresce upon hybridization. *Nature Biotechnology* **1996,** *14* (3), 303-308.

18.   Roberts, R. W.; Crothers, D. M., Specificity and Stringency in DNA Triplex Formation. *Proceedings of the National Academy of Sciences of the United States of America* **1991,** *88* (21), 9397-9401.

19.   Tsourkas, A.; Behlke, M. A.; Rose, S. D.; Bao, G., Hybridization kinetics and thermodynamics of molecular beacons. *Nucleic Acids Research* **2003,** *31* (4), 1319-1330.

20.   Wang, K.; Tang, Z.; Yang, C. J.; Kim, Y.; Fang, X.; Li, W.; Wu, Y.; Medley, C. D.; Cao, Z.; Li, J.; Colon, P.; Lin, H.; Tan, W., Molecular engineering of DNA: molecular beacons. *Angewandte Chemie-Internaltional Edition* **2009,** *48* (5), 856-70.

21.   Zhang, D. Y.; Seelig, G., Dynamic DNA nanotechnology using strand-displacement reactions. *Nature Chemistry* **2011,** *3* (2), 103-113.

22.   Chen, S. X.; Zhang, D. Y.; Seelig, G., Conditionally fluorescent molecular probes for detecting single base changes in double-stranded DNA. *Nature Chemistry* **2013,** *5* (9), 782-789.

23.   Chen, Y. J.; Groves, B.; Muscat, R. A.; Seelig, G., DNA nanotechnology from the test tube to the cell. *Nature Nanotechnology* **2015,** *10* (9), 748-760.

24.   Zhang, D. Y.; Winfree, E., Control of DNA Strand Displacement Kinetics Using Toehold Exchange. *Journal of the American Chemical Society* **2009,** *131* (47), 17303-17314.

25.   Zadeh, J. N.; Steenberg, C. D.; Bois, J. S.; Wolfe, B. R.; Pierce, M. B.; Khan, A. R.; Dirks, R. M.; Pierce, N. A., NUPACK: Analysis and Design of Nucleic Acid Systems. *Journal of Computational Chemistry* **2011,** *32* (1), 170-173.

26.   Armitage, B.; Ly, D.; Koch, T.; Frydenlund, H.; Orum, H.; Schuster, G. B., Hairpin-forming peptide nucleic acid oligomers. *Biochemistry* **1998,** *37* (26), 9417-9425.

27.   Kushon, S. A.; Jordan, J. P.; Seifert, J. L.; Nielsen, H.; Nielsen, P. E.; Armitage, B. A., Effect of secondary structure on the thermodynamics and kinetics of PNA hybridization to DNA hairpins. *Journal of the American Chemical Society* **2001,** *123* (44), 10805-10813.

28.   Petersen, K.; Vogel, U.; Rockenbauer, E.; Nielsen, K. V.; Kolvraa, S.; Bolund, L.; Nexo, B., Short PNA molecular beacons for real-time PCR allelic discrimination of single nucleotide polymorphisms. *Molecular and Cellular Probes* **2004,** *18* (2), 117-122.

29.   Kuhn, H.; Demidov, V. V.; Coull, J. M.; Fiandaca, M. J.; Gildea, B. D.; Frank-Kamenetskii, M. D., Hybridization of DNA and PNA molecular beacons to single-stranded and double-stranded DNA targets. *Journal of the American Chemical Society* **2002,** *124* (6), 1097-1103.

30.   Kuhn, H.; Demidov, V. V.; Gildea, B. D.; Fiandaca, M. J.; Coull, J. C.; Frank-Kamenetskii, M. D., PNA beacons for duplex DNA. *Antisense & Nucleic Acid Drug Development* **2001,** *11* (4), 265-270.

31.   Wang, Z. H.; Zhang, K.; Shen, Y. F.; Smith, J.; Bloch, S.; Achilefu, S.; Wooley, K. L.; Taylor, J. S., Imaging mRNA expression levels in living cells with PNA center dot DNA binary FRET probes delivered by cationic shell-crosslinked nanoparticles. *Organic & Biomolecular Chemistry* **2013,** *11* (19), 3159-3167.

32.   Canady, T. D.; Telmer, C. A.; Oyaghire, S. N.; Armitage, B. A.; Bruchez, M. P., In Vitro Reversible Translation Control Using gammaPNA Probes. *Journal of the American Chemical Society* **2015,** *137* (32), 10268-75.

33.   Stender, H., PNA FISH: an intelligent stain for rapid diagnosis of infectious diseases. *Expert Review of Molecular Diagnostics* **2003,** *3* (5), 649-655.

34.   Baerlocher, G. M.; Vulto, I.; de Jong, G.; Lansdorp, P. M., Flow cytometry and FISH to measure the average length of telomeres (flow FISH). *Nature Protocols* **2006,** *1* (5), 2365-2376.

35.   Orum, H.; Nielsen, P. E.; Egholm, M.; Berg, R. H.; Buchardt, O.; Stanley, C., Single-Base Pair Mutation Analysis by Pna Directed Pcr Clamping. *Nucleic Acids Research* **1993,** *21* (23), 5332-5336.

36.   Chiou, C. C.; Luo, J. D.; Chen, T. L., Single-tube reaction using peptide nucleic acid as both PCR clamp and sensor probe for the detection of rare mutations. *Nature Protocols* **2006,** *1* (6), 2604-2612.

37.   Goldman, J. M.; Zhang, L. A.; Manna, A.; Armitage, B. A.; Ly, D. H.; Schneider, J. W., High affinity gammaPNA sandwich hybridization assay for rapid detection of short nucleic acid targets with single mismatch discrimination. *Biomacromolecules* **2013,** *14* (7), 2253-61.

38.   Zhao, C.; Hoppe, T.; Setty, M. K. H. G.; Murray, D.; Chun, T. W.; Hewlett, I.; Appella, D. H., Quantification of plasma HIV RNA using chemically engineered peptide nucleic acids. *Nature Communications* **2014,** *5*.

39.   Das, J.; Ivanov, I.; Montermini, L.; Rak, J.; Sargent, E. H.; Kelley, S. O., An electrochemical clamp assay for direct, rapid analysis of circulating nucleic acids in serum. *Nature Chemistry* **2015,** *7* (7), 569-75.

40.   Das, J.; Ivanov, I.; Sargent, E. H.; Kelley, S. O., DNA Clutch Probes for Circulating Tumor DNA Analysis. *Journal of the American Chemical Society* **2016,** *138* (34), 11009-11016.

41.   Hu, J. X.; Corey, D. R., Inhibiting gene expression with peptide nucleic acid (PNA)-peptide conjugates that target chromosomal DNA. *Biochemistry* **2007,** *46* (25), 7581-7589.

42.   Tonelli, R.; Purgato, S.; Camerin, C.; Fronza, R.; Bologna, F.; Alboresi, S.; Franzoni, M.; Corradini, R.; Sforza, S.; Faccini, A.; Shohet, J. M.; Marchelli, R.; Pession, A., Anti-gene peptide nucleic acid specifically inhibits MYCN expression in human neuroblastoma cells leading to cell growth inhibition and apoptosis. *Molecular Cancer Therapy* **2005,** *4* (5), 779-86.

43.   Good, L.; Awasthi, S. K.; Dryselius, R.; Larsson, O.; Nielsen, P. E., Bactericidal antisense effects of peptide-PNA conjugates. *Nature Biotechnology* **2001,** *19* (4), 360-364.

44.   Doyle, D. F.; Braasch, D. A.; Simmons, C. G.; Janowski, B. A.; Corey, D. R., Inhibition of gene expression inside cells by peptide nucleic acids: effect of mRNA target sequence, mismatched bases, and PNA length. *Biochemistry* **2001,** *40* (1), 53-64.

45.   Dragulescu-Andrasi, A.; Rapireddy, S.; He, G.; Bhattacharya, B.; Hyldig-Nielsen, J. J.; Zon, G.; Ly, D. H., Cell-permeable peptide nucleic acid designed to bind to the 5'-untranslated region of E-cadherin transcript induces potent and sequence-specific antisense effects. *Journal of the American Chemical Society* **2006,** *128* (50), 16104-12.

46.   El-Andaloussi, S.; Johansson, H. J.; Lundberg, P.; Langel, U., Induction of splice correction by cell-penetrating peptide nucleic acids. *Journal of Gene Medicine* **2006,** *8* (10), 1262-1273.

47.   Cheng, C. J.; Bahal, R.; Babar, I. A.; Pincus, Z.; Barrera, F.; Liu, C.; Svoronos, A.; Braddock, D. T.; Glazer, P. M.; Engelman, D. M.; Saltzman, W. M.; Slack, F. J.,

MicroRNA silencing for cancer therapy targeted to the tumour microenvironment. *Nature* **2015,** *518* (7537), 107-10.

48.   Bahal, R.; McNeer, N. A.; Quijano, E.; Liu, Y. F.; Sulkowski, P.; Turchick, A.; Lu, Y. C.; Bhunia, D. C.; Manna, A.; Greiner, D. L.; Brehm, M. A.; Cheng, C. J.; Lopez-Giraldez, F.; Ricciardi, A.; Beloor, J.; Krause, D. S.; Kumar, P.; Gallagher, P. G.; Braddock, D. T.; Saltzman, W. M.; Ly, D. H.; Glazer, P. M., In vivo correction of anaemia in beta-thalassemic mice by gamma PNA-mediated gene editing with nanoparticle delivery. *Nature Communications* **2016,** *7*.

49.   Demidov, V. V.; Potaman, V. N.; Frank-Kamenetskii, M. D.; Egholm, M.; Buchard, O.; Sonnichsen, S. H.; Nielsen, P. E., Stability of peptide nucleic acids in human serum and cellular extracts. *Biochemical Pharmacology* **1994,** *48* (6), 1310-3.

50.   Egholm, M.; Buchardt, O.; Christensen, L.; Behrens, C.; Freier, S. M.; Driver, D. A.; Berg, R. H.; Kim, S. K.; Norden, B.; Nielsen, P. E., PNA hybridizes to complementary oligonucleotides obeying the Watson-Crick hydrogen-bonding rules. *Nature* **1993,** *365* (6446), 566-8.

51.   Sahu, B.; Sacui, I.; Rapireddy, S.; Zanotti, K. J.; Bahal, R.; Armitage, B. A.; Ly, D. H., Synthesis and characterization of conformationally preorganized, (R)-diethylene glycol-containing gamma-peptide nucleic acids with superior hybridization properties and water solubility. *Journal of Organic Chemistry* **2011,** *76* (14), 5614-27.

52.   Sahu, B.; Chenna, V.; Lathrop, K. L.; Thomas, S. M.; Zon, G.; Livak, K. J.; Ly, D. H., Synthesis of conformationally preorganized and cell-permeable guanidine-based gamma-peptide nucleic acids (gammaGPNAs). *Journal of Organic Chemistry* **2009,** *74* (4), 1509-16.

53.   Yeh, J. I.; Shivachev, B.; Rapireddy, S.; Crawford, M. J.; Gil, R. R.; Du, S. C.; Madrid, M.; Ly, D. H., Crystal Structure of Chiral gamma PNA with Complementary DNA Strand: Insights into the Stability and Specificity of Recognition and Conformational Preorganization. *Journal of the American Chemical Society* **2010,** *132* (31), 10717-10727.

54.   Rapireddy, S.; He, G.; Roy, S.; Armitage, B. A.; Ly, D. H., Strand invasion of mixed-sequence B-DNA by acridine-linked, gamma-peptide nucleic acid (gamma-PNA). *Journal of the American Chemical Society* **2007,** *129* (50), 15596-15600.

55.   Sacui, J.; Hsieh, W. C.; Manna, A.; Sahu, B.; Ly, D. H., Gamma Peptide Nucleic Acids: As Orthogonal Nucleic Acid Recognition Codes for Organizing Molecular Self-Assembly. *Journal of the American Chemical Society* **2015,** *137* (26), 8603-8610.

Chapter 5:   Achieving Increased Strand Displacement on SPR and Future Directions

5.1   Introduction

In chapter 2 we observed that the γPNA-γPNA percent strand displacement reactions saturated at 50% measured by SPR. In brief, we hypothesized that the saturation effect was due to non-specific binding of the injected sense γPNA with the chip-immobilized DNA. Hence, we speculated that if a different immoblized DNA was used, thus a different sequence, this may lead to a higher percent strand displacement. In this brief chapter, we apply a different immobilized DNA sequence and demonstrate ~100% strand displacement using our SPR method.

5.2   Results

In chapter 2 the immobilized DNA generated off-target sense γPNA binding. To investigate if higher strand displacement could be achieved, we immobilized a truncated DNA (trDNA) strand that is still able to bind the antisense γPNA with 10-base complementarity. TrDNA does not contain the 5-additional bases of the DNA target used in chapter 2. These 5-bases are found in the mRNA target and are in sequence register, but are non-complementary to the antisense γPNA toehold (**Table 5.1**).

Table 5.1 Sequence of the immoblized DNA targets and γPNA probes[a]

DNA Target (Ch. 2)[a]	5'-BTTTTTAGACCCAAGCTTTCA-3'
trDNA Target (Ch. 5)[a]	5'-BTTTTTAGACCCAAGC-3'
Antisense γPNA	$H_2N-K-TCTGGGTTCG$TGATA$-H$
Sense γPNA	$H-AGACCCAAGC$ACTAT$-K-NH_2$

a. B = Biotin

We used the same γPNAs given in chapter 2 (**Table 5.1**) to carry out the strand displacement reaction. After antisense association, which resulted in ~120 response unit (RU) change, we injected 100 nM and 300 nM sense γPNA over the chip. Over the course of a 600 second injection, we observed ~110 RU and ~115 RU decreasing change with 100 nM and 300 nM sense γPNA over a 600 second injection, respectively (**Figure 5.1**). The injection of 0 nM sense γPNA resulted in no observable change in response, indicating that the injection of the sense γPNA is needed for strand displacement (**Figure 5.1**). We incorporated the 1500 second buffer wash step in anticipation that complete sense-mediated displacement may not occur. Hence, this additional buffer wash would allow for any non-specific interactions to dissociate, and result in additional response change. Nevertheless, the additional buffer wash step is not needed because we achieved ~100% displacement during the sense γPNA injection.
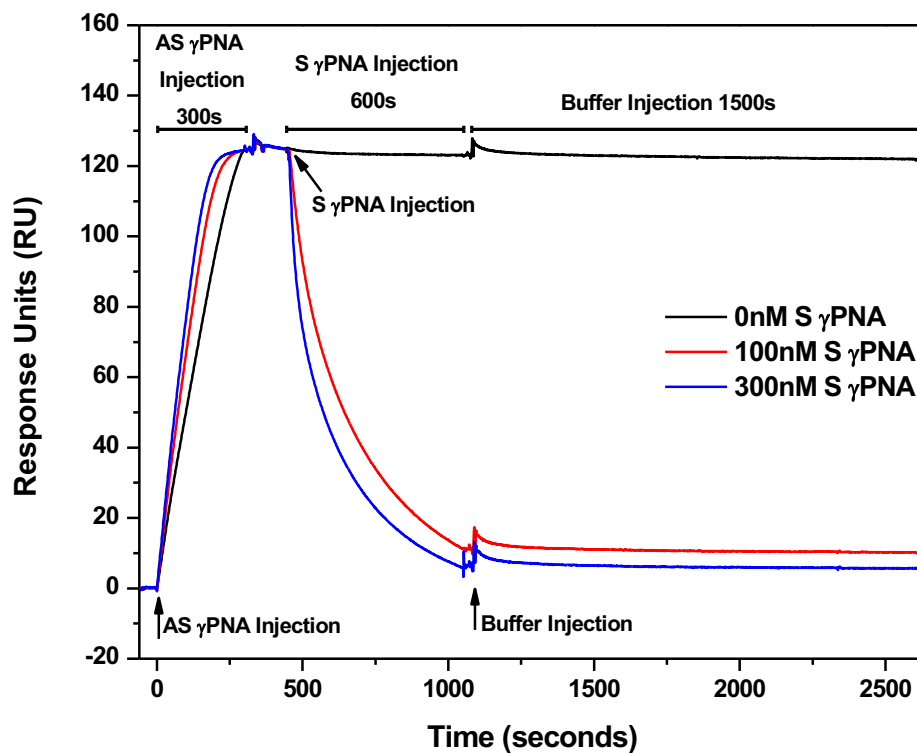
Figure 5.1 Antisense (AS)-sense (S) γPNA strand displacement measured by SPR.

5.3   Conclusions

We demonstrate near complete sense-mediated displacement of the surface bound

antisense γPNA. The high displacement achieved is likely due to the lack of non-specific

binding between the sense γPNA and the immobilized DNA. Although we did not

directly inject the sense γPNA over the immobilized DNA, the fact that we get near 100%

displacement provides strong evidence that sense γPNA non-specific interactions are

negligible.

5.4 Methods and Materials

All SPR experiments were performed on a Biacore T100 instrument (GE Healthcare) equipped with a four-channel sensor chip and all displacement data is presented in triplicate average. The commercially-available chip is coated with a carboxylmethyl dextran matrix that allows further functionalization with streptavidin via a standard NHS-EDC coupling procedure. Immobilization of streptavidin was continued until 6000 response units (RU) of the protein were captured on each of the four channels (flow cells). The final step of the sensor design involved non-covalent capture of the 5'-biotinylated DNA targets (~120 RU) on the respective flow cells bearing immobilized streptavidin.

Each experiment was preceded by injection of a solution containing 20 nM of the antisense γPNA oligomer for 300 s (flow rate = 30 μL/min). A dissociation time of 60 s was incorporated after the injection to allow for diffusion of unbound antisense oligomers from the sensor surface. The subsequent displacement assay was then performed by injecting a solution containing a fixed concentration of the sense γPNA (flow rate = 30 μL/min) and monitoring the sensor response over 600 s. A buffer wash step was conducted for 1500 s. Subsequently, each displacement cycle was ended by introducing a pulse of a regeneration cocktail (1 M NaCl, 10 mM NaOH) for 30 s at a flow rate of 50 μL/min. This cocktail serves to release any residual antisense/sense oligomers and is followed by a buffer injection (150 s, flow rate = 30 μL/min) to reestablish a baseline prior to the next displacement cycle.

5.5   Future Directions

In this thesis, we demonstrated reversible hybridization, in a cell-free and SPR context, by connecting a 5-mer toehold domain to complementary γPNAs. Looking toward future applications which leverage this thesis work, achieving transient control of a target gene of interest *in vivo* would be an exciting forward direction. For example, turning off (antisense) and then on (sense) a primary gene involved in development would be an obvious target. Furthermore, delivering the γPNAs to the cell by direct injection would be a relatively simple way to deliver the γPNA *in vitro* and avoid many delivery/trafficking challenges. Additionally, the method of reversible γPNA hybridization may be useful in applications or methods where transient binding is desirable. For example, hybridization capture and release of a target strand of interest is often used in many sequencing preparations.[1] The incorporation of high affinity and selectivity of γPNA in hybridization capture systems is beneficial, but the release of the target strand from the capture γPNA may be difficult due the high duplex stability. Hence, application of the strand displacement method present in this thesis would allow for easy target release without altering temperature or buffer conditions. Another potential use of the strand displacement method is to allow for RNA study on SPR. In general, RNA immobilization on SPR is not conducted because of the harsh buffer washes used in chip regeneration, which cleaves the RNA. Previous work has circumvented this issue by immobilizing a capture γPNA on the SPR surface that partially binds to an RNA (**Figure 5.2**).[2]
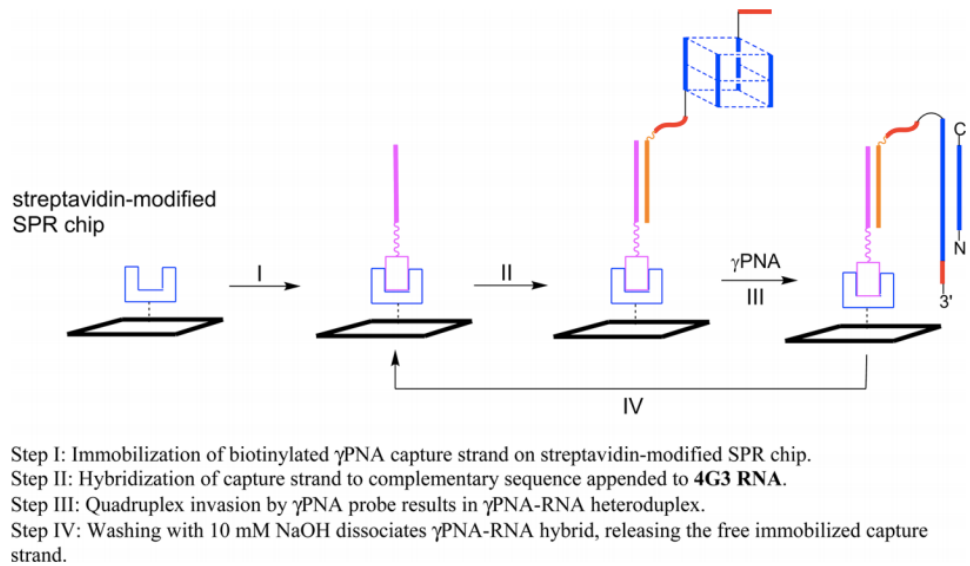
144

Step I: Immobilization of biotinylated γPNA capture strand on streptavidin-modified SPR chip.
Step II: Hybridization of capture strand to complementary sequence appended to **4G3 RNA**.
Step III: Quadruplex invasion by γPNA probe results in γPNA-RNA heteroduplex.
Step IV: Washing with 10 mM NaOH dissociates γPNA-RNA hybrid, releasing the free immobilized capture strand.

Figure 5.2 Hybridization of a target RNA to an immoblized γPNA. Figure adapted from reference 2.

After RNA capture, the subsequent injection of a γPNA is conducted, thus allowing for study of the RNA-γPNA interaction. However, under this method, chip regeneration dissociates the captured RNA from the capture γPNA, thus requiring a new RNA injection after each wash. Replenishing RNA after each regeneration may be tolerated if the RNA molecule is readily available, however this requirement may be prohibitive for some rare or expensive RNA samples (e.g. biologically derived or modified RNA targets). The application of toehold probes to this system would allow for direct binding of RNA and numerous probe injections for association/dissociation binding studies. Specifically, the injection of a complementary γPNA (sense) would mediate the displacement of the RNA-bound γPNA probe (antisense), thus regenerating the chip without requiring a harsh buffer wash and resupply of RNA to the chip surface (**Figure 5.3**).
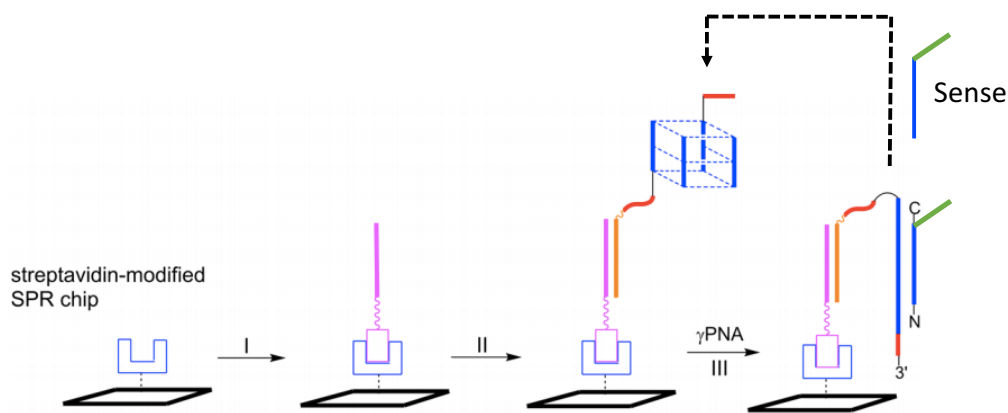
Figure 5.3 Release of a γPNA probe to RNA target by sense-mediated strand displacement (dashed arrow). Figure adapted from reference 2.

Future work may also consider understanding the relationship between strand displacement energetics and kinetics and γPNA design. For example, investigating toehold and branch migration length as a function of strand displacement kinetics may provide valuable insights towards future designs. In addition, acquisition of this energetic/kinetic data would allow for directly comparing γPNA systems to analogous DNA systems, which would aid in understanding the affinity and selectivity benefits, and potential downsides, of γPNA. Beside the addition or subtraction of bases in the toehold or branch migration domains, the incorporation of carbon spacers between the toehold and branch migration domains may present another way to modulate the strand displacement kinetics. Specifically, by separating the toehold domain from the branch migration domain by spacer incorporation (e.g. miniPEG units) the overall kinetics of strand displacement are likely to change because of the spatial separation of the last toehold base from the first branch migration base. The adjustment of the spacer length may present another method to tune the kinetics of the reaction, beside just changing the toehold length or the respective GC content.

5.6   References

1.   Mamanova, L.; Coffey, A. J.; Scott, C. E.; Kozarewa, I.; Turner, E. H.; Kumar, A.; Howard, E.; Shendure, J.; Turner, D. J., Target-enrichment strategies for next-generation sequencing (vol 7, pg 111, 2010). *Nature Methods* **2010,** *7* (6), 479-479.
2.   Oyaghire, S. N.; Cherubim, C. J.; Telmer, C. A.; Martinez, J. A.; Bruchez, M. P.; Armitage, B. A., RNA G-Quadruplex Invasion and Translation Inhibition by Antisense gamma-Peptide Nucleic Acid Oligomers. *Biochemistry* **2016,** *55* (13), 1977-1988.2.